RTG "Functionalization of Semiconductors"

Seminar 2014

San Sebastián, Spain, 31.07.2014 – 01.08.2014

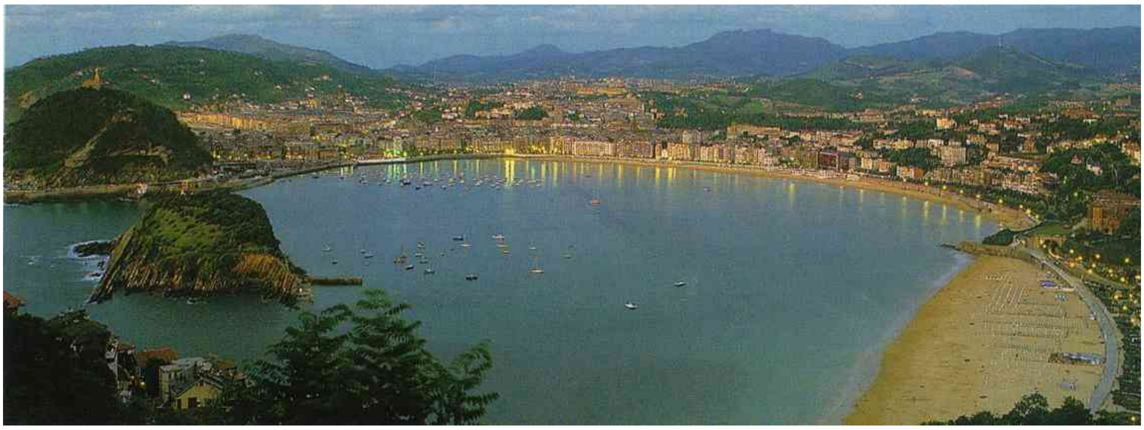

Research Summaries

supported by: Deutsche Forschungsgemeinschaft

Graduiertenkolleg 1782
„Functionalization of Semiconductors“

Workshop & Seminar

San Sebastian, Spain, july 28th – august 1st

Seminar program (august 1st):

Topic area A: Nanoscale layer structures for the functionalization of Silicon

9.00 – 9.30: K. Jandieri
"Band alignment at (GaB)(AsP) / GaP interface: Theoretical suggestions from different experiments"
9.30 – 9.50: P. Springer, S. W. Koch, and M. Kira
"New Approach to Calculate Excitonic Wave Functions in Indirect Semiconductors"
9.50 – 10.10: R. Woscholski, M. Stein, M. Drexler, A. Rahimi Iman and M. Koch
"Optical properties and carrier dynamics of III/V semiconductors"
10.10 – 10.30: N. Knaub, A. Beyer, P. Ludewig and K. Volz
"Quantitative STEM HAADF analysis of dilute Bi containing GaAs"

Topic area C: Control of functionalization

10.30 – 10.50: K. Werner, A. Beyer, K. Volz and W. Stolz
"Atomic Processes during the MOCVD of Gallium on Si (001)"
10.50 – 11.10: J. O. Oelerich, A. Stegmüller, K. Werner, A. Beyer, R. Tonner, W. Stolz, K. Volz and S. D. Baranovskii
"Computer Simulation of Growth Kinetics of Compound Semiconductors"

11.10 – 11.40: BREAK

11.40 – 12.00: M. Reutzel, G. Mette, M. Dürr, U. Koert and U. Höfer
"Breaking the O-C-bond: adsorption of diethyl ether on Si(001)"
12.00 – 12.20: S. Laref and R. Tonner
"DFT Calculations of TETRAHYDROFURAN on Si(001)-4x2"
12.20 – 12.40: A. Pick and G. Witte
"Site-selective Perylene-Deposition onto Microcontact-Printed Organothiols on Au-surfaces"

Topic area B: Nanoparticles

12.40 – 13.00: J. Eußner and S.Dehnen
"Functional binary and ternary Organotin Chalcogenides"
13.00 – 13.20: N. Rosemann and S. Chatterjee
"Time-resolved photoluminescence-studies on AuSn-X clusters"
13.30 – 13.40: A. M. Abdelmonem, B. Pelaz and W. J. Parak
"ZnO Nanoparticles: Synthesis and surface Modification for Biological Applications"
13.40 – 14.00: U. Kaiser, N. Sabir, M. Schneider, D. Jimenez de Aberasturi, W. J. Parak and W. Heimbrodt
"Energy transfer characteristics of Mn doped CdS/ZnS quantum dots"

Poster program (july 30th, 16.00 – 19.00):

Topic area A: Nanoscale layer structures for the functionalization of Silicon

E. Sterzer, A. Beyer, K. Werner, R. Straubinger, W. Stolz. C. v. Hänisch, J. Sundermeyer and K. Volz
"Nitrogen incorporation in GaAs using alternative precursors containing As-N and Ga-N bonds"

T. Wegele, A. Beyer, M. Zimprich, K. Jandieri, W. Stolz and K. Volz
"Investigations Focused on the Local Composition Determination of Dilute Nitride Quaternary Material Systems Grown on Si-substrates"

A. Ott, A. Beyer, A. Ruiz Perez, B. Kunert, W. Stolz and K. Volz
"Investigation of antimonide-based materials grown on exactly oriented (001) silicon substrate"

S. Gies, M. Zimprich, T. Wegele, C. Kruska , A. Beyer, W. Stolz, K. Volz and W. Heimbrodt
"Optical Spectroscopy of Novel III-V-Semiconductor-Heterostructures"

J. Kuhnert, P. Ludewig, K. Volz and S. Chatterjee
"Photo-modulated reflection and temperature-dependent photoluminescence studies of Ga(AsBi) bulk and quantum well structures"

C. Berger, U. Huttner, M. Mootz, M. Kira, S. W. Koch, J.-S. Tempel, M. Aßmann, M. Bayer, A. M. Mintairov, and J. L. Merz
"Microscopic Theory of Semiconductor Lasers"

L. Kraft and H. Jänsch
"An NMR-Approach to semiconductor burried interfaces"

Topic area B: Nanoparticles

N. Sabir, P. del Pino and W. J. Parak
"Mn doped CdS, CdS/ZnS Nanoparticles Synthesis and characterization"

B. Pelaz and W. J. Parak
"Surface modification of nanoparticles"

P. del Pino and W. J. Parak
"Smart Particles for Bio-Apps"

J. P. Eußner and S. Dehnen
"Functional Binary and Ternary Organotin Chalcogenide Clusters"

Topic area C: Control of functionalization

A. Ostapenko and G. Witte
"Preparation and characterization of phosphonic acid based self-assembled monolayers on Zn0 substrates"

M. Lipponer, N. Armbrust, **M. Dürr** and U. Höfer
"Reaction dynamics of exemplary organic molecules on Si(001) - a molecular beam study"

A. Stegmüller and R. Tonner
"MOVPE" Growth Phenomena of III/V Semiconductor studied by DFT

P. Rosenow and R. Tonner
"DFT-Study on the Adsorption of MOVPE-Precursors on III/V Semiconductors on Silicon and on Properties of III/V-Semiconductor Quantum Well Materials"

Topic area A:

Nanoscale layer structures for the functionalization of Silicon

New MOVPE Precursor Molecules for Highly Efficient Casting of Nitrogen into III-V Semiconductor Materials

Wolf Schorn, Katrin Schlechter, Eduard Sterzer, Kerstin Volz, Wolfgang Stolz,
Jörg Sundermeyer

*Faculty of Chemistry, Faculty of Physics and Materials Science Center,
Philipps Universität Marburg, Hans-Meerwein Str. 4 and 6*

1. Introduction

Within our GRK 1782 research project A1 we are aiming to develop new volatile MOVPE precursor molecules that combine group 13 (B, Al, Ga, In) alkyl and hydride functionalities with an anionic low molecular weight N,N-chelate ligand motif. The goal is to lower the high activation barrier, the high deposition temperature and the large excess of ammonia or other nitrogen sources typically needed during casting of substantial amounts of N atoms via MOVPE into the GaAs and InP growth process, and into meta-stable III-V semiconductor materials, in particular.

2. Results

2.1 Design, Synthesis and XRD Structure Determination of MOVPE Precurors

The low energy of N-N bond cleavage in hydrazine has prompted us to use 1,1-dimethylhydrazine (DMH), an established nitrogen source in MOVPE, as building block for volatile and even liquid boranes, alanes, gallanes and indanes. In order to stabilize these covalent molecules, we established the class of N,N'-bis-dimethylamino-acetamidine (BDMA) substituents. Our ligand synthesis follows a condensation of an active iminoester of acetic acid with two equivalents of DMH [1] (Scheme 1):

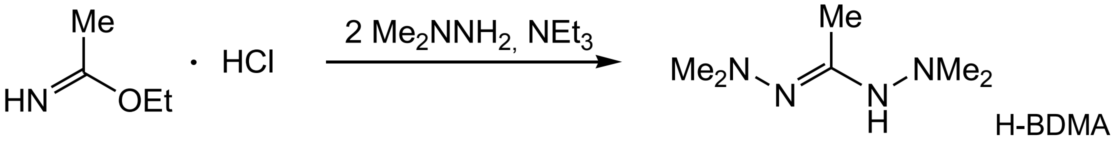

Scheme 1: Synthesis of H-BDMA

The reaction of Me_3M (M = Al, Ga, In) with H-BDMA leads to elimination of methane and formation of low-melting, subliming and pentane soluble inorganic ring compounds $Me_2M(BDMA)$, which were characterized via single-crystal XRD analyses (Fig. 1).

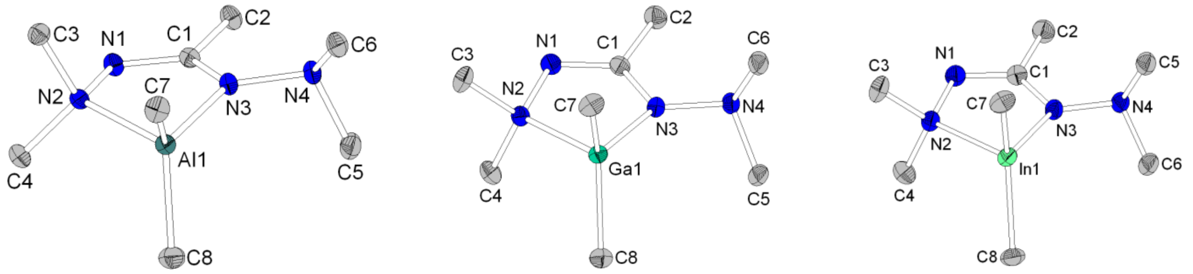

$Me_2Al(BDMA)$
m.p. 41 °C

$Me_2Ga(BDMA)$
m.p. 47 °C

$Me_2In(BDMA)$
m.p. 47 °C

Figure 1: XRD structure analyses of $Me_2M(BDMA)$ precursor molecules

The synthesis of corresponding group 13 hydrides is a challenging goal outlined in our GRK proposal. The absence of any metal-carbon bond in the precursor minimizes the danger of undesired carbon incorporation during the MOVPE process. This problem becomes immanent in the presence of the lighter elements boron and aluminum. The binary hydrides are hazardous gases (B_2H_6), non-volatile polymers $[AlH_3]_x$ or thermally (> -30°C) highly unstable compounds Ga_2H_6 or $[InH_3]_x$. We found, that our BDMA ligand stabilizes molecular ternary hydride compounds of these elements. Most of them are non hazardous liquids easy to condense. Our synthesis process chain for hydrido boranes, alanes and gallanes is displayed in Scheme 2 [1,2]:

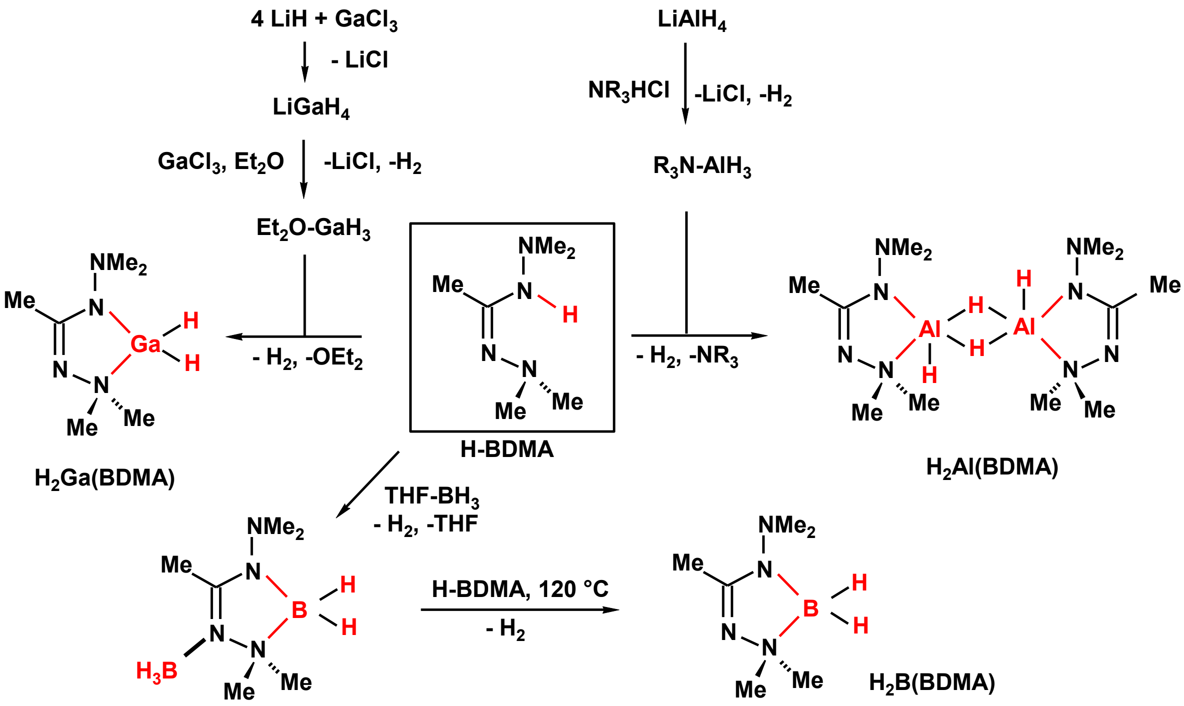

Scheme 2: Synthesis of group 13 hydrides stabilized by BDMA

Single-crystal XRD structure analyses were performed at low temperature in order to evaluate the monomer or dimer nature of these molecular hydrides (Fig. 2):

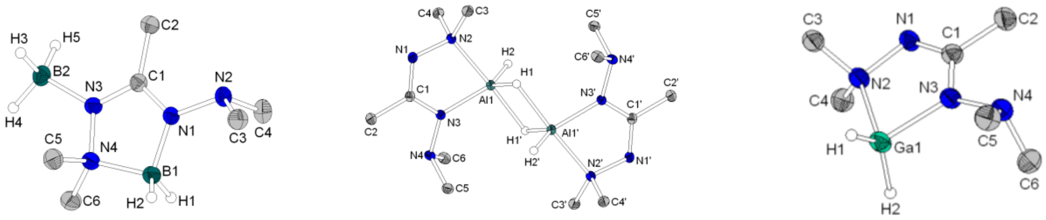

$H_2B(BDMA)(BH_3)$ $H_2Al(BDMA)$ $H_2Ga(BDMA)$

Figure 2: XRD structure analyses of $H_2M(BDMA)$ precursor molecules

2.2 MOVPE Studies

The liquid $H_2Ga(BDMA)$ precursor was synthesized on a 20 gram scale, purified, condensed into a bubbler and used in MOVPE studies [4]. Nitrogen incorporation was determined by XRD measurements (X-Ray Diffraction). We achieved a GaNAs/GaAs growth of up to 0.8% N in combination with conventional Ga and As precursors (TEGa, TBAs) as shown in Fig. 3. The origin of the observed growth rate increase is interpreted as an efficient MOVPE process incorporating not only N but also Ga from the new precursor. Growth conditions without TEGa during GaNAs growth confirmed this interpretation. Room temperature photoluminescence (PL) measurements (Fig. 4) of not annealed sample show the expected band gap shift per % N.

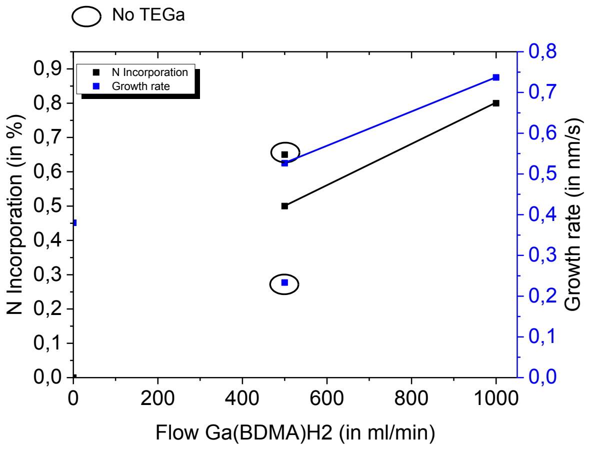

Figure 3: With increasing $H_2Ga(BDMA)$ flow, N incorporation and the growth rate increase. The encircled data points represent the sample without TEGa.

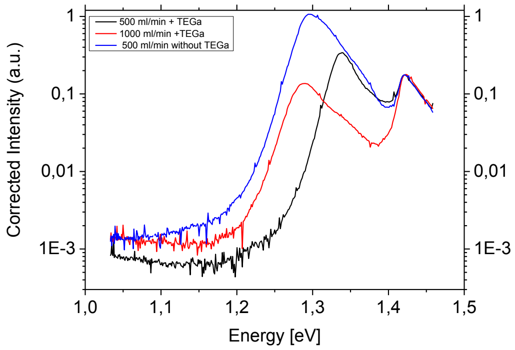

Figure 4: Room temperature PL measurements on not annealed samples (same as shown in Fig. 3).

3. Conclusions

We have managed to establish a new class of group 13 alkyls and hydrides suitable for synchroneous nitrogen and group 13 metal gas phase epitaxy at relatively low deposition temperatures. The key feature of these precursors is a molecular skeleton incorporating two 1,1-dimethylhydrazine building blocks with labile N-N bonds.

4. Outlook

In our current work [3] we plan to optimize the large scale synthesis and purification of group 13 BDMA precursor molecules. We develop the synthesis of a corresponding set of bis-dimethylamino-formamidinato (BDMF) compounds (R^1 = H) and of mono-dimethylamino-acet- and formamidinato compounds (R^2 = alkyl). We try to optimize the thermal decomposition paths and precursor volatility via variation of all substituents R^1, R^2 and X next to the central atom M. In addition, the growth and incorporation characteristics using the novel precursors will be studied in detail.

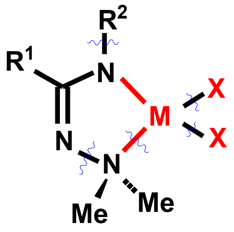

5. References

[1] W. Schorn, „Amidrazone, Hydrazidine und Formazane: Hydrazin-basierte Liganden zur Darstellung flüchtiger Metallverbindungen“, Dissertation Marburg 2012.
[2] J. Sundermeyer, W. Schorn, R. Karch, “Metal complexes with N-aminoamidinate ligands as precursors for chemical vapor deposition processes”, WO2012113761 (A1).
[3] K. Schlechter, ongoing research towards the dissertation.
[4] E. Sterzer, Master thesis, to be submitted august, 2014.

MOVPE Growth of Dilute Bismide Ga(AsBi) Quantum Well Structures for High Efficiency IR Laser Devices

P. Ludewig, N. Knaub, Z. Bushell, L. Nattermann, E. Sterzer, W. Stolz, K. Volz

Faculty of Physics and Material Sciences Center, Philipps-Universität Marburg

Dilute bismide Ga(AsBi) based lasers diodes are promising candidates for high efficiency IR light sources. The incorporation of only a small amount of Bi into GaAs decreases the temperature sensitivity of the emission wavelength compared to conventional III/V semiconductors hence less cooling of the devices is needed. Furthermore, if the Bi content is above 10.5 %, the spin-orbit splitting becomes larger than the bandgap which is due to the band anticrossing in the valance band. In this case auger loss processes could be suppressed leading to higher efficiencies and less heating of the devices. However, Ga(AsBi) is highly metastable which leads to segregation of bismide at the surface and the formation of metallic droplets during growth. In order to incorporate a significant amount of Bi into GaAs low growth temperatures are required and all growth parameters need to be adjusted very carefully.

Ga(AsBi)/GaAs quantum well (QW) and bulk structures were grown by metal organic vapor phase epitaxy (MOVPE) on exact GaAs (001) substrates. All liquid precursors as triethylgallium (TEGa), trimethylaluminum (TMAl), tertiarybutylarsine (TBAs) and trimethylbismuth (TMBi) were used to enable growth temperature as low as 375 °C to 450 °C. The structure of the samples was investigated by as scanning transmission electron microscopy (STEM), high resolution X-ray diffraction (HR-XRD) and atomic force microscopy (AFM). The optical properties were studied by room temperature photoluminescence (PL) measurements.

If all parameters are adjusted carefully Ga(AsBi) layers with Bi fractions up to 5% in good quality can be realized without any formation of metallic droplets. It was found, that the incorporation of Bi into GaAs is limited depending on the applied growth temperature and growth rate and can be influenced by the V/V ratio. Surplus Bi then segregates to the surface and can incorporate into subsequent layers or form metallic droplets if it is not evaporated by a growth interruption at higher temperatures. All samples show a significant PL signal already after growth which can further be improved by annealing at temperatures between 600 °C and 700 °C. The PL peak shifts by about 80 meV / % Bi which is in a good agreement with the theory. The introduction of (AlGa)As barriers grown at 625 °C improves the electronic confinement of the Ga(AsBi) quantum wells compared to pure GaAs barriers and therefore allows the growth of laser diodes. First experiments on a Ga($AsBi_{0.022}$)/(AlGa)As SQW device show promising threshold currents in the range of 800 mA/cm² at an emission wavelength of 950 nm. In addition, Ga(AsBi) laser structures with Bi > 4% were realized that showed lasing operation at low temperatures and indicate a reduced temperature sensitivity of the emission wavelength.

Quantitative STEM HAADF analysis of dilute Bi containing GaAs

Nikolai Knaub, Andreas Beyer, Tatjana Wegele and Kerstin Volz

Material Sciences Center and Faculty of Physics, Philipps-Universität Marburg

Introduction

Our field of research in the framework of the GRK „Functionalization of Semiconductors“ is the quanitative analysis of dilute III/V semiconductors such as Ga(AsBi) or Ga(NAs) on an atomic scale. These dilute III/V semiconductors became very promising materials for optical and electronical devices because the dilute elements have a significant influence on the semiconductors‘ band structure. Since the samples (e.g. Ga(AsBi)) were grown by metal organic vapour phase epitaxy (MOVPE) under metastable growth conditions [1], a homogeneous distribution of the dilute atoms is not automatically given and thus the structure has to be examined.

Results

For the characterization of dilute Bi containing GaAs we use the high angle annular dark field (HAADF) method via the scanning transmission electron microscope (STEM), which is also known as the so called Z-contrast imaging. Thus the measured intensity is approximately proportional to Z^2 (Rutherford-scattering). The imaging was performed with a double spherical aberration corrected JEOL JEM 2200 FS, operating at 200 kV.

For a quantitative evaluation and comparison with the experiment, image simulations are unavoidable. We used the HREM package [2] which is based on a fast Fourier transformation (FFT) multislice method. Here, a supercell of a certain thickness is divided in many slices (usual slice thickness is the thickness of a unit cell). However, the simulated probe interacts with each slice separately where the scattering and thus the intensity is calculated. At the end the final intensity is the sum of the particular slice intensities. To evaluate the simulated (as well as the experimental) images we used the integrated intensity method combined [3]. By using this method one can create a histogram where the intensity distribution is shown. Figure 1a) depicts the group V intensity distribution of a simulated Ga(AsBi) supercell with 3.8% Bi and with a thickness of 5 nm. A huge peak at 0.0225 and two other smaller peaks at higher intensities are clearly visible. Since the scattered intensity is approximately proportionnal to Z^2, the highest peak belongs to the pure As containing columns. Knowing this, one can attribute the other peaks to the Bi distribution on the group V columns. Since we know the structure of the the supercell, it is possible to mark the columns which contain Bi atoms. Such a Bi distribution map is depicted in figure 1b). Here group V columns are marked (yellow) which contain two Bi atoms in a column. By knowing the x-y coordinates of these columns intensity and coordinates can be matched. This allows to identify how many Bi atoms are in each group V column.

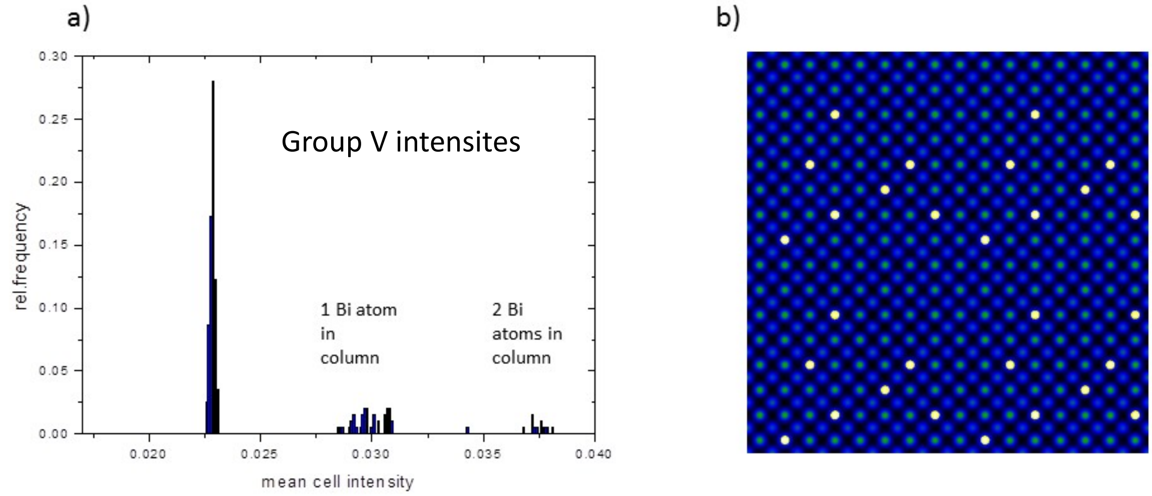

Therefore it can be concluded that the highest intensities in fig. 1a) belong to group V columns containing two Bi atoms and the intensities around 0.03 belong to group V columns containing one Bi atom.

Outlook

The presented results of the simulated images evaluation are promising for the comparison with experimental measurements. For real quantitative evaluation of single impurity atoms on the group V sublattice, also the sample preparation has to be improved further, allowing us to obtain much thinner samples.

[1] Ludewig et al., Journal of Crystal Growth 396 (2014), pp. 95 - 99
[2] Ishizuka K., Ultramicroscopy 90 (2002), pp. 71-83
[3] S.I. Molina et al., Ultramicroscopy 109 (2009), pp. 172-176

Investigations Focused on the Local Composition Determination of Dilute Nitride Quaternary Material Systems Grown on Si-substrates

T. Wegele, A. Beyer, M. Zimprich, K. Jandieri and K. Volz

Material Sciences Center and Faculty of Physics, Philipps-Universität Marburg

Introduction

Our investigations in the framework of the GRK „Functionalization of Semiconductors“ is focused on the quantitative analysis of dilute quaternary semiconductor materials grown by by metal organic vapour phase epitaxy (MOVPE) under metastable growth conditions, for example, Ga(NAsP), which is important as an active layer in laser structures to realize a laser on a Si substrate [1]. The quality of the layer depends on the local composition and on the distribution of the components that can be investigated only on the atomic scale using a scanning transmission electron microscope (STEM).

Results

The investigations of the quaternary semiconductor materials were performed using a JEOL JEM 2200 FS with a double corrected spherical aberration, operating at 200 kV. Especially the high-angle annular dark-field (HAADF-STEM) technique was applied, which makes the interpretation of the micrographs easier in comparison to the conventional TEM measurements because the scattered intensity is proportional to $Z^{1.6\text{-}2}$ [2] (Rutherford-like scattering [3]).

For evaluation of experimental results the integrated intensity method was used [4]. This method includes the identification of the peak positions in the micrographs, separation of the peaks belonging to the different sublattices, integration of the intensities within a certain radius around these peaks and at least creation of the histograms describing the distribution of the peak intensities. The optimal integration radius is a variable, which was also determined during our studies.

Characterization of our structures using Raman spectroscopy as well as photoluminescence spectroscopy [5] showed a change of the composition of the Ga(NAsP)-layers after annealing treatment, which is normally applied to increase the quality of the layers [6]. To assess what happens on a local scale, HAADF-STEM imaging of the Ga(NAsP)-layers was performed. Fig. 1 a) shows that the interfaces of the GaNAsP-layers become rougher with increasing temperature of the thermal treatment. Moreover, the HAADF-intensity of the Ga(NAsP)-layer decreases for higher annealing temperature. Along with that, we observe a HAADF-intensity increase of the neighboring GaP-layers. This means, that outdiffusion of the components of the Ga(NAsP)-layer takes place. Moreover, Ga(NAsP)-layers of the annealed specimens reveal some kind of defects, that show up in HAADF images as dark spots. For quantitave analysis of these defects the high resolution STEM images (Fig. 1 b)) were done for different scattering angles. The measurements at high scattering angles are more sensitive to the atoms with high Z, whereas the lighter atoms can be better detected at lower scattering angles [7]. The intensities in the dark spots and the bright regions in the Ga(NAsP)-layers were compared. The histogram for the intensities of group-V-sublattice at lower angle reveals a significant shift to the higher intensity values, it becomes broader and more asymmetric in the bright region. The skew direction shows that atoms with low Z were detected. This means, that bright region contains more N than dark region.

Outlook

To determine the N-content in the bright region simulations have to be done [8]. For that reason the exact knowledge of the sample thickness and microscope parameters are needed. We optimized the thickness determination of simple materials, e.g., GaP using simulated intensities. This can be used to determine the thickness of neighbouring Ga(NAsP)-layer, so we will be able to do reliable simulations.

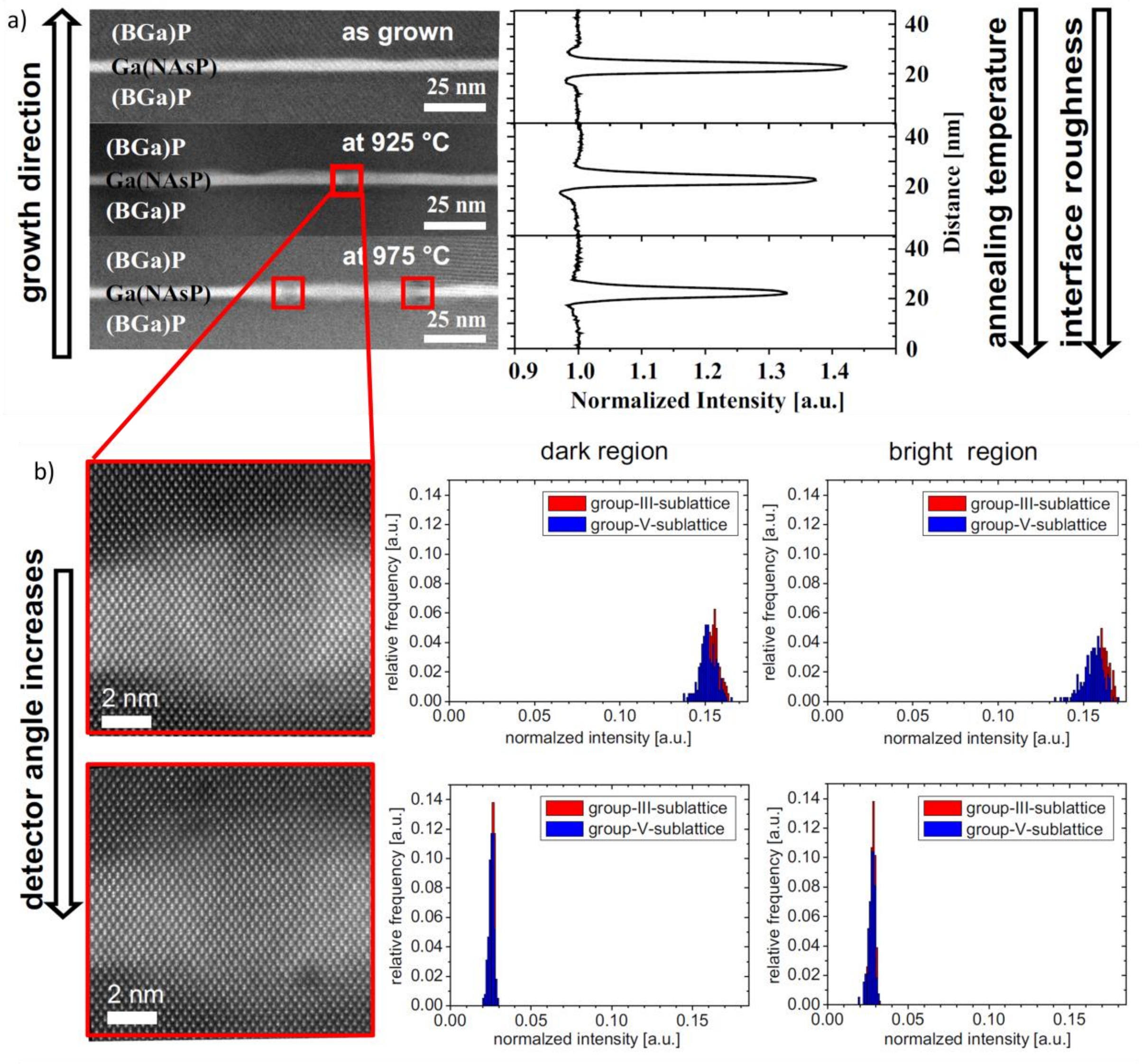

Fig. 1: ADF-STEM images of Ga(NAsP): a) low resolution HAADF images of the as-grown specimen and the specimens annealed at T=925 °C and T=975 °C with corresponding normalized intensity profiles. b) high resolution ADF-images of the specimen annealed at T=925 °C, measured at low (top) and high (bottom) scattering angles. The histograms describe the distributions of the intensities, evaluated from the dark and bright regions in the Ga(NAsP)-layer.

References

[1] S. Liebich, M. Zimprich, A. Beyer, C. Lange, D. J. Franzbach, S. Chatterjee, N. Hossain, S. J. Sweeney, K. Volz, B. Kunert and W. Stolz, Appl. Phys. Lett. 99, 071109 (2011)
[2] S. Pennycook, B. Rafferty, and P. Nellist, Microscopy and Microanalysis 6, 343 (2000).
[3] E. Rutherford, Philosophical Magazine 21, 669 (1911).
[4] J. M. LeBeau, S. D. Findlay, L. J. Allen, and S. Stemmer, Nano Lett. 10 (2010), 4405-4408.
[5] S. Gies, M. Zimprich, T. Wegele, C. Kruska, A. Beyer, W. Stolz, K. Volz, W. Heimbrodt, Journal of Crystal Growth, 402 (2014) 169-174.
[6] B. Kunert, D. Trusheim, V. Voßebürger, K. Volz, and W. Stolz, Phys. Stat. Sol. (a), 1 (2008) 114-119.
[7] Y. Kotaka, Appl. Phys. Lett.101, 133107 (2012).
[8] K. Ishizuka, Ultramicroscopy 90 (2002) 71-83.

Carrier Dynamics in (BGa)(NAsP)-materials on silicon

R. Woscholski, M. Stein, A. Rahimi-Iman, W. Stolz, M. Koch

Faculty of Physics and Material Sciences Center, Philipps-Universität Marburg

Introduction

The goal of my work performed in the framework of the GRK *functionalization of semiconductors* is to investigate the carrier dynamics of metastable nitrogenous and boracic III/V semiconductors on Silicon, fabricated in the framework of the GRK.

Work and Results

The band gap of the quantum well material lies at higher energies than the band gap-energy of the silicon substrate. As typical pump-probe measurements analyze the transmitted probe light, the spectral part that carries the absorption characteristics of the quantum wells will be absorbed when passing through the substrate.

Therefore the substrate of samples that are to be analyzed in a transmission setup needs to be removed. I compared different approaches for substrate removal or thinning with regard to their expenditure and feasibility: the etching of silicon with KOH and the mechanical sanding and polishing. To minimize irregularities in thickness when using chemical etching it is helpful to keep the etch time short. The etch rate of KOH is between one and two micrometers per minute at a temperature of 80°C. Therefore a substrate of several hundred micrometers thickness would need a mechanical thinning beforehand. Additional requirements for the glue used to stick the sample to a sapphire plate make sanding and polishing the preferable alternative for sample preparation.

Silicon has an indirect band gap. If the substrate is thin enough the absorption of the substrate is not dominating the absorption spectrum of the sample. This could be tested by comparing the linear absorption spectrum of prepared sample with a silicon substrate. The suitable substrate thickness lies between forty to seventy micrometers. Further sanding results in damaging the samples. Time-resolved photoluminescence (TRPL) measurements that were performed on both thinned and unprepared sample pieces proved that the quantum well structure has not been damaged by the preparation. Unfortunately the linear absorption showed neither at room temperature nor at 10K distinct features that would have allowed us to identify the band edge or the different excitonic resonances.

An interesting process of the carrier dynamics would be the observation of the Γ-X transfer, meaning the transfer of carriers from the Γ-point in the quantumwell to the X-point in the barrier. Depending on the strain and the nitrogen concentration, the energetic position of the barrier conduction band at the X-point might or might not lie near the first two energy levels of the quantum well. Depending on the exact alignment, which is to be investigated, this could result in a fast carrier transfer from the quantum well to the barrier which would have a major influence on the lasing characteristics of this material. In order to investigate this, TRPL measurements with different excitation wavelengths have been perforemed. However, no drastic changes in the decay time have been observed. This might be due to the GaP intermediate layers that separate the quantumwell material from the barriers to prevent the boron and the nitrogen from forming clusters. Samples with thinner intermediate layers, however, might show a different behavior.

Nevertheless, the time resolved photoluminesence of this sample revealed decay times in the range of a few nanoseconds and a faster and more pronounced non-exponential decay with rising excitation power (Fig. 1a). The comparison of the time-integrated and the initial photoluminescence intensities (Fig. 1b) indicates that this faster decay is probably due to a faster non-radiative recombination.

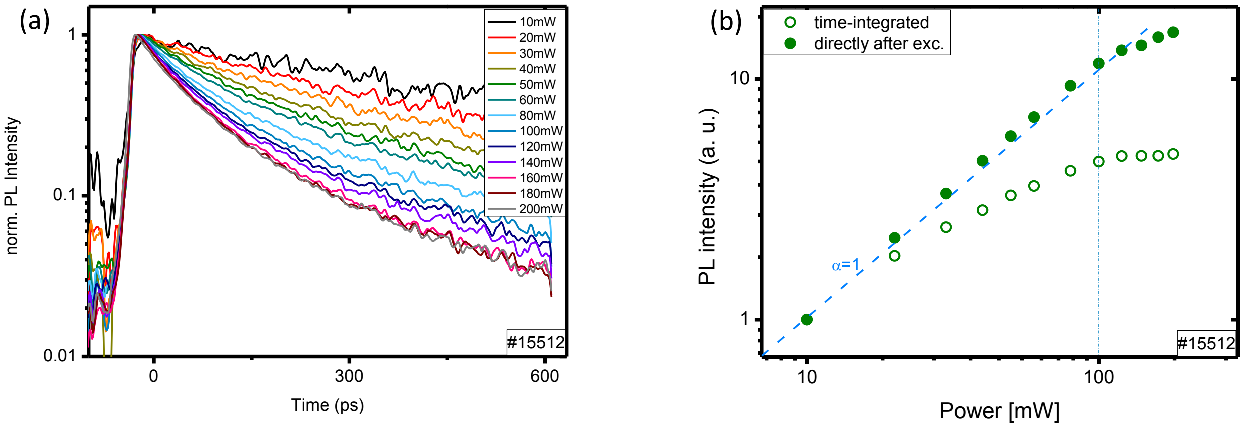

Figure 1: (a) Integrated transients for different excitation densities at T=10 K.
(b) Comparison of the initial and the time integrated PL intensities.

Conclusion and Outlook

Due to the sample structure and the material system, absorption measurements remain challenging while the samples are very much suited for photoluminesence measurements. To investigate Γ-X transfer samples with a certain barrier material and thin GaP intermediate layers will be fabricated by the WZMW. It is planned to study the influence of the composition and fabrication parameters on the carrier dynamics by photoluminesence measurements with excitation wavelength, power and temperature.

THz Effects on bulk GaAs

M. Drexler, R. Woscholski, A. Rahimi-Iman, M. Koch

Faculty of Physics and Material Sciences Center, Philipps-Universität Marburg

The interaction of an optically induced excitonic polarisation with strong electric fields that are in the terahertz (THz) frequency-range has been studied in various systems so far, within group IV, III-V, and II-VI materials [1]–[3]. However, most of these studies have been concerned with multiple quantum wells (MQW). Here we study a bulk GaAs sample being 1.1 µm thick glued to a sapphire substrate. Due to strain caused by the substrate, the heavy-hole (hh) and light-hole (lh) resonance exhibits a splitting of 1.6 nm.

The setup has previously been described in [1], [2]. Instead of a broad supercontinuum pulse, here we use the frequency-doubled output of an optical parametric amplifier. At an excitation wavelength of 820 nm, a pulse length of 120 fs and an excitation density of $4 \cdot 10^9$ photons/cm^2 the absorption is not broadened by the optical probe pulse itself. If the THz pulse is coincident with the optical pulse at the time-zero, a bleaching of both the hh- and lh-resonances is observed (Fig. 1). In fact, this bleaching exhibits a double-structure in time that resembles the temporal evolution of the THz pulse. This behavior differs from the II-VI MQW studies [2]. The Ge/SiGe MQW system studied in [1], however, shows a comparable time dependence of the transient absorption following the electric field.

When varying the electric field-strength of the THz-field (Fig. 2 (a)), the bleaching of both resonances at time-zero exhibit a threshold behavior.

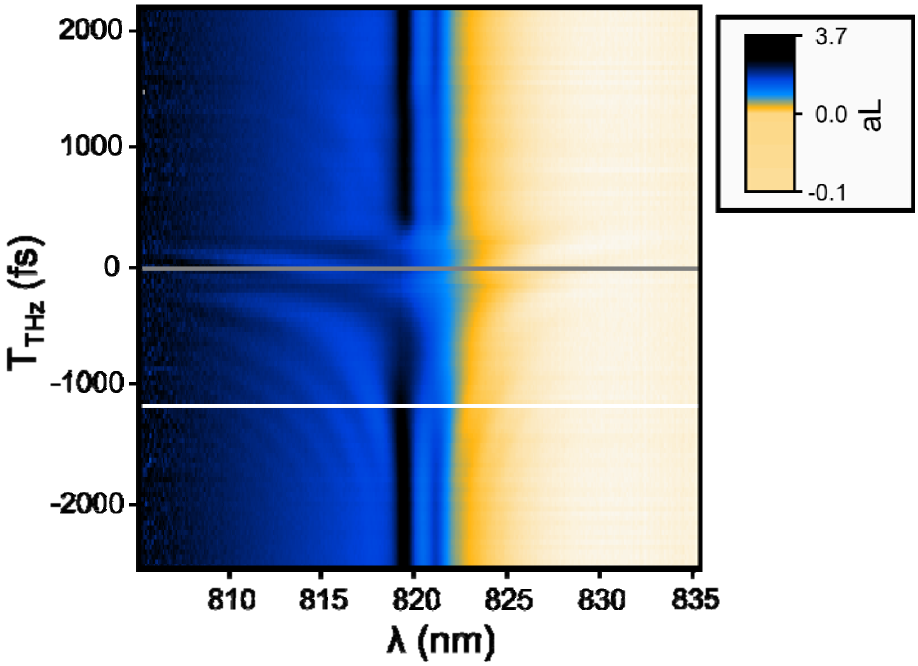

Fig. 1: *THz-induced changes in the absorption of a 1 µm bulk GaAs sample on a sapphire substrate at T=10 K for an electric field-strength of 9.4 kV/cm*

Another remarkable feature of the transient absorption is an oscillatory signal for negative time delays where the infrared probe pulse precedes the THz pulse (Fig. 1). From optical pump-optical probe experiments it is known that for negative time-delays the polarization induced by the probe pulse will dephase instantaneously when the pump pulse is present. In the spectral domain this manifests as coherent oscillations [4]. In this study, however, the polarization of the probe pulse dephases due to the impinging THz-field. The field-dependence of these coherent oscillations is shown in Fig. 2 (b) as changes in the differential absorption ΔαL for negative time-delays.

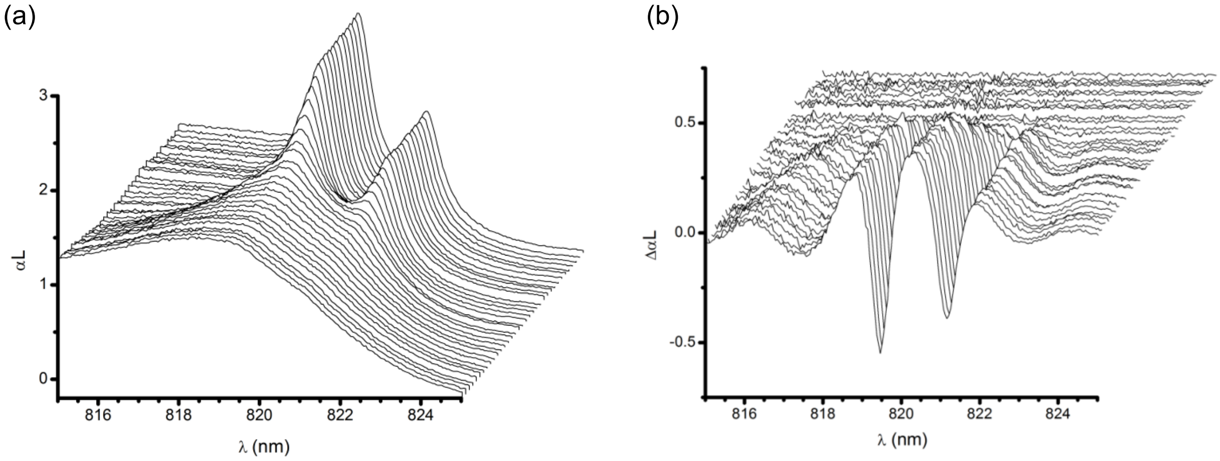

Fig. 2: *(a) THz field-dependent bleaching of the hh- and lh-resonances at a THz-delay time of* T_{THz}*=0 fs (grey horizontal line in Fig. 1.) in the linear absorption. (b) THz field-dependent coherent oscillations at a THz-delay time of* T_{THz}*=-1170 fs (white horizontal line in Fig. 1.) as seen in the differential linear absorption. The field-strength is varied from 0 kV/cm (back) to 9.4 kV/cm (front) within 35 steps for both cases.*

[1] N. S. Köster, A. C. Klettke, B. Ewers, R. Woscholski, S. Cecchi, D. Chrastina, G. Isella, M. Kira, S. W. Koch, and S. Chatterjee, “Controlling the polarization dynamics by strong THz fields in photoexcited germanium quantum wells,” *New J. Phys.*, vol. 15, no. 7, p. 075004, Jul. 2013.

[2] B. Ewers, N. Köster, R. Woscholski, M. Koch, S. Chatterjee, G. Khitrova, H. Gibbs, a. Klettke, M. Kira, and S. Koch, “Ionization of coherent excitons by strong terahertz fields,” *Phys. Rev. B*, vol. 85, no. 7, pp. 1–5, Feb. 2012.

[3] H. Hirori, M. Nagai, and K. Tanaka, “Excitonic interactions with intense terahertz pulses in ZnSe/ZnMgSSe multiple quantum wells,” *Phys. Rev. B*, vol. 81, no. 8, p. 081305, Feb. 2010.

[4] K. Kolata, N. Köster, A. Chernikov, M. J. Drexler, E. Gatti, S. Cecci, D. Chrastina, G. Isella, M. Guzzi, and S. Chatterjee, “Dephasing in Ge/SiGe quantum wells measured by means of coherent oscillations,” *Phys. Rev. B*, vol. 86, no. 20, p. 201303, Nov. 2012.

The effects of rapid thermal annealing on the disorder and composition of Ga(N,As,P) quantum wells on silicon for laser application

Sebastian Gies, Martin Zimprich, Tatjana Wegele, Carsten Kruska, Andreas Beyer, Wolfgang Stolz, Kerstin Volz, and Wolfram Heimbrodt

Faculty of Physics and Material Science Center, Philipps University Marburg,
D-35032 Marburg, Germany

Abstract

Realizing suitable light sources for optical data transmission on silicon is one of the major goals of optoelectronic integration nowadays. The quaternary Ga(N,As,P) is a promising candidate for this as it can be integrated monolithically on silicon. Here, we present an analysis of the annealing effects on Ga(N,As,P) quantum wells (QWs) on silicon using PL, PL excitation and raman spectroscopy as well as transmission electron microscopy (TEM).

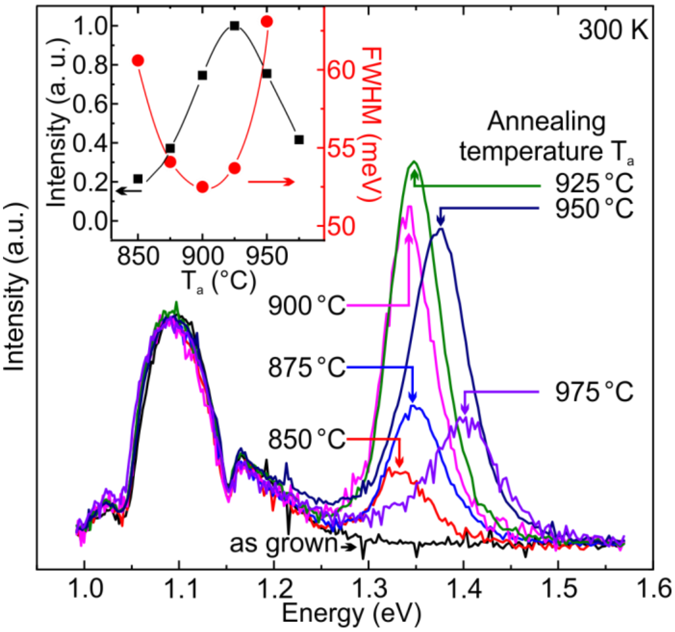

Figure 1: PL spectra of the Ga(N,As,P)-MQW samples at room temperature. The spectra a labeled according to the annealing temperature during RTA processing. The inset shows the integrated intensity and the FWHM as a function of T_a.

The samples consist of a 5 nm thick Ga($N_{0.07}$,$As_{0.82}$,$P_{0.11}$) QW between 5.6 nm GaP and 33 nm (B,Ga)P barriers. This unit is repeated 3 times and embedded in an optical confinement region of (B,Ga)(As,P) layers. As substrate Si was used. The growth was performed using metal-organic vapor-phase epitaxy at a growth temperature of 575 °C. After growth the samples underwent rapid thermal annealing for ten seconds at annealing temperatures T_a between 800 °C and 1000 °C. Figure 1 depicts the room temperature PL spectra of the samples. The spectra are normalized to the silicon emission at 1.09 eV. Around 1.35 eV the Ga(N,As,P) emission can be seen. For the as grown sample no emission could be observed. With increasing T_a the luminescence intensity undergoes a maximum at 925 °C. Additionally, the FWHM has a minimum around 900 °C. Therefore, we can determine the optimal T_a to be in this range. Most surprising is the fact, that the emission is monotonously blueshifted with increasing T_a. In addition to the PL we performed raman spectroscopy, observing a decrease of the GaAs-LO signal with increasing annealing temperature. This result is in perfect agreement with the PL measurement. The blueshift of the emission is caused by a As-P-exchange between the Ga(N,As,P) QW and the barriers. The amount of As-P-exchange can be estimated from raman spectroscopy to be approx. 10%. In order to get accurate access to the electronic changes we performed PLE spectroscopy revealing the excitation bands. Comparing these with QW calculations taking strain into account we could determine the As-P-exchange to be 5-10% for T_a = 975 °C. To further analyze the interplay of removing defects by annealing and creating new ones by As-P-exchange we studied the disorder of the Ga(N,As,P) QW. A two scaled disorder common for these materials was found [1,2]. Both disorder scales are minimal for T_a between 900 °C and 925 °C. This can be explained considering that the As-P-exchange leads to more microscopic defect (short ranged disorder) and may also generate well width fluctuations and strain fields (log ranged disorder). Finally, we examined the structure using TEM to directly examine the changes in QW morphology and composition. The HAADF-images and corresoponding intensity profiles further support decreasing QW quality and a reduction in As content with increasing T_a. To sum up, we found that the annealing process necessary to increase the optical properties of the Ga(N,As,P) QW are inevitably accompanied by an As-P-exchange between QW and barrier, leading to a blueshift of the emission.

References

[1] C. Karcher et al., Journal of Luminescence **133**, 125 (2013).
[2] C. Karcher et al., Phys. Rev. B **82**, 245309 (2010).

Type-II Excitons in (Ga,In)As/Ga(N,As)-quantum wells on GaAs

Sebastian Gies, Philip Hens, Carsten Kruska, Wolfgang Stolz, Kerstin Volz,
and Wolfram Heimbrodt

Faculty of Physics and Material Science Center, Philipps University Marburg,
D-35032 Marburg, Germany

Abstract

Quantum Well (QW) structures are used in many semiconductor devices. These systems inevitably contain interfaces, that influence the charge carriers. Since the recombination of the excitons takes place across the interface their properties are influenced by the interface, making type-II excitons an excellent probe to study internal interfaces. Here, we present an analysis of the recombination of spacially indirect (type-II) excitons in (Ga,In)As/Ga(N,As)-MQWs on GaAs.

The MQW structures under investigation were grown epitaxially using metal-organic vapor-phase epitaxy. On the GaAs substrates a 10 nm thick (Ga$_{0.76}$,In$_{0.24}$)As was grown. This layer is followed by a GaAs barrier of varying thickness between 1 and 7 nm and a QW consisting of Ga(N,As). The nitrogen content in this QW was chosen to be 0.5% to have type-I samples and 5% to have type-II samples. The final capping consists of 45 nm GaAs. No post-growth annealing was applied. Figure 1 shows the luminescence spectra of the type-II samples for different GaAs interlayer thicknesses. For the sample with a 6 nm thick interlayer the type-I transition of the (Ga,In)As is clearly visible at 1.250 eV. Additionally a broad IR-band around 0.8 eV is visible. This is most likely because of the EL2 level of the GaAs substrate. For decreasing interlayer thicknesses the type-I transition disappears and a new peak arises at approx. 0.950 eV. This is because of the type-II transition between the electron in the Ga(N,As) QW and the heavy hole (hh) in the (Ga,In)As. The type-II luminescence does not occur for the thickest interlayer because the special separation of electron and hole is too big. The type-I samples containing 0.5% of nitrogen only show the type-I (Ga,In)As transition, which is lowest in energy (not depicted). The inset shows the result of a quantum well calculation using the transfer matrix method. In this calculation we take strain into account. Conjuction of experiment and calculation reveal the heterooffest between the conduction bands of Ga(N,As) and GaAs to be 600 meV. For the heavy hole band within the

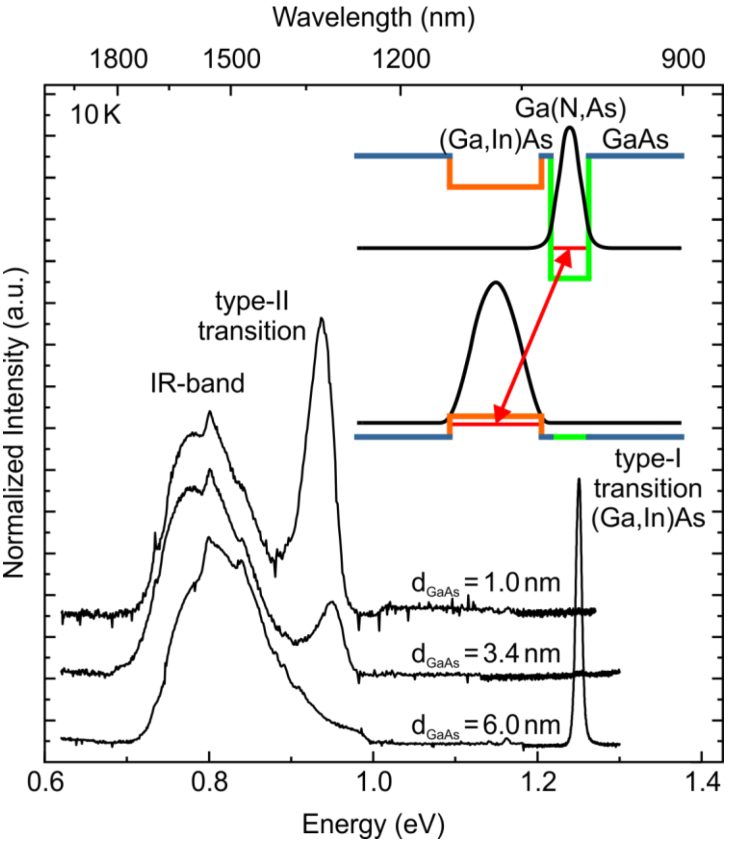

Figure 1: Low temperature PL spectra of the (Ga,In)As/Ga(N,As) type-II samples for different interlayer thicknesses. The inset shows the bandoffsets of the MQW structure and the energy levels and probability density of electron and hole contributing to the type-II transition.

errorbars no offset was found. Furthermore, we find the electron and the heavy hole wavefunction to be strongly confined to their respective QW supporting the explanation for the absence of the type-II transition in the PL spectra for a 6 nm thick interlayer. Additionally, we performed PL experiments using varying excitation intensities. These measurements reveal a second indirect transition for high excitation intensities. This transition is most likely because of the e1-hh2 transitions, which is possible because the selection rules are weakend for indirect transitions. Finally, we aim to present time resolved mearurements of the type-I and type-II transitions to reveal the recombination dynamics of the type-II transitions and their interplay with interface properties such as interlayer thickness and quality.

Microscopic Calculation of the Luminescence Spectra of Dilute Bismide Systems

B. Breddermann, A. Bäumner, P. Springer, S. W. Koch

Department of Physics and Material Sciences Center, Philipps-Universität Marburg

The strong modifications to the band structure introduced by bismuth incorporation promise the possibility of band gap engineering leading to applications in active and passive semiconductor optical devices [1]. Of special interest is the long-wavelength operation of GaAs-based optical devices in which Auger recombination can be suppressed by proper engineering of the band structure through targeted introduction of bismuth into the system [2, 3].

In order to analyze experimental results obtained in the group of Prof. Volz, we calculated the photoluminescence (PL) spectra of $GaBi_xAs_{1-x}$ samples for different bismuth content x solving the time dynamics of the photon-assisted polarization and coupled microscopic quantities such as the photon-number-correlation and carrier distributions. To theoretically account for the bismuth incorporation into the system we used a sp^3s^* tight-binding supercell and a 14-band $\mathbf{k}\cdot\mathbf{p}$ approach [4] to calculate the band structure appropriately. This method accounts for several effects such as Bi-related resonant states undergoing valence band anti-crossing (VBAC) and interactions with extended states of the GaAs valence band edge [5].

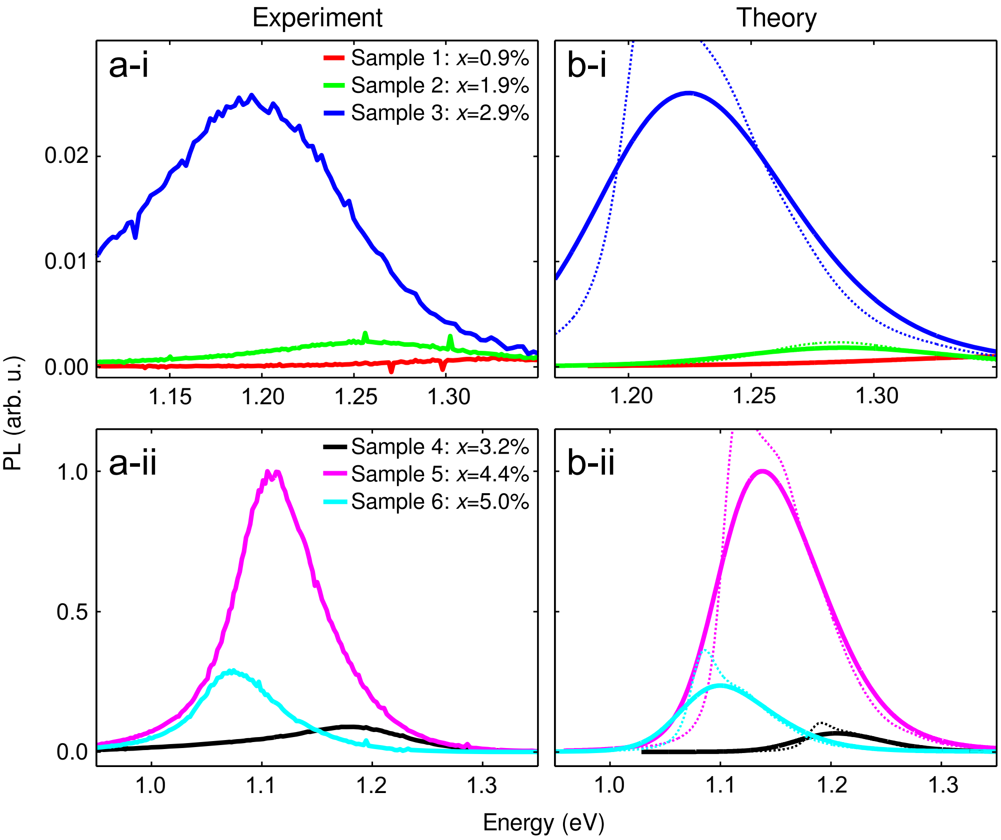

Fig. 1: *Comparison of (a) experimental and (b) theoretical photoluminescence spectra for different bismuth content x. The subframes i show lower contents compared to subframes ii. The solid (dotted) lines in (b) denote computations with (without) in homogenous broadening. All spectra are normalized with respect to the PL peak of sample 5.*

As depicted in Fig. 1 [6], we could achieve an astonishing agreement between experimental (subfigures a-i and a-ii) and theoretical (subfigures b-i and b-ii) luminescence spectra for all investigated Bi contents. The trend of a strong redshift of the PL peak with increasing *x* could be reconstructed as well as the bleaching of the PL intensity with decreasing *x* up to a certain bismuth level (*x*=4.4%) by adjusting the carrier densities. This behavior can be explained by the sample purity which decreases with decreasing Bi continent due to a higher defect density.

Overall, we computed the band structure of diluted bismide systems using an effective 14-band $\mathbf{k}\cdot\mathbf{p}$ method. On this basis we computed the photoluminescence spectra for several bismide contents and found very good agreement with experimental findings.

[1] Y. Tominaga, K. Oe, M. Yoshimoto, Photo-pumped $GaAs_{1-x}Bi_x$ lasing operation with low-temperature-dependent oscillation wavelength, in: International Society for Optics and Photonics, SPIE OPTO, Bellingham, Washington, p. 827702.
[2] C.A. Broderick, M. Usman, S.J. Sweeney, E.P. O'Reilly, Semicond. Sci. Technol. 27 (2012) 094011.
[3] K. Alberi, J. Wu, W. Walukiewicz, K.M. Yu, O.D. Dubon, S.P. Watkins, C.X. Wang, X. Liu, Y.-J. Cho, J. Furdyna, Phys. Rev. B 75 (2007) 045203.
[4] M. Usman, C.A. Broderick, A. Lindsay, E.P. O'Reilly, Phys. Rev. B 84 (2011) 245202.
[5] S. Imhof, C. Bückers, A. Thränhardt, J. Hader, J.V. Moloney, S.W. Koch, Semicond. Sci. Technol. 23 (2008) 125009.
[6] B. Breddermann, A. Bäumner, S.W. Koch, P. Ludewig, W. Stolz, K. Volz, J. Hader, J.V. Moloney, C.A. Broderick, E.P. O'Reilly, Journal of Luminescence 154 (2014), pp. 95 - 98.

Towards Novel Redox Mediators for Dye-sensitised Solar Cells

Lars Hendrik Finger

AK Sundermeyer, FB Chemie, Philipps-Universität Marburg

In the frame of my PhD research within the GRK 1782 I am focusing on the development of alternative redox couples -the traditional I^-/I_3^- couple suffers from severe disadvantages- thereby facilitating the exciton dissociation into mobile electrons and holes at the TiO_2 semiconductor surface.[1] Polysulfides are prospective alternatives for the iodide tri-iodide redox couple in quantum dot[2,3] or dye sensitised solar cells.[4] Ionic liquids (ILs) offer a range of advantages for the application in organic solar cells, *e.g*. very low vapour pressure, wide electrochemical and thermal stability window. Hydrosulfide based ionic liquids were synthesised previously by salt metathesis reactions under aqueous conditions, and were employed in the synthesis of organic polysulfides.[2] It is a fact that the resulting substances cannot be easily purified from halogen and water residues which are highly undesirable for electrochemical applications. We wish to present an easy and completely halogen, metal and water free approach to hydrosulfide based ILs and low melting salts with organic cations.[5] Corresponding substances were prepared by introducing hydrogen sulfide gas into solutions of methyl carbonate based ILs (Scheme 1) which are easily accessible themselves from the appropriate nucleophiles (*e.g*. 1-ethylimidazole) and dimethyl carbonate.[6]

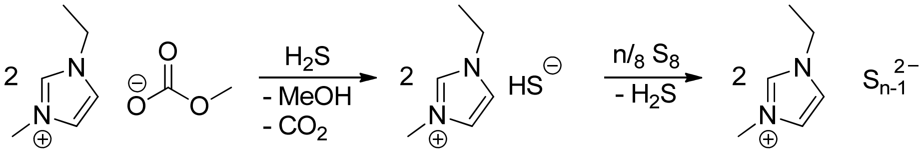

Scheme 1. Halogen free synthesis of hydrosulfide and polysulfide based ionic liquids.

A variety of cations has been employed ranging from alkyl-methyl-imidazolium, over alkyl-methyl-pyrrolidinium and –piperidinium to trialkyl-methyl-phosphonium ions. The compounds were characterized by NMR spectroscopy and elemental, single crystal XRD (Figure 1) and TGA/DSC analyses.

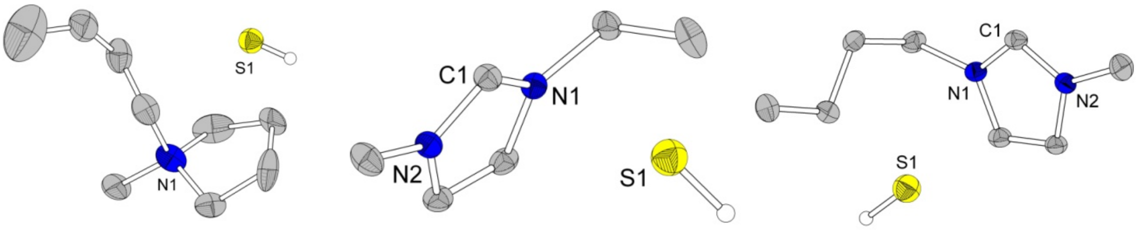

Figure 1. Molecular structures of butyl-methyl-pyrrolidinium hydrosulfide, ethyl-methyl-imidazolium hydrosulfide and butyl-methyl-imidazolium hydrosulfide.

The reactivity of the compounds was investigated primarily with respect to the dissolution of elemental sulfur under non-aqueous conditions (Scheme 1). Polysulfide based ILs with anions in the range S_2^{2-} to S_8^{2-} can be prepared in this manner. UV/Vis spectroscopic examination proved a mixture of polysulfides to be present (Figure 2) which is in agreement with the published literature where sulfur has been dissolved *e.g.*, in dicyanamide[7] and dithiocarbonate[8] based ILs. Cyclic voltammetry (Figure 2) was performed in order to evaluate the redox chemistry of the polysulfides.

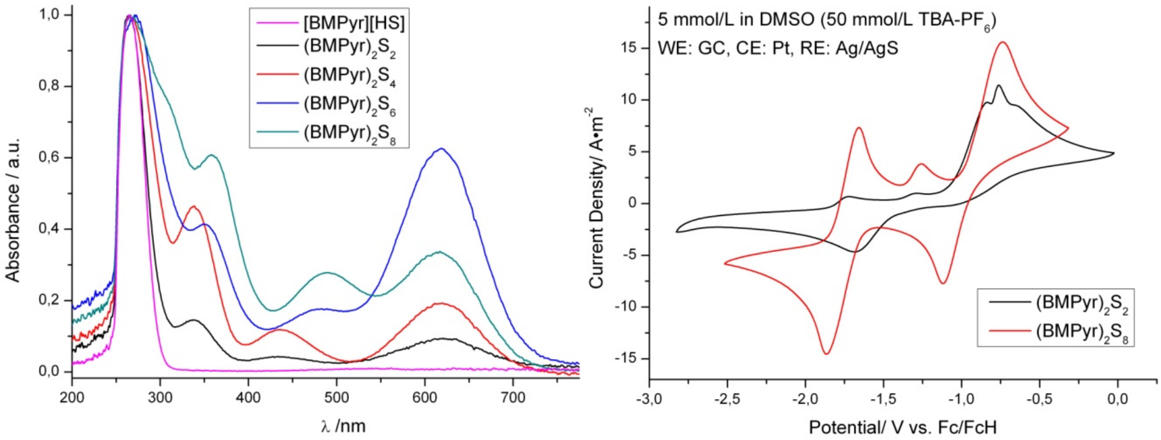

Figure 2. UV-Vis spectra and cyclic voltammetry of butyl-methyl-pyrrolidinium sulfides.

It is evident, that the redox chemistry of the compounds greatly depends on the sulphur content. While the disulfide salt shows only irreversible processes (φ_{ox}: −1.721 V, −0.833 V, −0.764 V, φ_{red}: −1.687 V) the formal octasulfide salt exhibits two reversible redox processes ($\varphi_{0,a}$: −1.762 V, $\varphi_{0,b}$: −0.929 V) and one additional irreversible oxidation (φ_{ox}: −1.258 V). Upon comparison with literature values[7] the reversible redox processes can be attributed to the following redox reactions:

$$\varphi_{0,a}:\ \ 2\,S_4^{2-} \rightarrow S_8^{2-} + 2\,e^-$$

$$\varphi_{0,b}:\ \ S_8^{2-} \rightarrow S_8 + 2\,e^-$$

Detailed experiments with a new spectroelectrochemical cell set up, which is currently in development, will allow a confirmation of these results.

Furthermore we were able to extend our novel procedure to the higher homologues *i.e.* organic salts with hydroselenide and hydrotelluride anions. This was accomplished by preparing the corresponding hydrogen chalcogenide gas *in situ* from the bis(trimethylsilyl)selenide or telluride and methanol (Scheme 2).

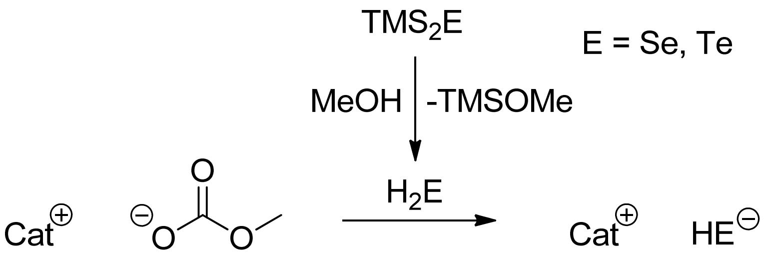

Scheme 2. Halogen free synthesis of hydroselenide and hydrotelluride based ionic liquids.

References:

1. G. Boschloo and A. Hagfeldt, *Acc. Chem. Res.* **2009**, *42*, 1819–1826.
2. V. Jovanovski, V. González-Pedro, S. Giménez, E. Azaceta, G. Cabañero, H. Grande, R. Tena-Zaera, I. Mora-Seró, J. Bisquert, *J. Am. Chem. Soc.* **2011**, *133*, 20156-20159.
3. V. Gonzáles-Pedro, Q. Shen, V. Jovanovski, S. Giménez, R. Tena-Zaera, T. Toyoda, I. Mora-Seró, *Electrochimica Acta* **2013**, 100, 35-43.
4. H. Tian, E. Gabrielsson, Z. Yu, A. Hagfeldt, L. Kloo, L. Sun, *Chem. Commun.* **2011**, *47*, 10124-10126.
5. L. H. Finger, *Halogen Free Synthesis of Hydrosulfide and Polysulfide Based Ionic Liquids*, EuCheM2014 Tallinn, Molten Salts and Ionic Liquids XXV, 6-11 July **2014**, Tallinn, Estonia, Oral and Poster Presentation.
6. R. Kalb (PROIONIC), *PCT Int. Appl.,* WO2008/052861, **2008**; G. Degen, C. Stock (BASF), WO2009/040242, **2009**.
7. N. S. A. Manan, L. Aldous, Y. Alias, P. Murray, L. J. Yellowlees, M. C. Lagunas, C. Hardacre, *J. Phys. Chem. B* **2011**, *115*, 13873-13879.
8. E. Boros, M. J. Earle, M. A. Gilea, A. Metlen, A.-V. Mudring, F. Rieger, A. J. Robertson, K. R. Seddon, A. A. Tomaszowska, L. Trusov, J. S. Vyle, *Chem. Commun.* **2010**, *46*, 716-718.

Topic area B:

Nanoparticles

Functional Binary and Ternary Organotin Chalcogenides

Jens P. Eußner, S. Dehnen

Fachbereich Chemie, Philipps-Universität Marburg

Investigations of group 14 chalcogenidometalates have increasingly attracted attention due to potential technological applications requiring semiconducting, photoconducting, non-linear optical, catalytic or ion exchange properties.[1] The last years afforded a large number of organotin chalcogenide clusters with different size and topology.[2] In a previous work the stepwise formation of binary organotin sulfide clusters was investigated by ^{119}Sn NMR titration experiments in combination with DFT calculations.[3]

Starting from functional organotin halides R^FSnX_3 (R^F = functional organic ligand, X = Cl, Br, I) functional binary organotin chalcogenides can be obtained by reaction with $(Me_3Si)_2E$ (E = S, Se, Te). Further reaction with transition metal complexes (ML_n) can yield functional ternary clusters. In every step of this route, reactions in the functional periphery of the clusters with organic molecules with complementary reactivity (R^x) can chemically modify the organic shell. This can come along with rearrangement of the inorganic cluster core. The reaction scheme for the generation of functional (ternary) organotin chalcogenides is outlined in Scheme 1.

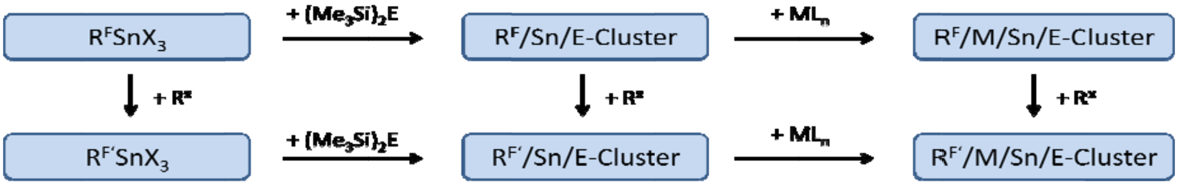

Scheme 1. *Synthetic route for the generation of functional (ternary) organotin chalcogenide clusters. R^F, $R^{F'}$ = functional organic substituent; X = (Cl, Br, I); R^x = organic molecule with complementary reactivity; E = (S, Se, Te); ML_n = transition metal complex.*

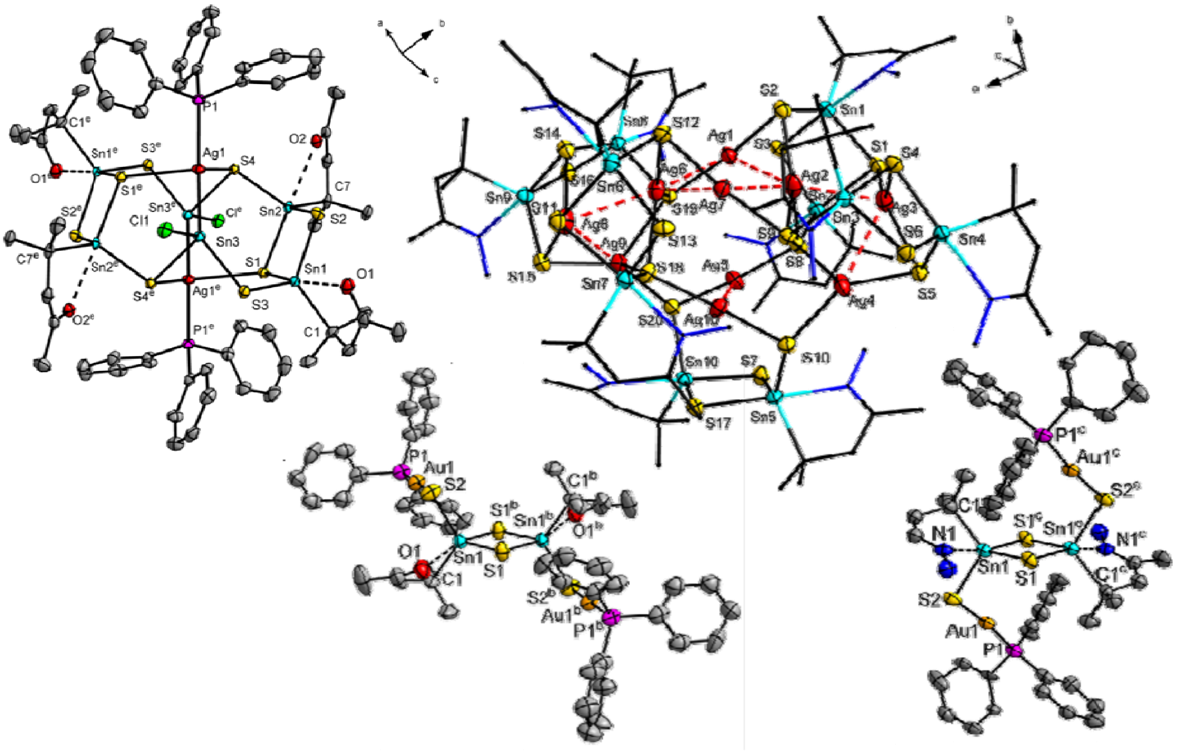

Figure 1. *Molecular structures of* ***2*** *(up left),* ***3*** *(up right, organic substituents denoted as sticks),* ***4*** *(bottom left), and* ***5*** *(bottom right) in the crystal; ellipsoids drawn at 50 % probability without H atoms.*

Our most recent work focused on ternary complexes of group 11 elements. Reaction of $[(R^1Sn)_3S_4Cl]$ (**A**, R^1 = $CMe_2CH_2C(Me)O$) with $[Cu(PPh_3)_3Cl]$ and $(Me_3Si)_2S$ yielded the ternary mixed-valence cluster $[(R^1Sn^{IV})_4(Sn^{II}Cl)_2(CuPPh_3)S_{10}]$ (**1**). The corresponding reaction with $[Ag(PPh_3)_3Cl]$ yielded $[(R^1Sn^{IV})_4(Sn^{II}Cl)_2(AgPPh_3)S_{10}]$ (**2**). The complexes comprise M–Sn bonds (M = Cu, Ag). Additional reaction with hydrazine hydrate yielded $[(R^2Sn)_{10}Ag_{10}S_{20}]$ (**3**, R^2 = $CMe_2CH_2C(Me)NNH_2$). This ternary complex does not exhibit additional phosphine groups. Reaction with $[Au(PPh_3)Cl]$ and $(Me_3Si)_2S$ yielded $[(R^1Sn)_2(AuPPh_3)_2S_4]$ (**4**). The reaction with hydrazine hydrate led to the formation of $[(R^2Sn)_2(AuPPh_3)_2S_4]$ (**5**) under conservation of the inorganic core but with different orientations of the {SAuPPh3} moieties. The molecular structure of **2**−**5** in the crystal are shown in Figure 1. Substitution of the PPh_3 groups in the Au complexes by PMe_3 yielded the corresponding complexes $[(R^{1,2}Sn)_2(AuPMe_3)_2S_4]$ (**6**, **7**). In these complexes, different types of Au···Au interactions are present: **6** exhibits *intra*molecular Au···Au interaction, while the transformation of the organic substituent promotes *inter*molecular Au···Au interaction in **7**.

In conclusion, several new ternary functional organotin sulfide complexes have been synthesized and characterized. The choice of the very group 11 metal M – although added as similar complexes $[M(PPh_3)_xCl]$ (M/x = Cu/3, Ag/3, Au/1) – causes specific coordination environments that affect the molecular structures. Accordingly, the products exhibit different compositions and topologies. It was shown for the first time that functionalized ternary M/Sn/S complex can undergo further derivatization.

Additionally, we have recently started investigation of the deposition of binary functionalized clusters on Si surfaces in collaboration with K. Volz and A. Gries. As a preliminary result, we seem to observe a non-crystalline, but monomolecular coverage of the surface. These studies are currently repeated and will be complemented by further experiments in the near future.

Future synthetic work will focus on further reactions in the organic periphery of the ternary clusters, including the introduction of multidentate phosphine ligands as well as the reaction with multifunctional hydrazines. We envisage proving the general accessibility of other organo-functionalized, ternary transition metal tin chalcogenide clusters in the presented way, in order to obtain a variety of different compositions and thus tunable properties.

References

[1] a) R. R. Chianelli, T. A. Pecoraro, T. R. Halber, W. H. Pan, E. I. J. Stiefel, *J. Catal.* **1984**, *86*, 226–230; b) J. B. Parise, Y. Ko, J. Rijssenbeek, D. M. Nellis, K. Tan, S. Koch, *J. Chem. Soc., Chem. Commun.* **1994**, 527; c) R. L. Glitzendanner, F. L. Di Salvo, *Inorg. Chem.* **1996**, *35*, 2623–2626; d) C. L. Bowes, G. A. Ozin, *Adv. Mater.* **1996**, *8*, 13–28; e) U. Simon, F. Schüth, S. Schunk, X. Wang, F. Liebau, *Angew. Chem. Int. Ed. Engl.* **1997**, *36*, 1121–1124; f) C. R. Evenson IV, P. K. Dorhout, *Z. Anorg. Allg. Chem.* **2001**, *627*, 2178–1282; g) J. Llanos, C. Mujica, V. Sanchez, O. J. Pena, *J. Solid State Chem.* **2003**, *173*, 78; h) S. Bag, P. N. Trikalitis, P. J. Chupas, G. S. Armatas, M. G. Kanatzidis, *Science* **2007**, *317*, 490–493; i) B. D. Yuhas, A. L. Smeigh, A. P. Samuel, Y. Shim, S. Bag, A. P. Douvalis, M. R. Wasielewski, M. G. Kanatzidis, *J. Am. Chem. Soc.* **2011**, *133*, 7252–7255.

[2] a) Z. Hassanzadeh Fard, L. Xiong, C. Müller, M. Hołyńska, S. Dehnen, *Chem. Eur. J.* **2009**, *15*, 6595-6604. b) J. P. Eußner, S. Dehnen, *Z. Anorg. Allg. Chem.* **2012**, *638*, 1827−1832. c) M. Wagner, T. Zoller, W. Hiller, M. H. Prosenc, K. Jurkschat, *Chem. Commun.* **2013**, *49*, 8925−8927. d) B. Mairychová, T. Svoboda, M. Erben, A. Růžička, L. Dostál, R. Jambor, *Organometallics* **2013**, *32*, 157−163. e) B. E. K. Barth, B. A. Tkachenko, J. P. Eußner, P. R. Schreiner, S. Dehnen, *Organometallics* **2014**, *33*, 1678−1688.

[3] J. P. Eußner, B. E. K. Barth, E. Leusmann, Z. You, N. Rinn, S. Dehnen, *Chem. Eur. J.* **2013**, *19*, 13792−13802.

Towards Connection of Chelating Ligands and Ruthenium Complexes to Tin/Sulfur Clusters

Eliza Leusmann and Prof. Dr. Stefanie Dehnen*

Faculty of Chemistry and Material Sciences Center, Philipps-Universität Marburg

In recent years, the design of ruthenium complexes has attracted great interest due to their properties, which are useful for diverse applications: the utilization of Ru(II) complexes ranges from dye-sensitized solar cells[1] and chromophores[2] to water oxidation[3], for instance. Many of these complexes include chelating *N*-donor ligands like terpyridines.[1]

In our group, we have developed ligands for organotetrel-chalcogenide cages, especially a double-decker-like RSn/S cluster based on an inorganic Sn_4S_6 core, to make the organic shell reactive toward further functionalization. Starting out from a keto-functionalized ligand R = CMe_2CH_2COMe, reactions with hydrazine-derivatives have been successful (Scheme 1). [4,5]

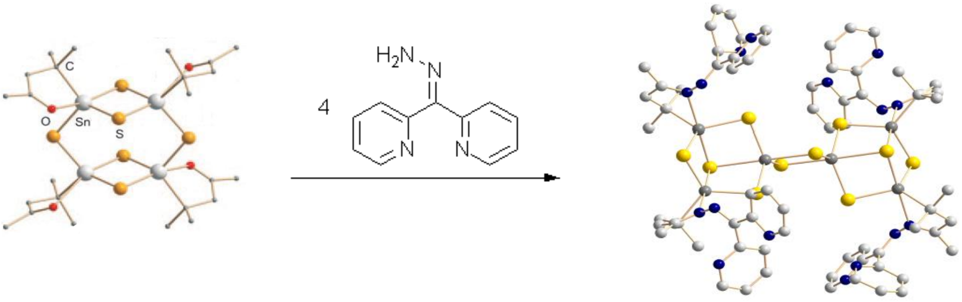

Scheme 1: Core-rearrangement and functionalization of the double-decker-like cage [$(RSn)_4S_6$] (R = CMe_2CH_2COMe) upon reaction with 2,2'-(hydrazonomethylene)dipyridine.

To combine the versatile properties of the inorganic cluster core with the potentially applicable properties of Ru(II) complexes, one of our current aims is to attach these to an Sn/S cage. This can be achieved following different ways: either by functionalization of the Sn/S cluster with a suitable donor ligand and subsequent Ru(II) sequestration, or by attachment of one of the ligands of a pre-formed Ru(II) complex to the cluster. So far, it was possible to exemplarily trap Zn(II) ions by the 2,2'-(hydrazonomethylene)dipyridine-substituted cluster shown above (Scheme 2, left).[5] Also the connection of acetylruthenocene to the Sn/S cluster was successful (Scheme 2, right)[6], indicating the possibility to covalently bind ruthenium complexes to the Sn/S core.

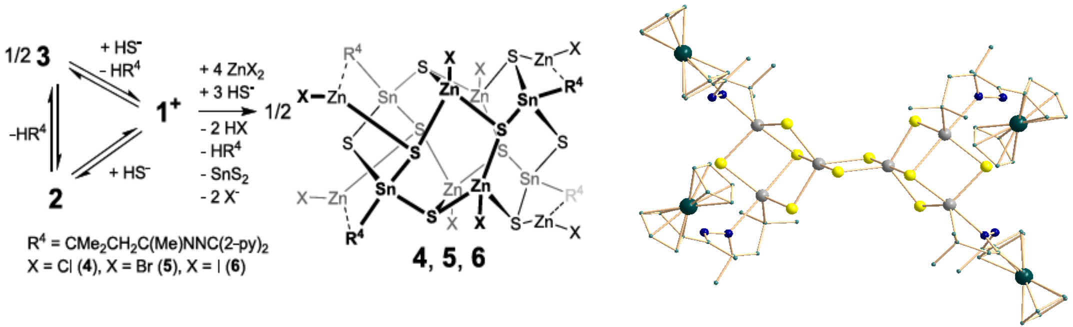

Scheme 2: Trapping of Zn(II) ions by the 2,2'-(hydrazono-methylene)dipyridine-substituted cluster[5] (left) and tethering of hydrazine-derivatized ruthenocene to the Sn/S cluster (right)[6].

In the recent past, we concentrated on the synthesis of hydrazine ligands or their organic derivatives and on their attachment to the Sn/S cluster. We have been successful with diverse acetonaphthenes, anthracenes, acetylquinolines, quinolines, phenanthrolines and, most important, bipyridines[7] (Scheme 3):

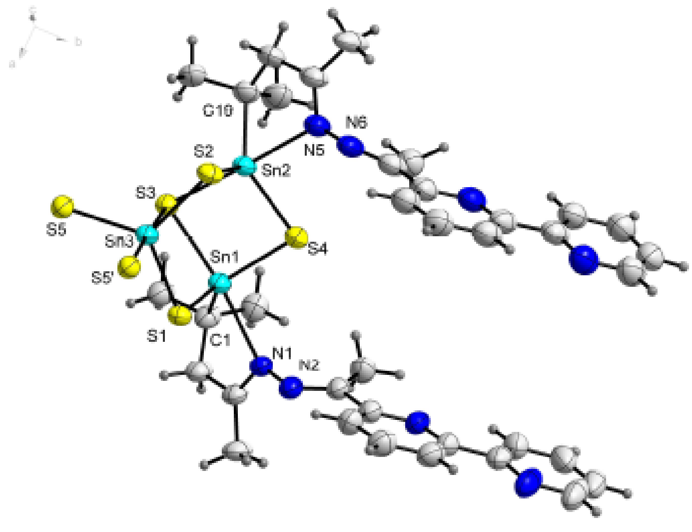

Scheme 3: 2,2'-bipyridine, attached to an Sn/S cluster via azine groups.

We were able for the first time to covalently bind a ligand to the cluster which is not only a chelating one, but which is also known to build complexes with ruthenium easily. We were also able to find out that the Lewis-acidity of transition metal ions influences the azine-group, which is therefore often split. Currently we focus on transition metal complexes in oxidation state 0 like [$Mo(CO)_6$] or [$W(CO)_6$].

As many of the synthesized ligands are planar and aromatic ones, we now plan to investigate their interdependency with semi-conductor surfaces in collaboration with research groups in the Physics Department. A few examples potentially suitable clusters are shown in scheme 4.

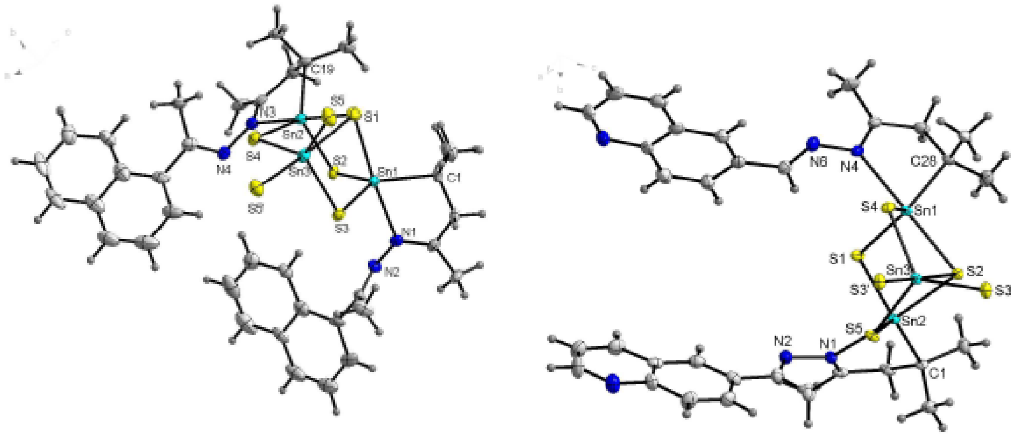

Scheme 4: Molecular structures of the asymmetric unit of an Sn/S cluster with an anthracene-derivative (left) and a quinoline-derivative (right) as polyaromatic ligands.

(1) P. G. Bomben, T. J. Gordon, E. Schott, C. P. Berlinguette, Angew. Chem. **2011**, 123, 10870-10873. (2) K. C. D. Robson, C. P. Berlinguette et al., Inorg. Chem. **2011**, 50, 5494-5508. (3) B. Radaram, X. Zhao et al., Inorg. Chem. **2011**, 50, 10564-10571. (4) Z. Hassanzadeh Fard, L. Xiong, C. Müller, M. Hołyńska, S. Dehnen, Chem. Eur. J. **2009**, 15, 6595-6604. (5) B. E. K. Barth, E. Leusmann, K. Harms, S. Dehnen, *Chem. Commun.* **2013**, *49*, 6590-6592. (6) E. Leusmann, M. Wagner, N. W. Rosemann, S. Chatterjee, S. Dehnen, *Inorg. Chem.* **2014***, 53,* 4228 – 4233. (7) E. Leusmann, F. Schneck, S. Dehnen, *in preparation*.

Ternary Intermetalloid Clusters and Zintl Anions: Reactions of Binary Zintl Anions with Lanthanide Complexes

Bastian Weinert, Prof. Dr. Stefanie Dehnen

Department of Chemistry and Material Sciences Center, Philipps-Universität Marburg

Introduction

Intermetalloid clusters,[1] which combine main group (semi-)metals with transition metal clusters, belong to the most recent developments in the field of *Zintl* anion chemistry and physics.[2] So far, the clusters have usually been obtained by reacting solutions of *Zintl* phases A_4Tt_9 or A_3Pn_7 (A: alkali metal, Tt: tetrel, Pn: pnictogen), which comprise homoatomic anions, in liquid NH_3 or *en*/[2.2.2]crypt with transition metal compounds.

However, due to a relatively high charge, most of the phases with molecular tetrel polyanions, e.g. A_4Tt_4, show poor solubility,[3] which has complicated reactions of further species. To overcome this problem, and to add another degree of freedom regarding the electron number of the resulting clusters, we recently extended this approach by using binary *Zintl* anions with a combination of Group 14/15 elements as well-soluble precursors, namely $[Sn_2Sb_2]^{2-}$, $[Sn_2Bi_2]^{2-}$, with only 2− charge according to the *Zintl-Klemm-Busmann*[4] pseudo element concept. This has led to the generation of a large variety of ternary anions such as $[Pd_3@Sn_8Bi_6]^{4-}$, $[Ln@Sn_7Bi_7]^{4-}$ and $[Ln@Sn_4Bi_9]^{4-}$ (Ln = La, Ce).[5,6]

Results

Our current investigations have again extended this field by transferring our so far approach to the Group 13/15 elemental combinations $[GaBi_3]^{2-}$ and $[InBi_3]^{2-}$.[7] Here, we present first results of this variation (fig. 1) that indicate the subtle influence of charges, atomic radii and Lewis basicities of the involved elements.

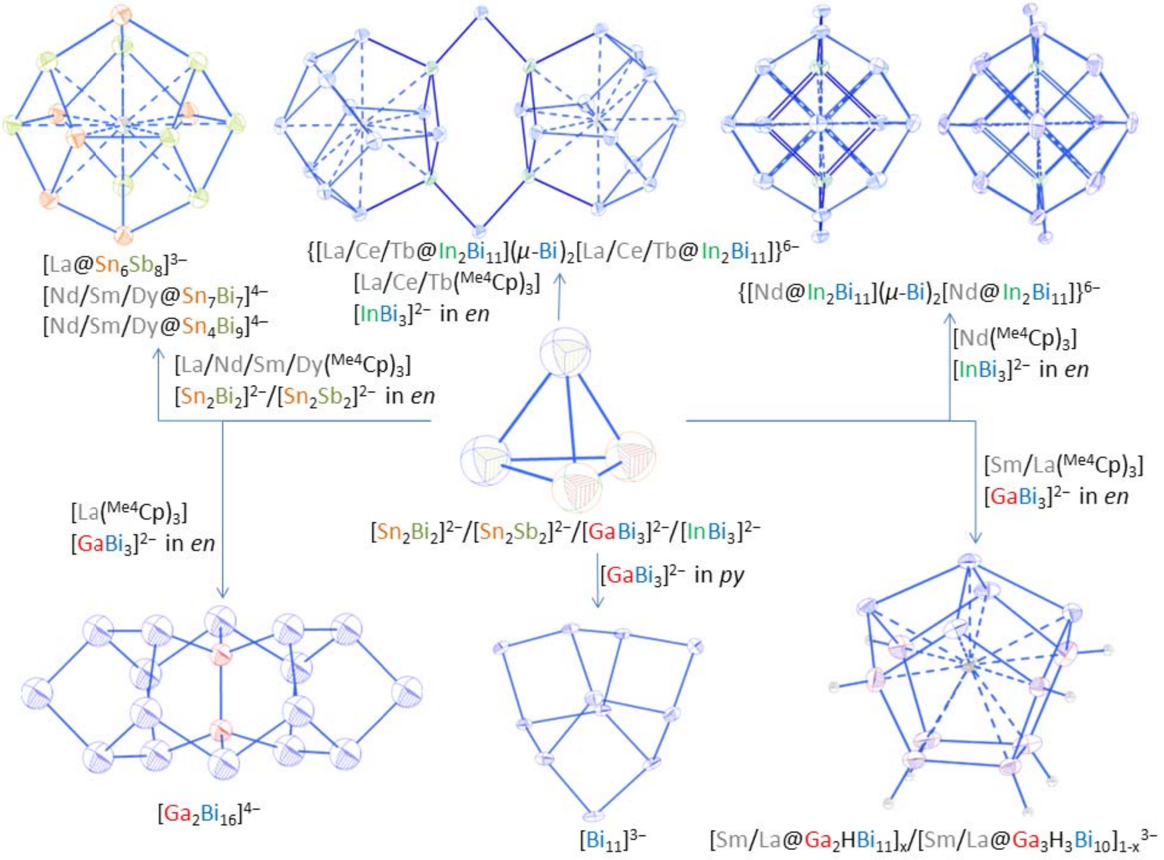

Fig.1: Reaction scheme with resulting intermetalloid clusters and Zintl anions.

We obtained clusters with novel structures and/or different charges, $\{[La/Ce/Nd@In_2Bi_{11}](\mu\text{-}Bi)_2[La/Ce/Nd@In_2Bi_{11}]\}^{6-}$ or $[La@Sn_6Sb_8]^{3-}$.[8,9] We were able to firstly synthesize protonated ternary intermetalloid clusters $[Sm@Ga_2HBi_{11}]_x/[Sm@Ga_3H_3Bi_{10}]_{1-x}{}^{3-}$,[9] which brings us closer to both directed functionalization and uncharged and therefore even better soluble species. Furthermore we could achieve bismuth rich polyanions, that were generally unknown to date – such as $[Bi_{11}]^{3-}$ and $[Ga_2Bi_{16}]^{4-}$.[9] Besides characterization of the compounds, our studies include the elucidation of formation mechanisms and electronic structures of the uncommon intermetalloid cages and their complex behavior in solution.

Conclusions

We performed ^{71}Ga, ^{1}H, ^{13}C, HSQC and HMBC nuclear magnetic resonance, mass spectrometry, infrared spectroscopy and quantum chemical investigations. We can now explain the whereabouts of the lanthanide precursor ligands, which had been unclear for a long time. Additionally, we could prove our concept of using binary Zintl anions as being an efficient approach in generating new intermetalloid clusters, and we were able to widen the field by use of Group 13/15 anions. Even anions that have been missing for long are now available via our method.

Outlook: what is planned?

We are interested in depositing our binary and ternary anions onto semiconductor surfaces via crystallization from solution or via gas phase anion deposition, for example in an electric field. Furthermore we are planning to selectively decompose our compounds to generate binary, ternary or quaternary phases and to prove their application as heterogeneous catalysts.

References

[1] T. F. Fässler, S. D. Hoffmann, *Angew. Chem. Int. Ed.* **2004**, *43*, 6242;

[2] S. Scharfe, F. Kraus, S. Stegmaier, A. Schier, T. F. Fässler, *Angew. Chem. Int. Ed.* **2011**, *50*, 3630;

[3] M. Waibel, F. Kraus, S. Scharfe, B. Wahl, T. F. Fässler, *Angew. Chem. Int. Ed.* **2010**, *49*, 6611;

[4] W. Klemm, E. Busmann, *Z. Anorg. Allg. Chem.* **1963**, *319*, 297;

[5] F. Lips, R. Clérac, S. Dehnen, *J. Am. Chem. Soc.* **2011**, *133*, 14168;

[6] F. Lips, M. Hołyńska, R. Clerac, U. Linne, I. Schellenberg, R. Pöttgen, F. Weigend, S. Dehnen, *J. Am. Chem. Soc.* **2012**, *134*, 1181;

[7] L. Xu, S. C. Sevov, *Inorg. Chem.* **2000**, *39*, 5383;

[8] B. Weinert, F. Weigend, S. Dehnen,* *Chem. Eur. J.* **2012**, *18*, 13589–13595;

[9] B. Weinert, F. Müller, K. Harms, R. Clerac, S. Dehnen, 2014, *submitted*;

[10] B. Weinert, A.R. Eulenstein, R. Ababei, S. Dehnen, *Angew. Chem.* 2014, *126*, 4792-4797; *Angew. Chem. Int. Ed.* 2014, *53*, 4704-4708.

Optical properties of organotin sulfide clusters

Project B4: Nils Rosemann and Sangam Chatterjee

Optics & Laser Spectroscopy Group – Faculty of Physics, Philipps-Universität Marburg

Chalcogenide clusters in combination with various different ligands offer a large variety of structural and physical properties. By changing the combination of cluster and ligand, their properties can be tuned to fit the desired purpose, e.g., optimized light harvesting in organic solar cells[1].

To identify the impact of different ligands, we study a series of three different organotin sulfide clusters, based on the same core but with different functional groups. The structures are visualized in Fig.1 a-c. Structure **1** (Fig. 1a) consists of two (R^{1}Sn-Cl$_1$) fragments that are bridged by 2 μ-S ligands. The other two have a central {R^{1,3}Sn(μ-S)}$_2$ unit that is terminated by two {Au(PPh$_3$)(μ-S)} groups, these units point away from the central Sn$_2$S$_2$ ring and show a trans arrangement of Cl-Sn1-S2-Au1 in case of **2** (Fig. 1b) but a cis arrangement in **3** (Fig. 1c).

First, we studied the absorption of the clusters in crystalline phase. Already the macroscopic appearance in optical transmission microscopy reveals a different shape for each specimen. **1** forms brown crystals with clean facets, **2** forms a nearly translucent film on the soda-lime glass substrate, while **3** form colorless needles. To quantify the color impression we measure the linear absorption using a microscopy setup with reflective optics yielding a spatial resolution of below 10μm. A deuterium-arc lamp is used as light source for the UV and a tungsten halogen lamp for VIS/NIR range. For detection, a compact spectrometer equipped with a Si-photodiode array is used. The absorption of all structures is summarized in Fig. 1a. A distinct broad-band absorption is found for **1**, while the other two structures exhibit a more step like absorption towards 400nm. Additionally, all samples display a pronounced absorption peak in the NIR-range. The signatures are centered at 960, 970, and 995nm for **1**, **2**, and **3**, respectively.

The complexity of the structure as revealed by X-ray diffraction[2] infers a high potential for a non-isometric response. Thus, we investigated the polarization dependence of the absorption. Especially **1** shows a strong polarization dependence of the absorption, cf. Fig. 2. Next, we corroborate these findings by investigating the clusters in solution. The measurements are performed using a Cary 300 UV/VIS spectrometer in the 200-800nm

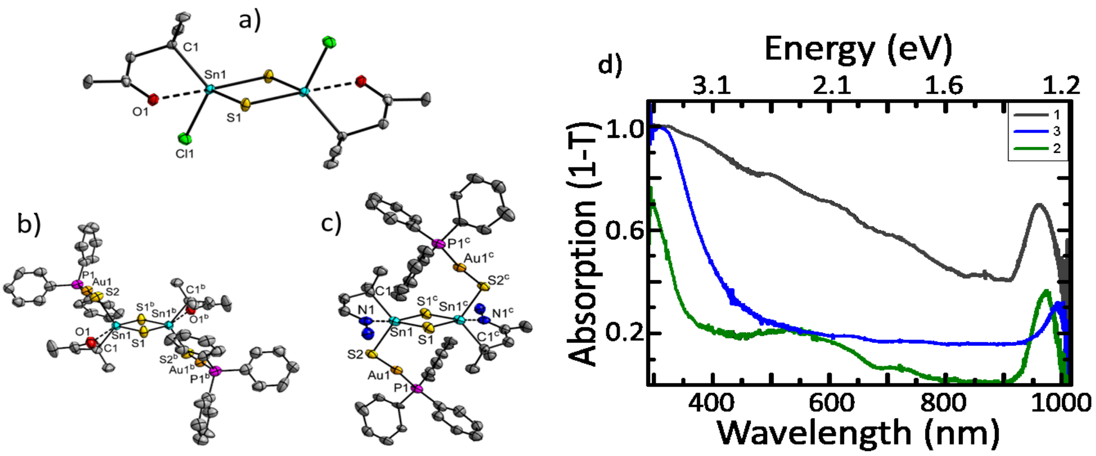

Figure 1: *Conformation of **1** (a), **2** (b) and **3** (c). Absorption spectra of all structures in solid state phase (d).*

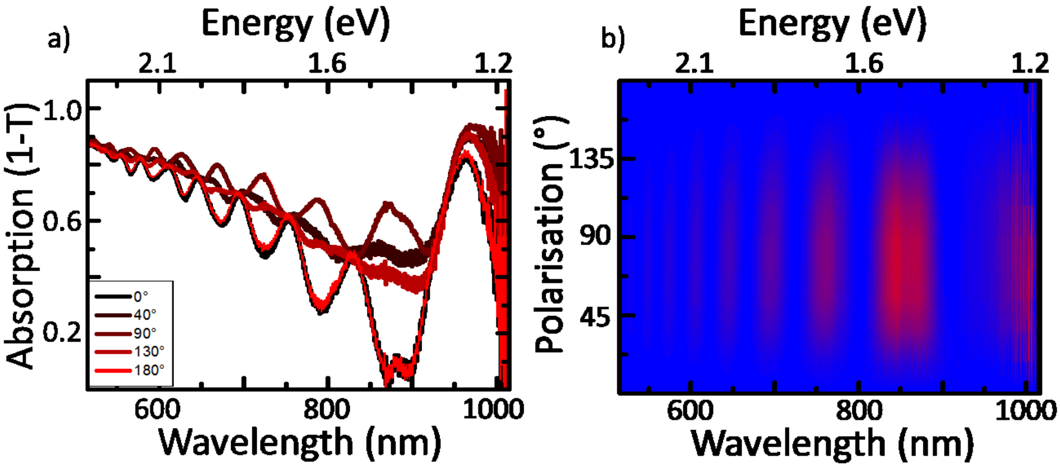

Figure 2: *Polarization-dependent absorption spectra of* ***1****-crystallites (a). False-color plot of the change in absorption (b).*

range. The solvent dichloromethane (DCM) limits the spectrum to 235nm. The absorbance of all the structures is shown in Fig. 3a. All specimen exhibit absorption below 380nm. For high concentrations, additional strong and narrow peaks are found below 260nm.

Additionally, we perform a concentration dependence series to identify possible agglomerations effects. Exemplarily data for **1** are given in Fig. 3b. The integrated absorbance at different wavelength starts to level out for larger concentrations. This indicates that the absorbance is indeed affected by agglomeration effects; otherwise it would depend linear on the concentration.

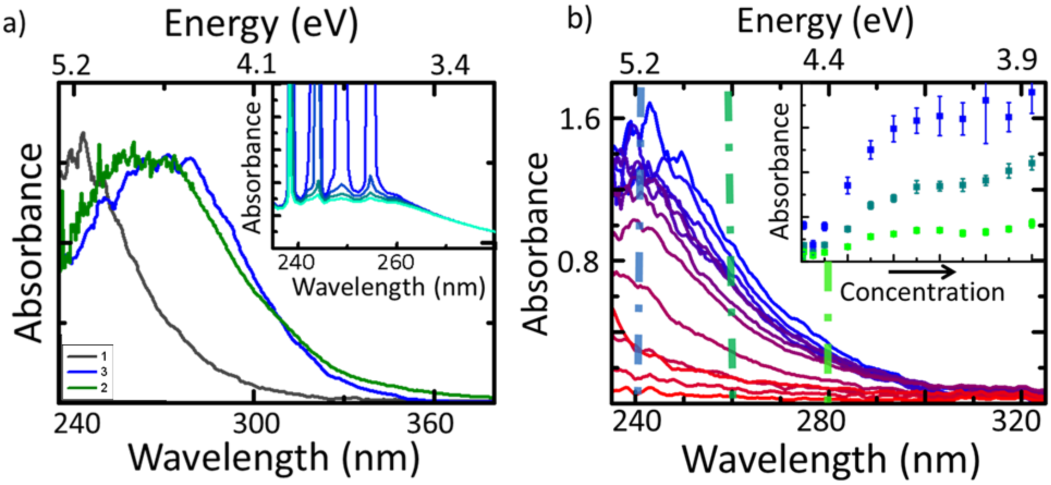

Figure 3: *Normalized absorption spectra of all structures in solution (a) Spectra for high concentration of* ***1*** *(inset of a). Absorption spectra of* ***1*** *in solution for different concentrations (b). Integrated absorbance at the wavelength indicated by dash-dotted lines (inset of b).*

[1] Kershaw S.V., et al.; Chem. Soc. Rev, 2013, **42**, 3033-3087

[2] Eußner, J. P., et al.*;* Chem. Eur. J., 2013, **19,** 13792-13802

Nanoparticles: Synthesis and Conjugation for the Bio-Applications

Abuelmagd M. Abdelmonem, Beatriz Pelaz, Wolfgang J. Parak
Fachbereich Physik, Philipps-Universität Marburg, Marburg, Germany
a_almagd@yahoo.com

Introduction

Increased fast growing interest has been paid to the synthesis and characterization of the different types of the nanomaterials both organic and inorganic (magnetic, flouescent and plasmonic nanoparticles) due to their unique physicochemical properties and their promising industrial, environmental and biological applications[1-6].

The major task of the current work has been focused on the synthesis, bioconjugation and characterization of different types of nanoparticles aiming to designing of multifunctional nanomaterials for bio-applications.

Results

Different types of water soluble nanoparticles of various surface modifications and high colloidal stability have been successively prepared and next are few examples:

- Magnetic nanoparticles e.g. Iron oxide, $CoPt_3$ and FePt nanoparticles
- Quantum dots, e.g. CdSe, CdS, CdSe/ZnS core shel QDs and ZnO nanocrystals
- Plasmonic nanoparticles e.g. AuNPs

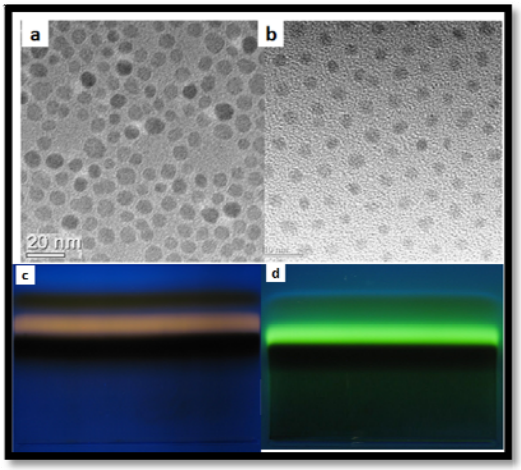

Fig.1: TEM images of iron oxide (a) and FePt (b) nanoparticles, gel electrophoresis images of water soluble polymer coated iron oxide nanoparticles functionalized with rhodamine (c) and Dy-495 (d)

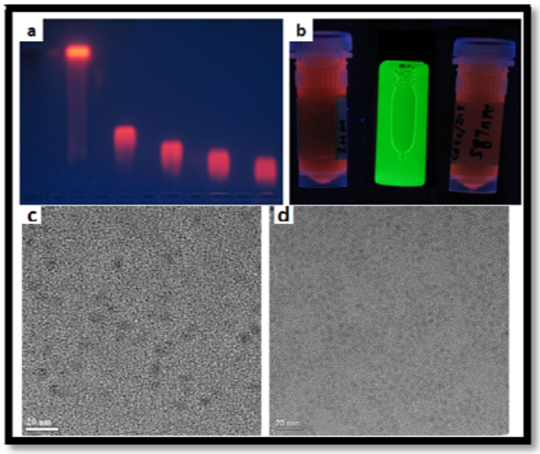

Fig.2: a) gel electrophoresis image of polymer coated red luminescent CdSe/ZnS QDs modified with different ratios of 2 kD diamine PEG, b) images of water soluble CdSe/ZnS, c) and d are TEM images of the polymer coated QDs

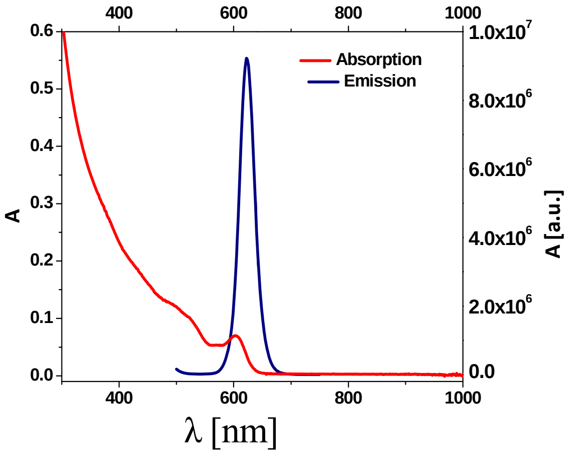

Fig.: Absorption emission spectra of the water soluble polymer coated red CdSe/ZnS QDs.

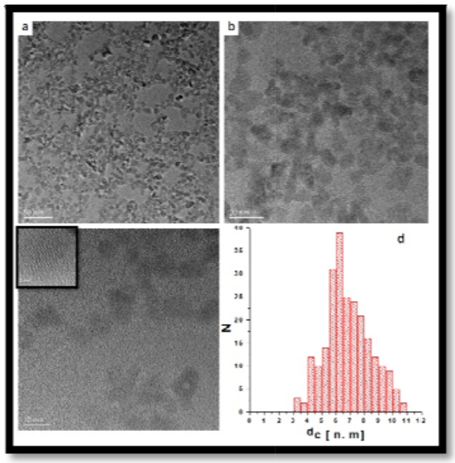

Fig.4: TEM images and size distribution histogram of the arginine capped ZnO nanocrystals. The average core diameter (dc)= 6.8± 1.9 nm

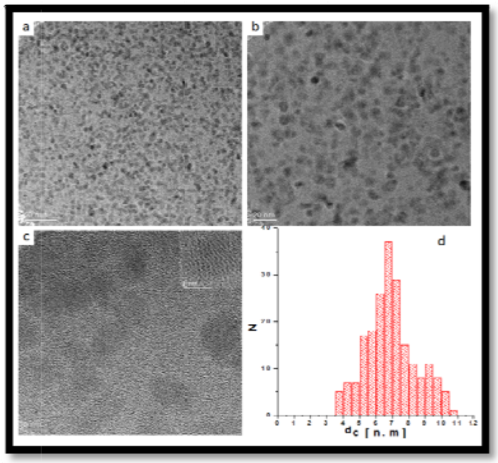

Fig.5: TEM images and size distribution histogram of the polymer coated ZnO nanocystals. The average core diameter (dc)= 6.7± 1.5 nm

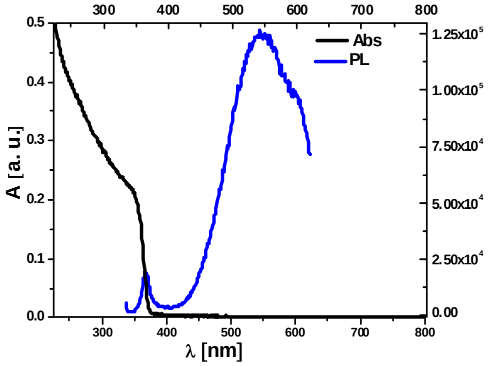

Fig.6: Absorption emission spectra of the positively charged (arginine capped) ZnO nanocrystals showing two fluorescence band one in the UV region with intensity max at 365nm and the other one in the visible region with intensity max at 521 nm. Excitation Wavelength is 335nm

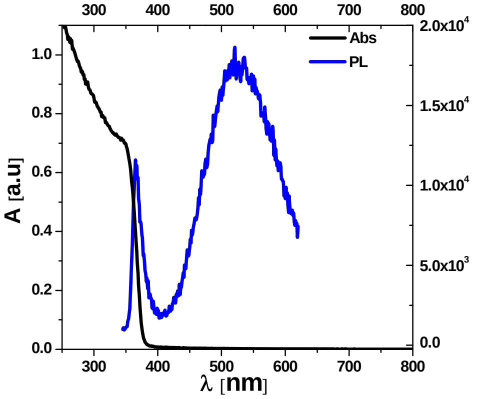

Fig.7: Absorption emission spectra of the polymer coated ZnO nanocrystals showing two fluorescence band one in the UV region with intensity max at 364nm and the other one in the visible region with intensity max at 543 nm. Excitation Wavelength is 325nm

Conclusions

Water soluble monodisperse nanoparticles with a high colloidal stability and different surface chemistry were obtained which might be of great importance for the biological applications.

Outlook: what is planned

Further studies are required to investigate the toxicological and environmental impact of some of the obtained nanoparticles especially the ZnO nanoparticles of different surface modifications (positively and negatively charged nanoparticles).

References

1. Dowling, A. P.,. *Nano Today* **2004,** 7, (12), 30-35.
2. Resch-Genger, U.; Grabolle, M.; Cavaliere-Jaricot, S.; Nitschke, R.; Nann, T.,. *NATURE METHODS* **2008,** 5, (9), 763-775.
3. Gao, R.; Liang, Z.; Tian, J.; Zhang, Q.; Wang, L.; Cao, G., NANO ENERGY 2013, 2, (1), 40-48.
4. Rasmussen, J.; Martinez, E.; Louka, P.; Wingettt, D., EXPERT OPINION ON DRUG DELIVERY 7, (2010), 1063-1077.
5. Prasanth, R.; Gopinath, D., APPLIED PHYSICS LETTERS, 102 (2013).
6. Tang, X.; Choo, E.; Li, L.; Ding, J.; Xue, J., LANGMUIR, 25 (2009), 5271-5275.

Mn doped CdS, CdS/ZnS Nanoparticles Synthesis and characterization

N. Sabir, P. del Pino, W. J. Parak

Philipps-University of Marburg, Renthof 7, 35037 Marburg, Germany

Over the last decade, Magnetic doped nanoparticles have gained increasingly more attention by researchers. These nanoparticles exhibit very unique and useful properties, enabling applications in fields such as biomedical diagnosis, solar cells, spintronics, light emitting diodes(LED) etc. Large Zeeman effects have been demonstrated in Mn-doped ZnS, ZnSe, and CdSe nanocrystals due to the presence of just few Mn^{2+} ions inside the nanocrystals.[1-9] Synthesis and characterization of Mn-doped CdS/ZnS core/shell nanocrystals [Fig.1,2], using a slightly modified method described previously by Yang et al., are discussed. [10]

References

[1] M. Shim, C. Wang, D. J. Norris, P. Guyot-Sionnest, MRS Bull.2001, 1005.
[2] J. D. Bryan, D. R. Gamelin, Prog. Inorg. Chem. 2005, 54, 47.
[3] D. J. Norris, A. L. Efros, S. C. Erwin, Science 2008, 319, 1776.
[4] D. Magana, S. C. Perera, A. G. Harter, N. S. Dalal, G. F. Strouse, J. Am. Chem. Soc. 2006, 128,2931.
[5] N. Pradhan, D. Goorskey, J. Thessing, X. Peng, J. Am. Chem.Soc. 2005, 127, 17586.
[6] D. J. Norris, N. Yao, F. T. Charnock, T. A. Kennedy, Nano Lett.2001, 1, 3.
[7] A. Nag, S. Chakraborty, D. D. Sarma, J. Am. Chem. Soc. 2008,130, 10605.
[8] S. E. Irvine, T. Staudt, E. Rittweger, J. Engelhardt, S. W. Hell, Angew. Chem. 2008, 120, 2725; Angew. Chem. Int. Ed. 2008, 47, 2685.
[9] Y. A. Yang, O. Chen, A. Angerhofer, Y. C. Cao, Chem. Eur. J.2009, 15, 1386.
[10] Yang et. al., *J. Am. Chem. Soc*; 2008, *130* (46), Pages: 15649–15661

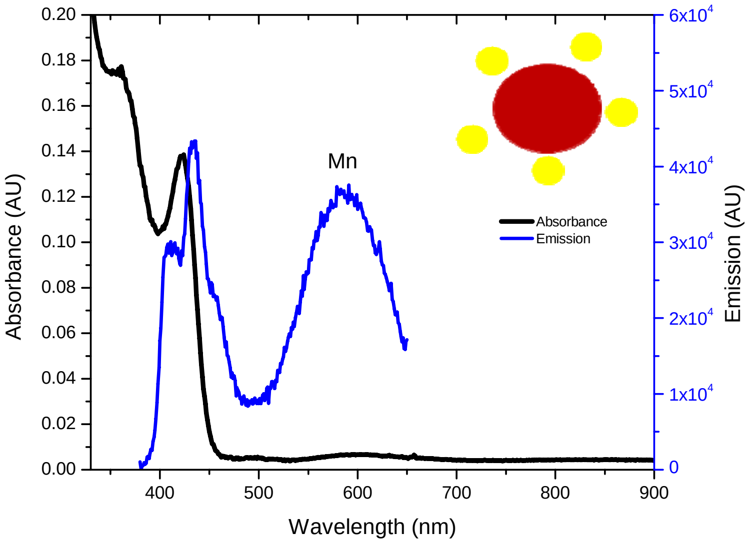

Figure 1a. Scheme1 : Uv-vis absorbance/emission spectra of Mn-CdS NPs

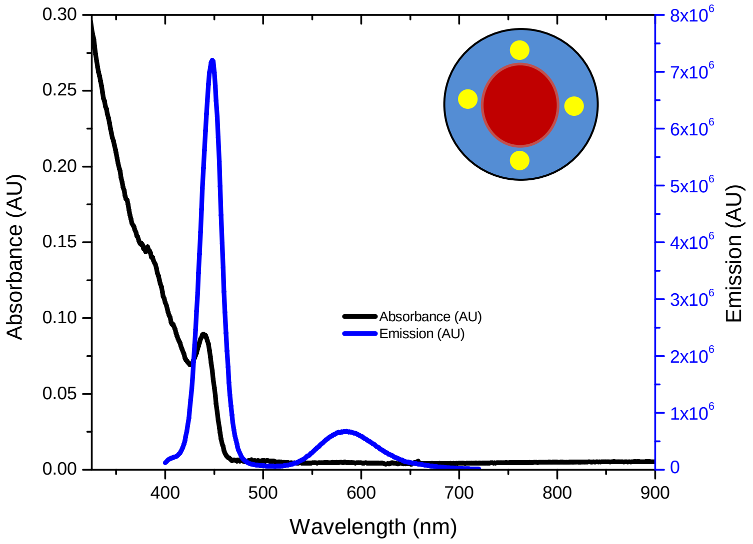

Figure 1b. Scheme2 : Uv-vis absorbance/emission spectra of CdS/Mn-ZnS NPs

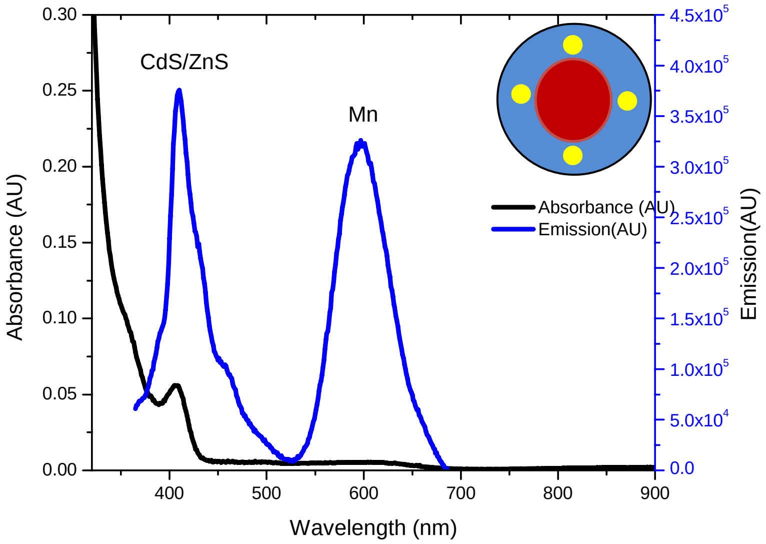

Figure 1c. Scheme3 : Uv-vis absorbance/emission spectra of CdS/Mn-ZnS NPs

Mn doped semiconductor quantum dots for time resolved multiplex sensing

U. Kaiser[1], R. Malinowski[1], M. Wilhelm[1], D. Jimenez de Aberasturi[2], N. Sabir[1],
C. Carrillo-Carrion[1], P. Del Pino[2], W. J. Parak[1], and W. Heimbrodt[1]

[1]*Department of Physics, Philipps University Marburg, Renthof 5, 35032 Marburg, Germany*
[2]*CIC Biomagune, Paseo de Miramon 182, 20009, Donostia – San Sebastian, Spain*

Introduction

Quantitative analysis of different analytes in a solution simultaneously is a very demanding topic for bio analytic applications. There is still a strong restriction of so called multiplex sensing with optical methods. Due to the broad luminescence bands of the used dye sensor molecules there is a limitation to simultaneously detection to only a few molecules at a time. With time dependent measurements of the dye molecules photoluminescence (PL) we want to overcome this obstacle. The basic idea is, to use dye sensors with the same spectral information, but with significant different time behavior of the PL. To obtain these different time characteristics we want to use Mn doped semiconductor quantum dots (QDs).

Results

In a first step we started with two model systems to proof the potential of time resolved multiplexing itself. On the one hand we synthesized gold nanoparticles (AuNPs) with an amphiphilic polymer shell. In the polymer shell of these AuNPs we embedded dye molecules (ATTO-590) with a PL maximum at 620 nm. To create our modified dye sensor we coupled the same molecules to the polymer shell of colloidal CdSe/ZnS QDs, yielding a luminescence maximum at the same spectral position as the ones bound to the AuNPs. In Fig.1 the transients of the individual samples are depicted, dye bound to AuNPs, CdSe/ZnS QDs and dye bound to the QDs. The dye molecules bound to the AuNPs show a mono-exponential decay behavior with a decay constant of 4.5 ns (red circles in Fig.1). The PL of the semiconductor QDs (black squares) on the other hand shows a typical bi-exponential decay with a long lifetime of 134 ns. The decay characteristics of the QDs are determined by a radiative transition and an energetically lower trap state.[1] The dye molecules bound to the CdSe/ZnS QDs (blue triangles) exhibit a decay behavior which is determined by the radiative lifetime of the isolated dye and the decay characteristics of the QD. This is due to the energy transfer from the QD to the dye molecules coupled to the shell of the CdSe/ZnS QD. The knowledge of the decay constants of the dye bound to AuNPs and QDs respectively leads to a unique determination of the mixing ratio of both dye types.[2]

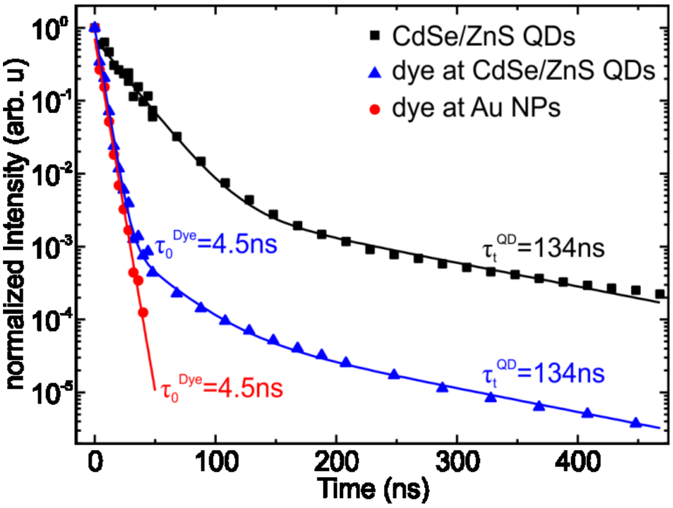

Fig.1: Measured PL decay for CdSe/ZnS quantum dots, dye bound to AuNPs, and dye bound to CdSe/ZnS QDs with respective fitting curves.

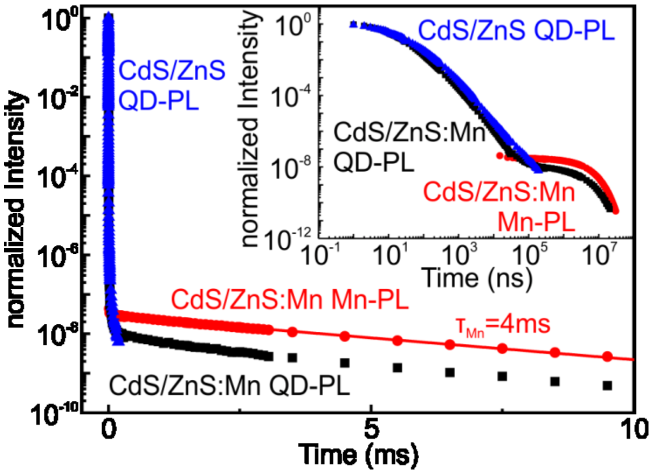

Fig.2: Decay of the PL for Mn doped and undoped CdS/ZnS QDs. The red line gives a mono-exponential fit for the Mn luminescence. The inset shows the same experimental data in a log-log-plot.

In a next step we synthesized CdS/ZnS QDs with a Mn doped ZnS shell.[3] The incorporated Mn leads to luminescence band around 580 nm. In Fig.2 the decay characteristics of Mn doped and undoped CdS/ZnS QDs are depicted. The PL of the undoped dots decays within a few microseconds following a power-law dependence (blue triangles). For Mn doped QDs the luminescence shows a significant change of the decay behavior. The Mn PL follows a mono-exponential decay with a lifetime of 4 ms (red circles). Interestingly, for the doped QDs the decay of the CdS core shows a slow mono-exponential decay as well (black squares). This indicates a transfer mechanism from the Mn states to the energetically higher QD states, probably via multi-step excitation. On the other hand, for short times after excitation the decay of the QD seems to be faster in the presence of Mn ions as well. This result indicates a donator and an acceptor like behavior of the Mn states. To test the Mn doped QDs for temporal multiplexing we attached different dye molecules, varying the spectral overlap of the Mn luminescence and the dye absorption, respectively. We not only observe a long lifetime of the dye luminescence due to the energy transfer from the Mn, but we are also able to tune the exact decay time of the dye between 0.7 and 2.1 ms.

Conclusion

Doping of the QDs with Mn atoms, which exhibit a long lifetime of the PL, gives us a tool at hand to yield dye molecules with a luminescence lifetime in the millisecond range. These dye molecules therefore are able to extend the previously investigated time resolved multiplexing system with two dye molecules even further.

Outlook

For future applications we want to extend this method to ion sensitive dye molecules. Therefore we want to couple different ion sensitive dye molecules to doped and undoped QDs. Additionally further investigations are needed on the Mn doped CdS/ZnS QDs to gain a better understanding of the energetic levels and the energy transfer pathways in these quantum dots.

---

[1] A. Efros *et al.*, Physical Review B **54**, 4843 (1996)
[2] U. Kaiser *et al.*, Journal of Applied Physics **104**, 041901 (2014)
[3] Y. Yang *et al.*, Journal of the American Chemistry Society **130**, 15649 (2008)
[4] T. Niebling *et al.*, Journal of Applied Physics **106**, 104701 (2009)

Topic area C:

Control of functionalization

Density functional study of tetrahydrofuran on Si(001)

Slimane LAREF, Ralf Tonner

Department of Chemistry, Philipps-Universität Marburg, Germany

Introduction:

Since previous decades, silicon (001) surface have drawn a great deal of attention because of their unique dimer termination [1-2]. The adsorption of organic molecules on silicon (Si) surfaces had many important properties such as improving physical and optical properties of semiconductor devices [1]. The well-known surface dimers on reconstructed Si(001) are highly reactive which leads in general to multiple adsorption sites and reaction pathways. Recently, experimenttal colleagues found motivating results [3], showing that tetrahydrofuran (THF) molecules exhibit a peculiar reactivity with the Si-dimer on the surface. Based on this outcome, we used density functional theory to elucidate the main chemical reactions of THF on Si(001)-c(4x2). All computational investigations were carried out within the Vienna *ab initio* simulation package (VASP) [4] with the exchange-correlation functional PBE [5] and semi-empirical dispersion corrections [6].

Results:

As an important first step toward optimizing experimental condition, we calculated the adsorption energies and the kinetic barriers as well as the key geometries that characterize the chemical reactions of the dissociated states. Essentially, we explored all possible adsorption geometries of THF on Si(001)-c(4×2), and we computed explicitly the most probable dissociated structures. The precursor state binds weakly on Si-dimer, on the other hand the final product shows strong chemical bonds over two adjacent dimers. Furthermore, we performed calculations of energy barriers for the key chemical processes of THF molecules on Si surface, and it turns out that the dissociation is barrierless across two Si-dimer rows (Fig. 1).

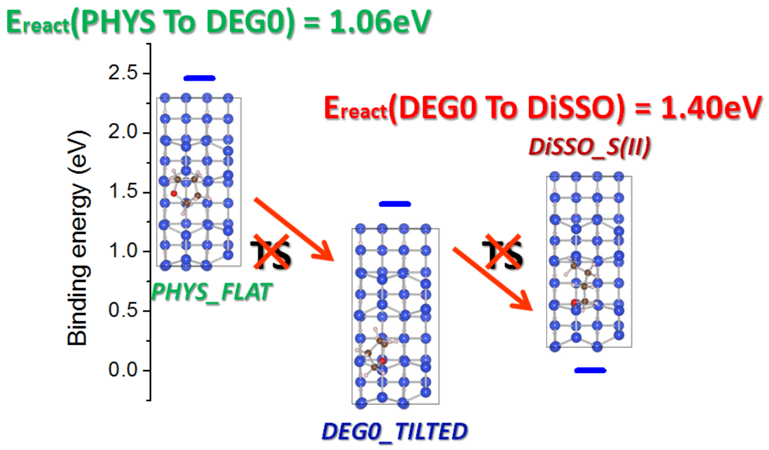

Fig. 1. *Key features of the reaction mechanism of THF molecule on Si(001)-c(4×2).*

Conclusions and perspective:

A notable conclusion of this study is that the dissociation of the THF molecule exhibits a very low energy barrier across two dimer rows. These theoretical studies are consistent with the experimental finding. In order to gain further insights into the chemical mechanism, we are currently simulating XPS spectra, and analyze the bonding situations via the newly implemented energy decomposition analysis (EDA) and natural bond orbital (NBO) for extended systems to understand the electronic interactions which are the main clue of the unique character of this system.

References:

[1] J. T. Yates, Science **279**, 335 (1998).
[2] R. A. Wolkow, Annu. Rev. Phys. Chem. **50**, 413 (1999).
[3] G. Mette, M. Reutzel, R. Bartholomäus, S. Laref, R. Tonner, M. Dürr, U. Koert, and U. Höfer, submitted.
[4] G. Kresse, J. Furthmüller Comput. Mater. Sci. **6**, 15 (1996), and Phys. Rev. B **54**, 11169 (1996).
[5] J. P. Perdew, K. Burke, M. Ernzerhof Phys. Rev. Lett. **77**, 3865 (1996).
[6] S. Grimme, J. Antony, S. Ehrlich, H. Krieg, J. Chem. Phys. **132**, 154104 (2010), and S. Grimme, S. Ehrlich, L. Goerigk J. Comp. Chem. **32**, 1456 (2011).

Quantum chemical investigations on the temperature-dependent hydrogen coverage of Si(001) under MOVPE conditions and electronic properties of III/V-semiconductors

Phil Rosenow, Ralf Tonner

Faculty of Chemistry and Material Science Center, Philipps-Universität Marburg

Introduction

Two aspects of the topical complex “III/V-semiconductor laser devices on silicon” are in the focus of this work. One is gaining an understanding on the chemical processes in metal organic vapor phase epitaxy (MOVPE) on an atomistic level. As a prerequisite, the dependence of hydrogen coverage of Si(001) on temperature has been studied for a thermodynamic equilibrium under MOVPE conditions. Surprisingly, research on this is scarce in the literature. While the interaction of a silicon surface and hydrogen has been studied extensively, the focus has mostly been on dynamic questions regarding the mechanism of hydrogen adsorption and desorption. Experimental studies on the desorption temperature have mostly been carried out under UHV conditions (e.g. TPD experiments). In a recent study, *in situ* reflectance anisotropy spectroscopy (RAS) has been employed under MOVPE conditions.[1] This can be used for comparison of computational results.

The second aspect is the electronic structure of III/V-semiconductor materials used in the construction of multi quantum well superstructures. The results of this study will be used in the group of S. W. Koch in order to compute optical properties of these systems. Since a certain numerical accuracy is required, suitable methods must be used. In order to model multinary systems, a unit cell with 64 atoms has been constructed as a compromise between freedom in choosing the composition and feasibility. The hybrid functional HSE06 and the meta-GGA functional MBJLDA have been proven rather accurate in tests with GaAs. Both can be adjusted to reproduce certain values (e.g. the band gap), if necessary. The popular GW method yields good results for GaAs as well, but is too computationally expensive for the bigger mixed system.

All calculations are carried out using the VASP code, which employs density functional theory with periodic boundary conditions and a plane wave basis set in conjunction with the projector augmented wave method.

Results

The thermodynamic properties of the silicon surface in different states of hydrogenation have been studied with several approaches. In a first approximation, surface phonons are assumed to compensate for different coverages and are thus neglected (*ab initio* thermodynamics, AITD). In the next steps, surface phonons are computed explicitly for intermediate coverage structures or interpolated from fully and non-covered structures. The two latter approaches yield results that only differ in details while providing a shift to higher desorption temperatures compared to the AITD approach. The desorption temperature is in good agreement with experiment when phonons are included. An immediate complete desorption without any intermediate coverages is predicted unless conformational entropy is taken into account.

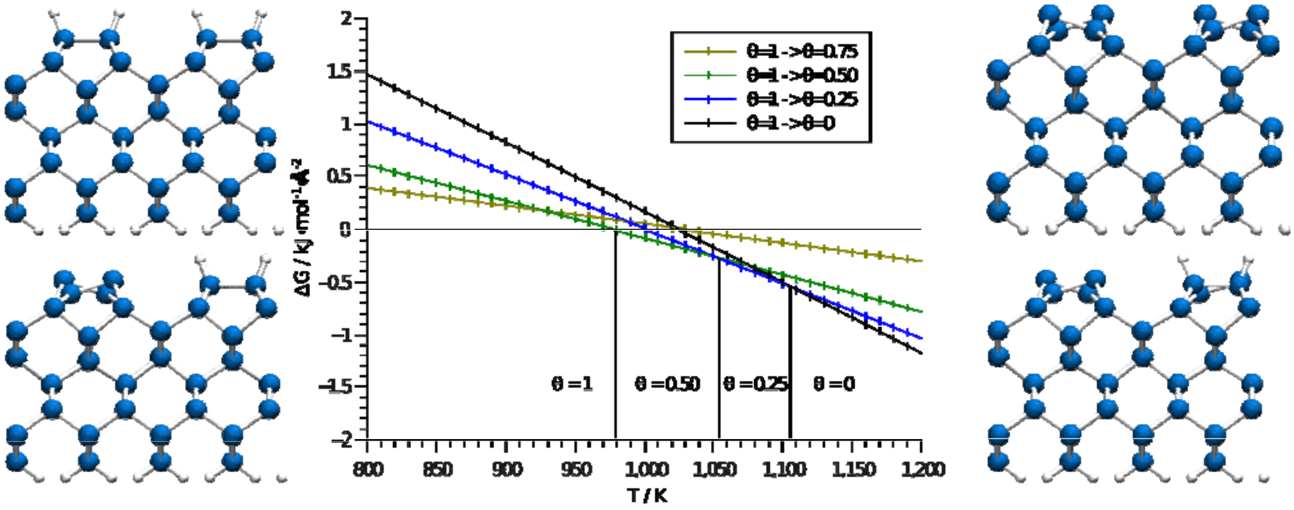

The computation of band structures for multinary III/V-semiconductor model systems with the required accuracy is still being worked on. The requirements in computational power and memory are the bottleneck that needs to be overcome. The choice of method has been based on the reproduction of the experimental band gap from a theoretically optimized structure.

Computed band gaps of GaAs in eV.

PBE	HSE06	optHSE	MBJLDA	MBJLDA$_{bgfit}$	Exp.
0.33	1.14	1.52	1.33	1.52	1.52

The HSE functional can be adapted to reproduce the experimental band gap by varying the amount of Hartree-Fock exchange and the range separation parameter (optHSE). This generally leads to good overall results. The MBJLDA functional contains a parameter that can likewise be varied (MBJLDA$_{bgfit}$). While this gives exactly the experimental band gap, the agreement of the carrier effective masses deteriorates in this procedure.

Conclusions and Outlook

From the thermodynamics calculations and in agreement with reported experimental observations it can be concluded that the Si(001) surface is (mostly) hydrogenated in a hydrogen atmosphere at typical MOVPE pressures for temperatures below approximately 950 K. At higher temperatures desorption will occur and lead to the clean Si(001)(4x2) surface around 1100 K. This allows to study adsorption reactions in the MOVPE process in a theoretically consistent manner, that reproduces experimentally observed conditions. In order to augment the thermodynamical studies, the effect of steps on the equilibrium properties could be included.

As for the band structure topic, the computational bottleneck still needs to be overcome. Once this has happened, band structures of various model systems can be computed and used in the computation of optical properties. The Ga(NAsP) model cell presented has been chosen such that it yields the lowest energy of some possible permutations of the guest atoms.

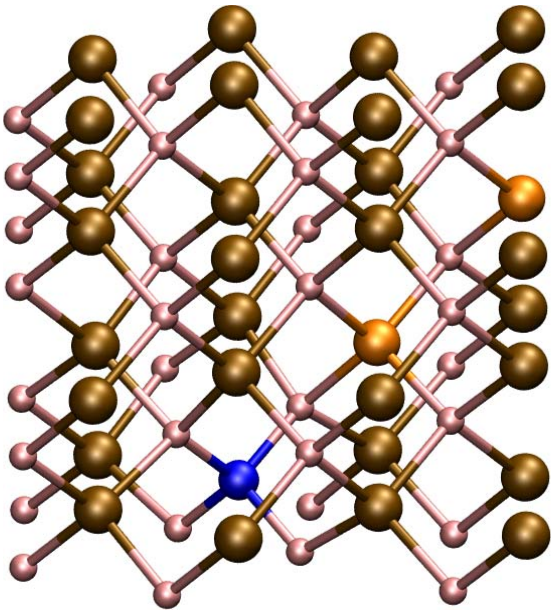

References

[1] Brückner *et al.*, *Appl. Phys. Lett.* **2011**, *98*, 211909.

Quantum Chemical Investigation of MOVPE Growth Processes of Galliumphosphide on Si(001)

Andreas Stegmüller and Ralf Tonner

Department of Chemistry, Philipps-Universität Marburg

Introduction

Mixed semiconductor materials from group 13 and 15 elements are developed and fabricated in a metal-organic vapour phase epitaxy (MOVPE) from single molecular precursors. The growth behaviour determines the material's structural composition and quality. It is hence crucial to optimize the growth conditions and intrinsic processes in order to achieve the integration of optically active materials onto silicon-based electronic devices. Elementary steps occurring in the reactor at different growth phases (see Fig. 1) are investigated within this project and preliminary results are presented in the following.

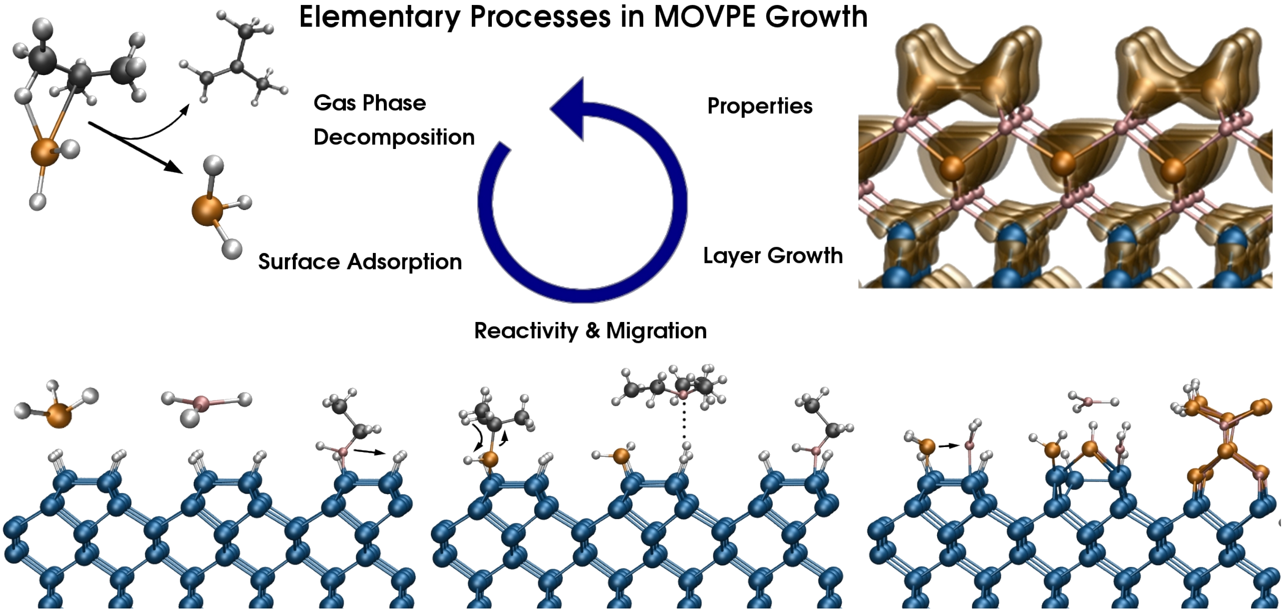

Fig.1: Schematic view of GaP/Si(001) MOVPE growth phases accessible to theoretical investigations including gas phase processes (1), surface adsorption (2) and reactivity (3), layer growth (4) and crystal properties (5).

Gas Phase Precursor Decomposition

Triethylgallane and *tert*-butylphosphine are carried into the low-pressure chamber in a hydrogen gas stream and flow over a heated Si substrate. A catalogue of 61 decomposition reactions was elaborated and Gibbs reaction energies (ΔG) were determined for temperatures between 450 and 675 °C on the MP2 and DFT (PBE-D3) levels of theory accompanied by CCSD(T) benchmark data.[1] The most important decomposition channels include β-hydride eliminations of the metal precursors, which exhibit favourable thermodynamics and moderate thermal barriers, and an equivalent “β-proton” elimination of *tert*-butylphosphine, which exhibits barriers about double as large as the former mechanism. Furthermore, unimolecular alkane- and H_2 eliminations as well as bimolecular decompositions assisted by the carrier gas are more likely at higher temperatures.
The mechanism of the “β-proton” elimination from group 15 alkyl molecules is not yet described in the literature and was analysed by quantum chemical tools (partial charges, canonical orbitals, energy decomposition and NOCV deformation densities). A 4-membered ring was determined as transition state structure, similar to the β-hydride mechanism with metal complexes, however, the electron flow of bond cleavage and formation is reversed. A partially positive H atom (H_{tr}) is

transferred from the β-position to the central pnictogen (atom E), where a covalent bond is being formed by the partially occupied H_{tr}-1s-orbital and the E-lonepair (comp. Fig. 2).

As the rate-deteriming step of the “β-proton” elimination of group 15 alkyl compounds is, in contrast to metal β-hydride mechanisms, the stretch of the C_α-E bond, the reaction barrier can be optimized by the choice of the ligand. Fig. 3 presents the tendency for electro-positive α-positions to exhibit lower electronic barriers.

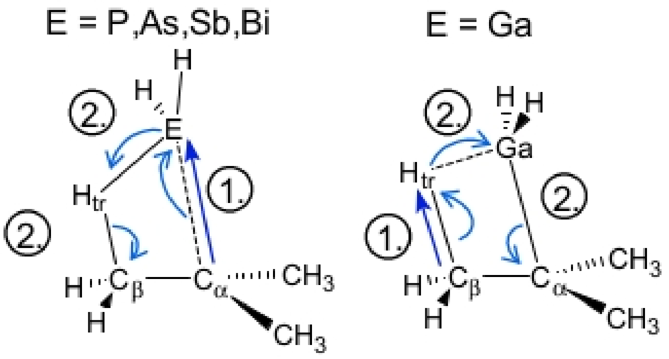

Fig.2: Schematic of reaction events in chronological order and electron flow for the β-H (H_{tr}) elimination for different mono-tert-butyl compounds of E.

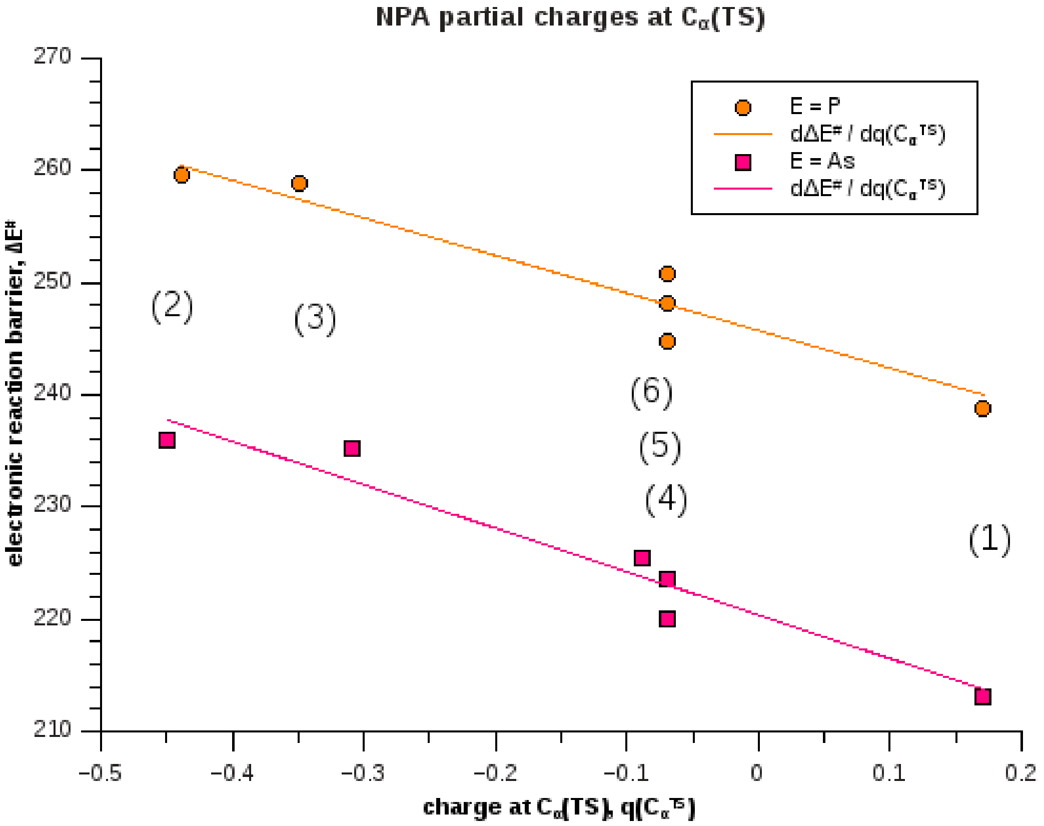

Fig.3: Electronic barriers [kJ mol^{-1}](PBE/TZ) of the above reaction for phosphines and arsines with different butyl ligands (1-6) in correlation with the partial charge of C_α at the transition state.

Surface Adatom Diffusion

Assuming complete precursor decomposition in the gas phase or early adsorption phase, surface diffusion barriers were investigated for individual adatom species. By DFT (PBE-D3) calculations of periodic slab supercell models of the bare Si(001) substrate with an *ideal* diamond-structure surface, the Ga and Si atoms were found to be significantly less hindered than the P atom. This as well holds true for a model cell with either Ga- or P-terminated GaP on top of Si in the same lattice. As a more realistic description of the interactions require the reconstruction of the surface as well as the inclusion of further influences – e.g. hydrogen passivation and reactivity – the origin of the decreased mobility of P adatoms on the semiconductor diamond lattice is still object of discussion. The electronic structure of the unreconstructed surface is complex and chemically activated. The transition states of the diffusion hops were analysed by partial charges and electron densities, however, a correlation with the height of the barriers could not yet be drawn.

Interface Formation and Chemical Properties

During growth at elevated temperatures the surface atoms of a MOVPE substrate are activated and may interact with each other and adsorbate species. Assuming an (ad-) atom mobility based on surface diffusion data presented above, atoms can change place, which may lead to a structural reorganization at the GaP/Si interface (a growth effect)[2]. The interface is not limited to the {001} facet any more but (re-) shapes towards thermodynamic minima controlled by kinetic growth arguments. The energetically most favourable *ideal* (i.e. along the constructed crystal planes) GaP/Si interfaces are Ga-terminated ones at {112} as identified by DFT calculations. GaP/Si(001) is stabilised in a reconstruction with one layer intermixing (i.e. adjacent Ga and Si within the interface atomic layer)[3]. Partial charges were determined by a projection of the periodic wavefunction of the interface structure onto a set of atom-centered functions and utilised to discuss the chemical environment of the interface atoms and the origin of observed stabilities.

References

[1] A. Stegmüller, P. Rosenow, R. Tonner, Phys. Chem. Chem. Phys., 2014, doi: 10.1039/C4CP01584C.
[2] Experimental observation by A. Beyer, K. Werner, K. Volz (2014); kinetic Monte Carlo simulation by J.-O. Oelerich, S. Baranovski (2014).
[3] W. A. Harrison, Surf. Sci., 1976, 55, 1-19.

Marburg, July 17th, 2014.

Breaking the O-C Bond: Reaction of Diethylether on Si(001)

Marcel Reutzel[1], Gerson Mette[1], Michael Dürr[1,2], Ulrich Koert[3], and Ulrich Höfer[1]

[1]*Fachbereich Physik und Zentrum für Materialwissenschaften, Philipps-Universität, D-35032 Marburg*
[2]*Institut für Angewandte Physik, Justus-Liebig-Universität Giessen, D-35392 Giessen, Germany*
[3]*Fachbereich Chemie, Philipps-Universität, D-35032 Marburg*
marcel.reutzel@physik.uni-marburg.de

Introduction

A promising possibility to compete with the challenges of miniaturization in semiconductor device physics is the functionalization of inorganic semiconductor surfaces with organic molecules [1]. In this context, it is important to understand the basic adsorption mechanisms and adsorption dynamics of organic molecules on these surfaces. Within the framework of the GRK 1782 we investigate the interaction of ether molecules on Si(001). Within the first two years in the GRK 1782, we have studied the adsorption behaviour of tetrahydrofuran (THF) [2] and diethylether on Si(001).

Results

Fig. 1 (a) to (c) show the Si(001) surface after dosing 0.2 ML diethylether at room temperature. It is possible to distinguish between symmetric (S, red) and asymmetric (A, orange) adsorption configurations extending over two dimer rows. In the empty state image [Fig. 1 (b)], both configurations consist of dark and bright contributions. In the filled state image [Fig. 1 (c)], only the dark features are clearly resolved. Taking this bias dependence into account, the bright features can be attributed to dangling-bond orbitals [3,4]. The black features are assigned to saturated dangling bonds and thereby to molecular fragments of diethylether adsorbed on Si(001).

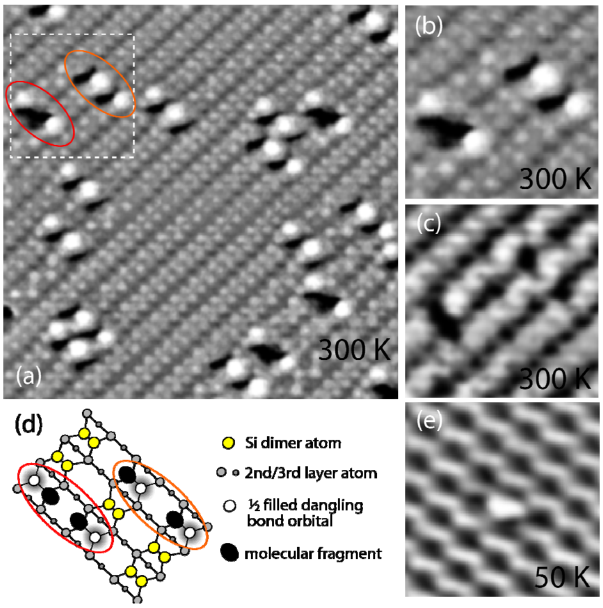

Fig. 1: *STM images of 0.02 ML diethylether on the Si(001) surface at T = 300 K (a-c) and T = 50 K (e). (a) At 300 K, the empty sate STM image (12.7x2.7 nm^2, +0.8 V, 0.5 nA) reveals symmetric (red) and asymmetric (orange) adsorption configurations across two dimer rows. (b) and (c) show empty (4.1x4.1 nm^2, +0.8 V, 0.5 nA) and filled (4.1x4.1 nm^2, -1.5 V, 0.5 nA) state blow-ups of the marked area in (a), respectively. (d) Sketch of the S and A adsorption configurations. (e) Low temperature STM (5x5 nm^2, +1.1 V, 0.3 nA) image with a coverage of 0.005 ML.*

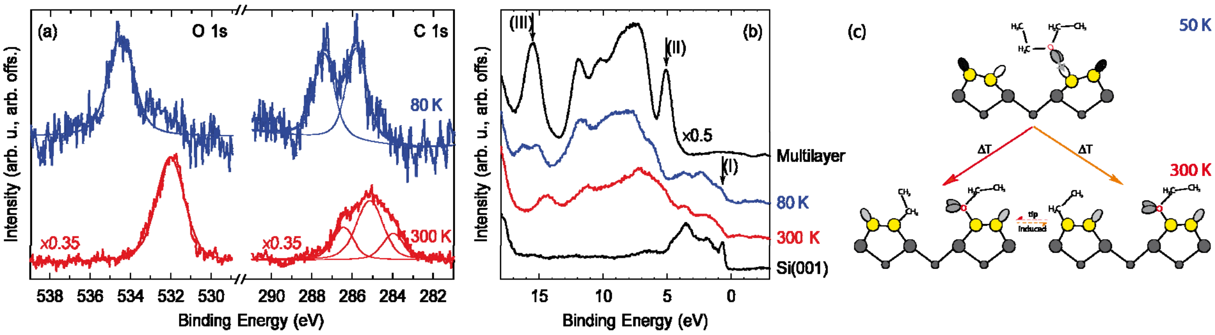

Fig. 2: *(a) Peak fitted O 1s and C 1s XPS spectra of diethylether on Si(001). All spectra were measured at liquid nitrogen temperature. The room temperature spectra were tempered to T = 300 K. (b) UPS spectra of a multilayer diethylether (black line, top), a submonolayer diethylether adsorbed at 80 K (blue) and 300 K (red) and of the clean Si(001) surface (black, bottom). (c) Ball and stick model of the adsorption pathway from the dative bonding situation at low temperature to the covalently attached room temperature configuration.*

Fig. 1 (e) shows an empty state STM image of the (4x2) reconstructed Si(001) covered by 0.005 ML diethylether after dosing at 50 K surface temperature. The zick-zack structure indicates the dimer rows with alternating buckling of the silicon-silicon dimer. The empty D_{Down} state appears bright in the empty state image. Diethylether adsorbs on-top of one silicon dimer, however, it is not possible to assign the features to the D_{Down} or the D_{up} state of the silicon-silicon dimer.

In order to learn more about the observed surface chemistry, X-ray photoelectron spectroscopy (XPS) was performed. In Fig. 2 (a), the O 1s and C 1s spectra reveal a phase transition from 80 K to 300 K.

At 80 K, the binding energy of the C 1s electrons is significantly higher than expected for covalently attached organic molecules on the Si(001) surface. Furthermore, the 1:1.1 intensity ratio of the two observed peaks is in agreement with a still intact diethylether molecule, a covalent binding situation can be excluded. The O 1s binding energy observed for a submonolayer of diethylether on Si(001) is higher than in a multilayer (not shown). The high binding energy of the O 1s electrons indicates a lower valence electron density at the oxygen atom. A dative bonding situation of the still intact diethyl ether can thus be concluded with the oxygen atom donating electron density into the Si(001) surface. At room temperature, the binding energy of the O 1s electrons is shifted towards a lower binding energy. It is in good agreement with a covalent O-Si bond [5]. A covalently attached oxygen atom requires a O-C bond cleavage. Such an ether cleavage of diethylether would result in an -O-C_2H_5 and a –C_2H_5 fragment. This is in good agreement with the room temperature C 1s spectra, which is well fitted with three peaks in a 1:2.2:0.8 intensity ratio. The three peaks can be attributed to CCO, CCH and CCSi bonds from highest to lowest binding energy and thereby to Si-O-C_2H_5 and Si-C_2H_5 adsorption configurations.

To get further information about the bonding situation, ultraviolet photoelectron spectroscopy (UPS) was performed [Fig. 2 (b)]. For the clean surface, the filled dangling-bond surface state D_{up} is clearly resolved (labeled I). For a Si(001) surface dosed with diethylether, the molecular orbitals of diethylether are resolved for binding energies E_B > 4 eV, depending on coverage and sample temperature. The UPS spectrum of a physisorbed multilayer is in good agreement with gas phase measurements [6]. At 80 K, the submonolayer spectrum is similar to the multilayer spectrum except for the highest occupied molecular orbital (HOMO, labeled II). This indicates a still intact molecule and a dative bonding situation due to the oxygen lone pair. Diethylether shows a linear molecular structure in the dative bonding situation at low temperature as well as in the dissociated form at room temperature. Therefore, only minor changes are observed between the low and the room temperature configuration in the UPS spectra [i.e. peak labelled (III)].

Conclusion and Outlook

In summary, we were able to observe a datively bonded ether molecule at low temperatures and the cleavage of an O-C bond at room temperature [Fig. 2 (c)]. These results are in perfect agreement with our former experiments on the adsorption of THF on Si(001) [2]. In future, we aim to study the adsorption kinetics from the low temperature to the room temperature configuration in more detail.

References

[1] J. T. Yates, Science, **279** (1998) 335-336.
[2] M. Reutzel, Research Summary GRK 1782, Hofheim 2013.
[3] G. Mette, C. H. Schwalb, M. Dürr, U. Höfer, Chem. Phys. Lett., **483** (2009), 209-213.
[4] M. Dürr, U. Höfer, Prog. Surf. Sci., **88** (2013), 61-101.
[5] H. N. Hwang, J. Y. Baik, K. S. An, S. S. Lee, Y. S. Kim, C. C. Hwang, B. S. Kim, J. Phys. Chem. B, **108** (2004), 8379-84.
[6] K. Kimura, Japan Scientific Press, Tokio, 1981.

Work Status for: Reaction dynamics of exemplary organic molecules on Si(001) – a molecular beam study

M. Lipponer[1], M. Dürr[1,2], and U. Höfer[1]

[1]*Fachbereich Physik, Philipps-Universität Marburg*
[2]*Institut für Angewandte Physik, Justus-Liebig-Universität Giessen*

1. Introduction

The functionalization of semiconductor surfaces by means of organic molecules is of great interest due to possible applications in the field of nanoelectronics [1]. A successful transition from a semiconductor substrate to a well ordered organic multilayer requires multifunctional molecules with a high chemoselectivity towards the semiconductor surface.

cyclooctyne (C_8H_{12}) is a highly strained cyclic molecule with a carbon-carbon triple bond that could meets these requirements. Since the sp-hybridized C-C bonds are only relaxed in a linear form, the cyclic form of the molecule leads to a very high strain within the ring. This strain gives reason to expect a high reactivity of the stiff C-C triple bond towards the silicon surface [2]. Mette et al. performed STM experiments to investigate the reactivity and the adsorption configurations on the Si(001) surface [3]. They found that the adsorption behaviour is both insensitive to (i) the surface temperature and (ii) hydrogen-distorted dangling bond configurations pointing towards a direct adsorption pathway. Especially the latter fact is more than uncommon for the adsorption of organic molecules on the Si(001) surface which usually includes an intermediate “precursor” state [1].

We thus investigated the adsorption dynamics of cyclooctyne on Si(001) by means of molecular beam techniques, second harmonic generation (SHG) and Auger spectroscopy. SHG was used to measure the cyclooctyne uptake during exposure while Auger spectroscopy was used to compare the resulting coverages after gas exposure. The experiments were performed at different surface temperatures to investigate the adsorption mechanism and dynamics.

2. Results

Before discussing the more recent results on the cyclooctyne / Si(001) surface reactions, we want to briefly summarize the studies discussed in the last research summary.

For ethylene and THF, we found that with increasing kinetic energy of the impinging molecules, the initial sticking coefficient decreases, as it is typical for a non-activated reaction channel. However, the decrease is much less pronounced in the case of THF when compared to C_2H_4/Si(001), pointing towards a more efficient energy dissipation in the former case. With increasing surface temperature, a decrease of the initial sticking coefficient is observed for both systems, which gives information on the energetics of the intermediate “precursor” states.

Figure 1 shows the temperature dependence of the initial sticking coefficients for all three different molecules. As discussed above, the temperature dependence for both ethylene and THF can be well described with an adsorption pathway via an intermediate precursor state (indirect adsorption). For cyclooctyne, a completely different behavior is observed: The sticking coefficient does not depend on the surface temperature, which confirms that the reaction proceeds via a direct reaction channel the results from the previous STM experiments, made in our group [1] (direct adsorption). Table 1 summarizes the evaluated differences in barrier heights ε_d-ε_a.

3. Conclusion

We performed molecular beam studies combined with SHG- and Auger-measurements to investigate the adsorption dynamics of cyclooctyne on Si(001). Our results clearly point towards a direct adsorption pathway, which is in agreement with previous STM investigations made in our group. The barrierless adsorption pathway of cyclooctyne via its C-C triple bond, together with its well-ordered adsorption structure at high coverage [3], makes it thus a good candidate for chemoselective adsorption and controlled growth of an inorganic/organic interface on Si(001).

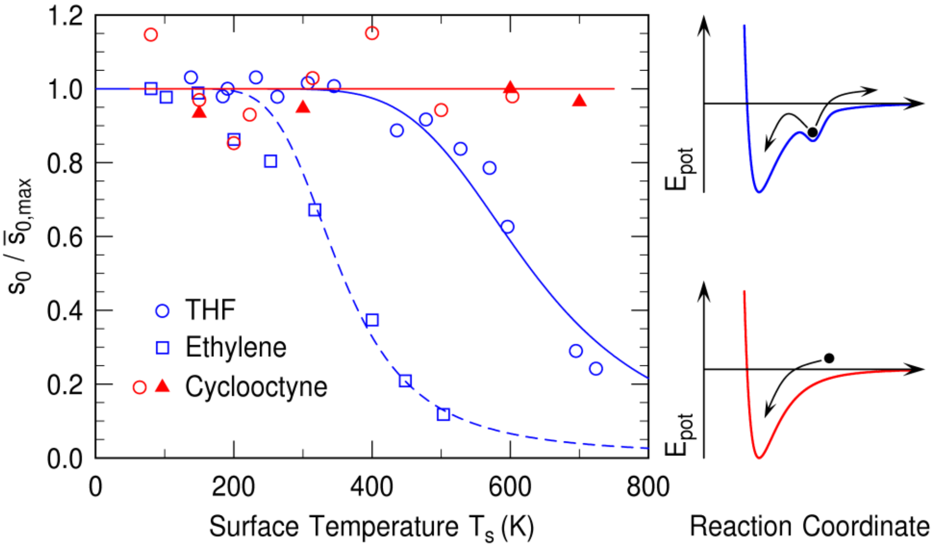

Fig 1: Normalized initial sticking coefficient s_0 of ethylene, tetrahydrofuran (THF) and cyclooctyne for different surface temperatures T_s. While the initial sticking coefficient $s_0(T_s)$ of ethylene and THF reveals an adsorption pathway via a precursor state (blue), cyclooctyne (red) shows no such behavior. Its surface reaction is independent of the surface temperature, which strongly points towards a direct adsorption pathway. Red triangles represent the resulting coverages evaluated by Auger spectroscopy after applying the same dose of cyclooctyne onto the surface. On the right side schematics for the indirect (blue) and indirect (red) adsorption pathways are shown.

Adsorbate	**Ethylene**	**THF**	**Cyclooctyne**
$\mathcal{E}_d$-$\mathcal{E}_a$ (eV)	**0.14**	**0.34**	**-**

Tab 1: Difference in barrier height within a precursor mediated adsorption pathway, evaluated with the temperature dependence of the initial sticking coefficient $s_0(T_s)$ [4]. For cyclooctyne no temperature dependence is observed, contradicting the existence of a precursor state.

4. Outlook

Right now we are investigating the adsorption dynamics of trimethylamine (TMA) on Si(001), which is an a excellent example for a Lewis acid-base reaction of an organic molecule with a semiconductor surface [5].

References

[1] Filler, Bent, Prog. Surf. Sci. 73 1 (2003)
[2] Turner, Jarrett, Goebel, and Mallon, J. Am. Chem. Soc. 95, 790 (1973)
[3] Mette, Dürr, Bartholomäus, Koert, Höfer, CPL 556 70 (2013)
[4] Lipponer, Armbrust, Dürr, Höfer, J. Chem. Phys. 136 144703 (2012)
[5] Hossain, Machida, Nagao, Yamashita, Mukai, and Yoshinobu, J. Phys. Chem. B 108, 4737 (2004)

Preparation and characterization of phosphonic acid based self-assembled monolayers on ZnO substrates

Alexandra Ostapenko, Gregor Witte

Molekulare Festkörperphysik, Philipps-Universität Marburg, Renthof 7, 35032 Marburg, Germany

Interfaces between semiconducting metal oxides and organic semiconductors have attracted considerable interest because of their applications in organic-inorganic hybrid systems such as transparent electrodes in light emitting devices or in dye-sensitized photovoltaic cells [1]. A promising way to control interfacial properties in such hybrid systems is the use of self assembled monolayers (SAMs) formed by covalently bond admolecules. Due to their ability to form robust bonds on metal oxides phosphonic acids are promising anchoring units for such SAMs or dye-molecules [2-5]. Though such modifications have already been successfully implemented in device applications, a microscopic understanding of the binding mechanism as well as the thermal and chemical stability of such molecular systems has not been achieved.

To derive a better understanding of the structure, binding strength and stability of such SAMs on metal oxides we have chosen the model system of the simplest aromatic molecule - phenylphosphonic acid (PPA, see Fig.1) linked to ZnO single crystals with different surface terminations: polar surfaces (O- and Zn- terminated) and non-polar surfaces (mixed-terminated). In contrast to widely used silanes, phosphonic acid chemisorbs on metal oxides without the formation of multilayers and form more robust films than silanes and carboxylic acid. However, these systems have been less thoroughly studied concerning the anchoring mechanisms in contrast to the commonly used thiol-based SAM's on metals such as gold or silanes coupled to silicon oxide. Moreover, the surface modification like the presence of H- or OH- groups affects the film formation [6,7]; therefore the role of hydroxylation of the various ZnO surfaces was also studied.

In contrast to most previous works that were carried out either for ZnO powder or sputtered partly mixed ZnO/ITO substrates [8,9], our approach focused on the preparation of SAMs with phosphonic anchor groups on single crystalline ZnO substrates. All surfaces were prepared by a recently introduced procedure [10] including initially Ar^+-sputtering followed by annealing in high pressure cell attached to the UHV-system allowing heating of the sample at a pure oxygen atmosphere at a pressure of 10 mbar which avoids the formation of oxygen vacancies upon heating. Subsequent SAM formation is done via immersion. To investigate the role of surface hydroxylation on the adsorbtion efficiency comparative films were prepared by organic molecular beam deposition method (OMBD) under UHV conditions. Additionally, ethanolic NaOH solution was used to modify surface with hydroxyl groups if it was needed.

To characterize the PPA films on the various ZnO substrates different experimental techniques were applied. High resolution X-ray photoelectron spectroscopy (XPS) and near edge x-ray absorption fine structure spectroscopy (NEXAFS) were performed at the HE-SGM dipole beamline of the synchrotron storage ring BESSY II in Berlin (Germany). The XPS core level intensities provide detailed information on the chemical composition and the relative surface coverage of the SAMs, while the quantitative analysis of the dichroism of the NEXAFS signal allows determining the average tilt angle of the phenyl backbone relative to the surface normal. Thermal stability of molecular films was studied by means of thermal desorption spectroscopy (TDS). Additional experiments as atomic force microscopy (AFM), low energy electron diffraction (LEED) helped us to control the substrate quality on the preparation steps.

To investigate the efficiency of the wet chemical surface hydroxylation of ZnO TDS measurements were performed at the mass of the OH-group for differently treated surfaces. Series of TDS measurements indicate, that even without NaOH dip OH- layer is formed after a few second of air exposure. Therefore, SAMs prepared via immersion (denoted as "hydroxylated"), have OH- surface termination in advance due to the sample transfer in the air. However, the fully hydroxylated surface (denoted as "NaOH modified") can be prepared only after chemical modifications (e.g. via NaOH dip).

To characterize the relative layer coverage high resolution X-ray photoelectron spectroscopy measurements were carried out. The relative coverage for differently prepared samples determined from the intensity ratios of the measured Zn 3s and P 2p XPS signals. Surprisingly, there is no clear indication that adsorption of PPA molecules occurs differently on the polar or non-polar surfaces. In spite of slightly larger PPA coverage on NaOH modified samples than on hydroxylated samples we cannot prove that –OH surface pretreatment plays significant role in the better film formation. On the contrary, UHV prepared PPA films exhibit higher amount of adsorbed molecules in a monolayer. We suggest the blocking of adsorbtion sites due to the adsorbed –OH or –H groups leads to another binding motive and therefore another packing density.

To complement the structural analysis and to characterize the orientational ordering adopted by PPA molecules, carbon edge X-ray absorption spectra were recorded. Measurements reveal nearly similar orientation for all PPA modified samples within an accuracy of +/- 5° hence indicating the presence of upright standing molecules with a tilt angle of about 87°. Hydroxilation of surface, made via NaOH dip, yields slightly but not significant smaller tilt angles. In case of ZnO-O samples, prepared by OMBD, reveal the PPA molecules ordered within a multilayer with the tilt angle of the aromatic moiety of about 75°. In turn spectra of a monolayer film exhibit similar features as films prepared by immersion.

Also the thermal stability of PPA-SAMs adsorbed on differently oriented ZnO samples had been studied. Interestingly, all PPA films of different surface termination and different film preparation exhibit an exceptional high thermal stability and reveal desorption signals only for surface temperatures above 650K. Actually two desorption peaks were observed at temperatures of $T_1 \approx 690$ K and $T_2 \approx 740$ K which are attributed to two different adsorption sites or the presence of both, bi- and tri-dentate species. By contrast multilayer of PPA (prepared by drying of PPA solution without ethanol rinsing) desorbs at the about 430 K.

In the present study we have demonstrated that well-defined PPA-monolayer films can be prepared on various single crystalline ZnO surfaces and by different preparation methods (immersion and OMBD). Surprisingly all wet chemically prepared films exhibit rather similar properties and depend only weakly on the actual surface termination: the molecules adopt an upright standing orientation with small variations of molecular tilt angle for both polar and non-polar surfaces; exhibit similar coverage; molecular films posses rather high thermal stability. Surface hydroxylation seems to change the adsorption geometry of PPA, though within the different hydroxylation degree (due to the NaOH dip, the automatically adsorbed species during the air contact or the presence of hydroxyl groups in the solvent) the properties hardly vary.

Finally we observed also an unexpected instability: After extended immersion times of several days we observed the formation of "star shaped" precipitations of crystalline needles.

EDX analysis of these structures reveal the contents zinc, phosphor, oxygen and carbon with the P:Zn ration is 1:1. Moreover they were found to by thermally extremely stable (more than 900K). This indicates a partial dissolving of the substrate upon immersion in PPA-solution and formation of new metal-organic compounds. This indicates a partial dissolving of the substrate upon immersion in PPA-solution and formation of new metal-organic compounds. In fact Mutin et al. reported in their review article [11] that some PA cause a dissolution-precipitation and formation of metal phosphonates or phosphinate phases which reflects some limitation of wet chemical processing on ZnO by PA. Remaining questions concern the understanding of this process and developing strategies to circumvent this dissolution.

Fig. 1 Phenylphosphonic acid (PPA)

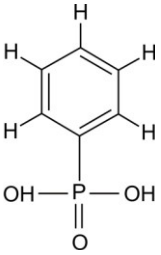

[1] Hagfeldt A. et al., Chemical Reviews, 110, 6595 (2010)
[2] Gupta S., Gleskova H., Organic Electronics, **13** (2013) 354-361
[3] Hubert Mutin P. et al., J. Mater. Chem., **15** (2005) 3761-3768
[4] Di Valentin C., Costa D., J. Phys. Chem., **116** (2012) 2819-2828
[5] Ma H., Acton O., H. Hutchins D. et al., Phys. Chem. Chem. Phys. **14** (2012) 14110-14126
[6] Hotchkiss et al., Accounts of Chemical Research, **45 (3)** (2012) 337-346
[7] Vioux, A. et al., Topics in Current Chemistry, **232** (New Aspects in Phosphorus Chemistry IV) (2004)145-174
[8] Gliboff M. et al., J. Phys. Chem. C, 117 (29), 15139-15147 (2013)
[9] Gouzman, I. et al., Surface Science, 600 (4), 773-781 (2006)
[10] Goetzen J., Witte G., Applied Surface Science, 258, 10144 - 10147 (2012)
[11] Mutin, P. H. et al., Journal of Materials Chemistry, **15**, (35-36), 3761-3768 (2005)

Site-selective Perylene-Deposition onto Microcontact-Printed Organothiolson Au-surfaces

André Pick & Gregor Witte

Faculty of Physics, Molecular Solids, D-35032 Marburg

Organic Semiconductors are promising materials for (opto)-electronic devices such as solar cells, light emitting diodes (OLEDS) and field-effect transistors (OFETs). On the other hand, e.g. single-crystal transistors allow fundamental studies of charge transport within the organic solid. A manual deposition of an organic single-crystal between two electrodes or the usage of conventional photolithography could lead to a destruction of the semiconductor. In addition, many applications require arrays of OFETS on the micron-scale with minimized cross-talk. Hence, it is crucial to control the nucleation of organic semiconducting crystals directly.

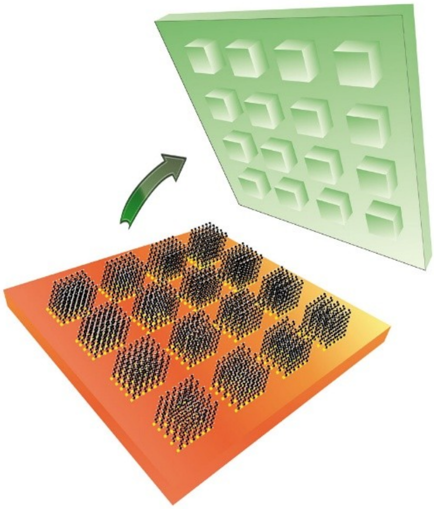

In order to achieve a site-selective deposition, soft lithography methods- such as microcontact-printing- have often been used. Here, active domains of nucleation are created by transferring an ink in patterns from a structured PDMS-stamp onto a surface. Especially molecules which tend to form self-assembled monolayers (SAMs) on a surface, were studied concerning their influence upon nucleation[1-4]. However, the mechanism of selective nucleation of organic semiconductors on a SAM still remains unclear.

Fig.1: Aliphatic thiols transferred onto a gold substrate

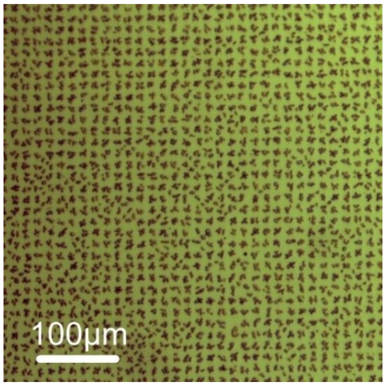

In this study we demonstrate the ability to control the site-selective nucleation of perylene crystallites by patterning gold-surfaces with self-assembling aliphatic organothiols. The semiconductor is deposited in UHV by means of organic molecular beam deposition from a resistively heated crucible, while the flux of molecules is measured with a quartz crystal microbalance.

Fig.2: Selectively grown crystallites on 1-Octadecanethiol/Au

As our aim is to analyze the origin of the selectivity, we compare the nucleation on differently prepared surfaces. Here we want to address several aspects:

1. influence of substrate roughness
   ➔ comparison between substrates of different local crystallinity

2. influence of chain length of SAMs

Fig.3: 1-Butanethiol, 1-Dodecanethiol, 1-Octadecanethiol

3. affect of their functional groups

Fig.4: 11-Mercapto-1-undecanol & 1H,1H,2H,2H-Perfluorodecanethiol,
both are compared with 1-Dodecanethiol

4. thickness of stamped thiol structures.

Regarding the chain-length of the thiolates we observe a contrast in sticking: the perylene-molecules stick to the shortest SAM at 300K, while for longer aliphatic backbones the sample has to be cooled to 275K in order to enable sticking. This can be attributet to the fact that a short SAM like the 1-Butanethiolate is defect-rich due to lower van-der-Waals interaction between the backbones, so that sticking is actually defect driven.

On the other hand, when comparing different functional groups, the hydrophobic species exhibit significantly lower sticking. Here the nature of the functional group regarding defects has to be taken into account. The hydroxyl group of 11-Mercapto-1-undecanol can form hydrogen bonds to neighboring molecules as well as to the substrate and thus induces less ordering, wich leads to an increased sticking behaviour. Apart from that, the presence of a thin water layer ontop of the hydrohphilic species could influence the sticking, although all SAMs were heated up to 350K in UHV.

The dependency of nucleation and growth on the thickness is highlighted for 1-Octadecanethiol and compared to the deposition of perylene within a thin liquid film of silicone-oil. This part of the study results from the fact that stamping thiols does not exclusively lead to monolayer formation. Often, ''puddles'' of a thiol are stamped which change the scenario drastically. We observe siteselectivity on thick structures of stamped 1-Octadecanethiol. As this material is waxy, we abstract the system to silicone-oil on a Si-wafer, instead of a thiol on gold.

[1] Briseno et al.: Patterning organic single-crystal transistor arrays. *Nature* **2006**, 444, 913-917
[2] Briseno et al.: Patterned growth of Large Oriented Organic Semiconductor Single Crystals on Self-Assembled Monolayer Templates. *J. Am. Chem. Soc.* **2005**, 127, 12164-12165
[3] Steudel et al.: Patterned growth of pentacene. *Applied Physics Letters* **2004**, Vol. 85, No. 23, 5550-5552
[4] Xu et al.: Selective deposition of organic molecules onto different densely packed self- assembled monolayers: A molecular dynamics study. *Chemical Physics Letters* **2011**, 507, 138-143

Deposition and physical characterization of graphene-like films on a Si (001) surface

K. Werner, A. Beyer, K. Volz and W. Stolz

Material Sciences Center and Faculty of Physics, Philipps-Universität Marburg

The two-dimensional carbon modification graphene has attracted great scientific interest in recent years. Exhibiting remarkable physical properties, as for example carrier mobilities as large as several thousands of cm²/Vs, it is an interesting material for fundamental research as well as for possible applications. Combining the well-established Si CMOS technology with graphene-based devices could lead to the next generation of high-speed electronics [1].

Currently graphene is mostly fabricated by chemical vapor deposition (CVD) on Cu substrates and transferred to the favored substrate after growth. This method though exhibits major drawbacks as e.g. the high cost originating from to complexity of the process, the defects in the graphene resulting from the transfer and the possibility of Cu contamination which cannot be accepted in CMOS fabrication lines. To avoid those drawbacks, we aim to deposit graphene on Si (001) by metal organic chemical vapor deposition (MOCVD) without the use of a transition metal. Our approach is to first pretreat the Si (001) substrates by depositing metallic gallium droplets, which we expect to have a catalytic effect on the decomposition of the carbon precursors and the graphene growth. This requires the controlled depositing of Ga on Si (001) by MOCVD, which was studied; the results will be presented in the following.

All investigated samples were grown in a horizontal MOCVD reactor system using H_2 as carrier gas. The Si (001) substrates were first treated by wet chemical etching followed by a high-temperature bake out in the MOCVD reactor directly before growth. For the Ga growth trimethyl gallium (TMGa) and triethyl gallium (TEGa) were used to study the influence of the precursor molecule on the grown structure. The reactor pressure was 50 mbar, while the growth temperature as well as the growth time and the Ga partial pressure were varied systematically to analyze the dependency of the Ga deposition on these parameters. To study the surface morphology samples were characterized by atomic force microscopy (AFM) in combination with selective etching with hydrochloric acid (HCl) as indication for metallic Ga, as HCl removes Ga while Si is unaffected by the etchant. To characterize the structural quality and the composition of the samples high angle annular dark field (HAADF) scanning transmission electron microscopy (STEM) reaching atomic column resolution in combination with energy dispersive X-ray spectroscopy (EDX) were used.

AFM images show that for both precursors used the Si surface is covered by mounds after the Ga deposition (Fig. 1(a) and 2(a)). Statistical analysis of the AFM measurements preformed for samples deposited with different growth conditions reveal that the size, height and density of those mounds clearly depends on the chosen precursor as well as growth temperature and time. While the structures deposited with TMGa could be etched of with HCl (Fig. 1(b)) leaving holes in the Si surface, this was not possible for the structures deposited with TEGa (Fig. 2(b)), indicating that the latter do not consist of pure metallic Ga. This difference is presumably due to the different reaction pathways for the two precursors. For the growth temperature range examined, it is assumed that TMGa decomposes by a hydrogen transfer process generating Ga, methane, hydrogen and carbon, while TEGa presumably decomposes primarily via β-hydride elimination yielding Ga, ethylene and hydrogen. It is expected that, due to the catalytic effect of the deposited metallic Ga, polyethylene chains build and deposit by the residual organic groups of the TEGa but not of the TMGa precursor molecule.

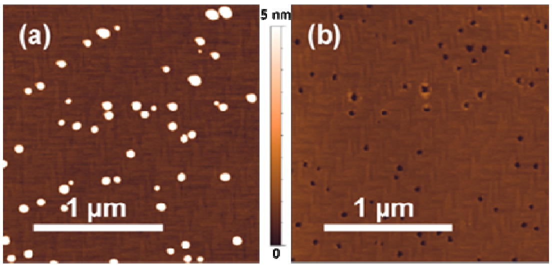

Fig. 1: AFM image of the Si surface after 15 s of TEGa deposition at 450°C before (a) and after selective etching with HCl (b)

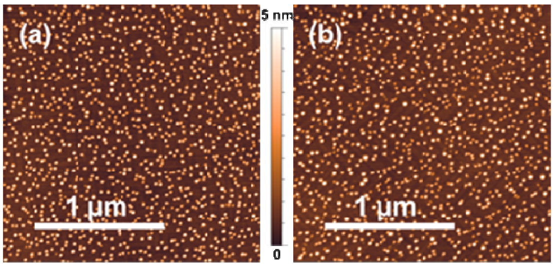

Fig. 2: AFM image of the Si surface after 10 s of TMGa deposition at 550°C before (a) and after selective etching with HCl (b)

STEM measurements for samples deposited with equivalent growth conditions exhibit that for both precursors used Ga diffuses into Si building pyramidal structures limited by the Si {111} lattice planes (Fig 3), which are energetically more stable in comparison with the Si (001) surface. Again, the size of the pyramidal structures depends on the growth conditions and decreases with decreasing temperature as well as with decreasing growth time. The structures are capped with an amorphous layer. As already discussed in the last section, for the sample deposited with TEGa we assume those mounds to be carbon containing. This prediction is also reinforced by results obtained by selective etching with organic solvents. For the structures grown with TMGa the origin and composition of the cap is not clear yet. It might partly form during the STEM sample preparation, but further investigation is needed. The sample deposited with TMGa exhibits stacking faults as can be seen in the inset in Fig. 3. Those are presumably caused by crystalline Si dissolving in the liquid Ga at growth temperature and recrystallizing at the boundaries of the Ga containing structure during the cooling down after growth due to the decreasing solubility of Si in Ga with decreasing temperature.

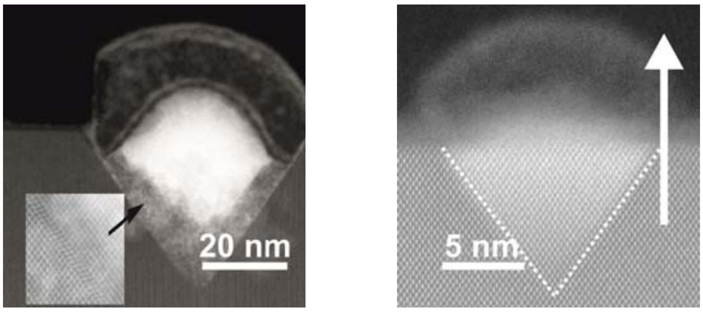

Fig. 3: HAADF STEM image of a sample after deposition of TMGa (left) and TEGa (right); growth conditions as for samples in Fig 1 and Fig 2 respectively

Some samples were annealed after growth in H_2 atmosphere at temperatures between 350°C and 800°C, as this temperature range might be suitable for a carbon deposition. For annealing temperatures above 800°C no Ga was found anymore at the surface of the samples deposited with both precursors. It might desorb from the surface or diffuse further into Si at this high temperature. For an annealing at lower temperatures structures build, which were more stable to etching with HCl. This might be due to a stronger intermixing of Si and Ga at the annealing temperatures, which might lead to a recrystallization of Si building a cap on the structure. But here, too, more work is needed.

As metallic Ga is needed as catalyst, the amorphous passivating cap on the mounds for the usage of TEGa as well as the intermixing of Ga and Si is presumably hindering the decomposition of the carbon precursors and the growth of graphene. To avoid this, the deposition of Ga on a thin GaP interlayer is studied. Also, the growth conditions for the Ga and for the carbon deposition need to be improved to prevent the described processes.

[1] K. Kim, J.-Y. Choi, T. Kim, S.-H. Cho, H.-J. Chung, A role for graphene in silicon-based semiconductor devices., Nature. 479 (2011) 338–44. doi:10.1038/nature10680.

Computer Simulations of Electronic and Atomic Kinetic Processes in Organic and Inorganic Semiconductors

Jan Oliver Oelerich and Sergei Baranovskii

Faculty of Physics and Material Sciences Center, Philipps-Universität Marburg

Computer Simulation of Growth Kinetics of GaP and Ga on Si (001)

Gallium (Ga) containing semiconducting III/V compounds on silicon (Si) are among the most promising materials for device application and functionalization. Particularly interesting is galliumphosphide (GaP) on Si since it is almost lattice matched with the diamond cubic Si lattice, eliminating strain as a source of unwanted physical effects at the interfaces. While the surface properties of the grown samples are easily accessible in experiments, it is comparatively hard to gain insight into the interface structures buried in the devices. In the past two years we developed a Kinetic Monte Carlo (KMC) simulation package for epitaxial growth of diamond cubic crystalline materials. The simulation allows us to study the kinetic aspects of the growth procedure and to gain insight into the sample structure during intermediate growth phases. The simulation was applied to two different phenomena, which are outlined below.

Melt-Back etching of Ga on Si (001)

In a recent experimental study of MOCVD of Ga on the Si (001) surface in the group of Prof. Dr. K. Volz and Dr. W. Stolz it was observed that the Ga atoms cluster on the surface and etch pyramidally shaped structures into the Si substrate. These voids are limited by Si (111) surfaces and, as seen in cross-sectional HAADF STEM images, filled with metallic Ga (see Fig. 1). We simulated the Ga deposition on Si (001) and found the sets of parameters that match the experimentally observed etching effects very well. An example snapshot of the Si substrate after the Ga growth is shown in Fig. 2 (Ga atoms are hidden).

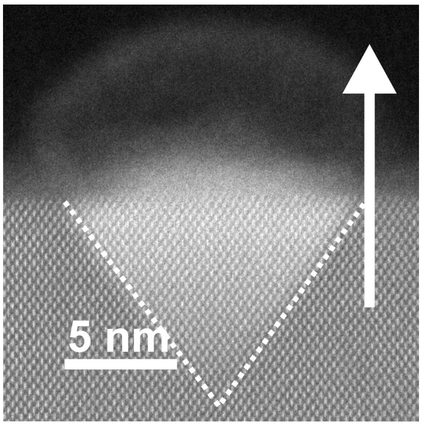

Figure 1: Cross-sectional HAADF-STEM image of the sample. The pyramidal structure limited by Si (111) planes (dashed lines) is clearly visible.

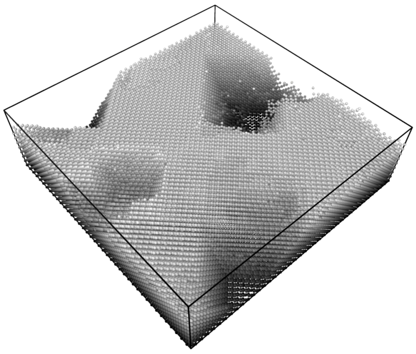

Figure 2: The Si substrate after the simulation. Ga fills the pyramidally shaped etching structures but is not shown here.

Several pyramidally shaped voids were etched by the Ga clusters into the substrate. These voids are mostly limited at the sides by the very stable Si (111) surface and filled with pure Ga, similar to the experimental findings.

Intermixing effects at the GaP on Si (001) interface

In another recent experimental study about MOVPE of GaP on Si (001), also carried out in the group of Prof. Dr. K. Volz and Dr. W. Stolz, significant intermixing effects of the Si substrate with the grown GaP crystal were observed: In the first seven to nine layers of GaP above the substrate decreasing amounts of Si are found. We simulated the deposition of GaP on Si with the KMC package and found that if one species of adatoms is less mobile than the others during self-organization of the GaP, significant intermixing is induced in the early stages of the growth. Our assumptions about the surface energy barriers were confirmed in ab-initio DFT studies by the group of Prof. Dr. R. Tonner. Comparisons between experiment and simulation are shown in Fig. 3. The figure shows the relative Si content of the simulation and experiment versus the number of layers in growth direction. It is apparent from the figure that both curves describe intermixing in about 8 ML around the interface.

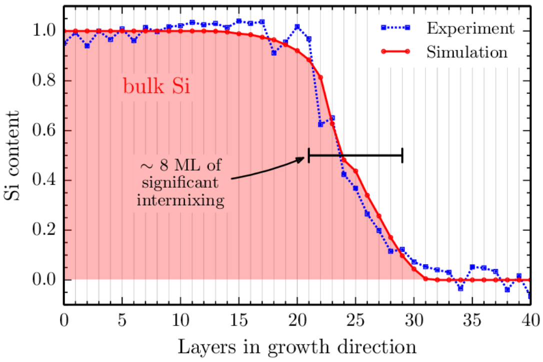

Figure 3: Relative amount of Si with respect to the layer number in growth direction.

Conclusion and Outlook

As demonstrated with the two examples above, we conclude that KMC simulations are a suitable tool to study kinetic processes during crystal growth procedures. There are many other interesting effects, to which our simulation can be applied, e.g., the growth of nanowhiskers or -wires and annealing effects of grown compound semiconductors. We are currently extending the simulation software to support simulation of quasi-liquid droplets on solid substrates.

Simulation of Electronic Kinetics in Organic Semiconductors

In the past two years we also focused on the simulation of the electronic transport and charge recombination in disordered organic materials.

Energy position of the transport path in disordered organic semiconductors

In disordered organic devices charge carriers move by a sequence of incoherent tunneling transitions between localized states, a transport mode called *hopping*. It is well known, that the localized states' energies are distributed following a Gaussian density of states (DOS) [1] and that there exists some particular energy level most significantly contributing to transport processes, the *transport energy*. However, there is no consensus among researchers on the exact position and the definition of this energy level. We suggested and implemented a new numerical procedure to determine the transport energy in organic semiconductors that ensures that the found energy level is indeed the most important energy for hopping transport in disordered materials [2].

Theory to carrier recombination in organic disordered semiconductors

While a concise and transparent theory for carrier recombination in inorganic materials existed for many years [3], this theory is restricted to certain parameter ranges that are not applicable to organic materials. We extended the theory, allowing its applicability to general cases of disordered systems [4]. By comparisons of numerical evaluations in the framework of this extended theory with experimental data for transient photoconductivity and photoabsorption we suggested a new way to infer the shape of the DOS in the disordered materials under study.

References

[1] J. O. Oelerich, D. Huemmer, and S. D. Baranovskii, *Phys. Rev. Lett.* **108**, 226403 (2012).

[2] J. O. Oelerich, F. Jansson, A. V. Nenashev, F. Gebhard, and S. D. Baranovskii, *J. Phys. Condens. Matter* **26**, 255801 (2014)

[3] J. Orenstein and M. Kastner, *Solid State Commun.* **40**, 85 (1981).

[4] A. Hofacker, J. O. Oelerich, A. Nenashev, F. Gebhard, and S. D. Baranovskii, *J. Appl. Phys.* **115**, 223713 (2014).

Optical Spectroscopy on Organic-Inorganic Hybrid Structures

I. Meyenburg, M. Kothe, A. Karthäuser, J. Falgenhauer*, M. Liebold**, T. Breuer,
J.Sundermeyer**, D.Schlettwein*, G. Witte and W. Heimbrodt

Philipps University, Physics department, Renthof 5, D-35032 Marburg
**Justus-Liebig-University, Institute of Applied Physics, Heinrich-Buff-Ring 16, D-35392 Gießen*
***Philipps University, Chemistry department, Hans-Meerwein-Straße, D-35032 Marburg*

Introduction

Understanding interface processes is crucial for improvements of existing and new functional materials based on organic-inorganic hybrids.

We studied organic-inorganic hybrids consisting of organic layers, e.g. pentacene, phthalocyanine, ruthenium based dyes and indoline dye on inorganic substrates by optical spectroscopy in the temperature range between 10K and room temperature.

Tension could be revealed as an interface relevant effect by studying Pentacene on ZnO [1]. Pentacene layers with different thickness show different exciton energy shifts with temperature variation. This is due to different temperature dependent expansion coefficients of the organic and inorganic material and the resulting tension between them. As a result a strong interface dipole in dependence of the temperature occurs.

Basic measurements are performed on organic-inorganic hybrid structures in order to learn about the influence of preparation method (OMBD and drop-coating) and substrate. Regarding the absorption spectra, in comparison to the organic molecules in solution, the spectra of thin solid layers are often broadened and even red-shifted due to weak intermolecular coupling and exciton formation, respectively.

Exciton recombination across type II organic-inorganic interface can give access to the level alignment and interface properties of the organic-inorganic semiconductor structures. Starting with material combinations known from dye sensitized solar cells (DSSC) which imply a charge transfer from organic to inorganic structure some promising hybrid systems are investigated in order to find a recombination of charge carriers across the interface. Different organic molecules, e.g. TiO-Phthalocyanine [4] and ruthenium dyes like N719 [2][3] have been studied on single crystalline rutile TiO2 and nanocrystalline anatase TiO2 substrates. Indoline dye D149 on mesoporous ZnO is a recently studied hybrid [5] structure. A typeII recombination is detected by photoluminescence spectroscopy (see figures).

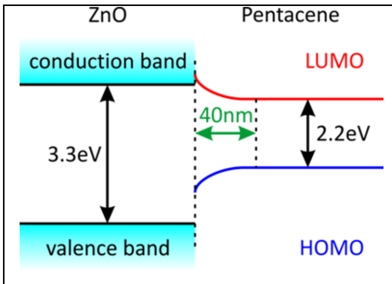

Left:
The bandgap of ZnO/pentacene at the interface at low temperature. The band bending is caused by strong different thermal expansion coefficients.

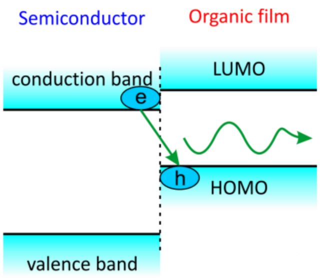

Right:
The recombination of spatially indirect excitons enables the precise determination of the organic-inorganic level alignment.
In DSSC the excited dye electron in the LUMO transfers into the conduction band and may recombine back to the HOMO.

Results

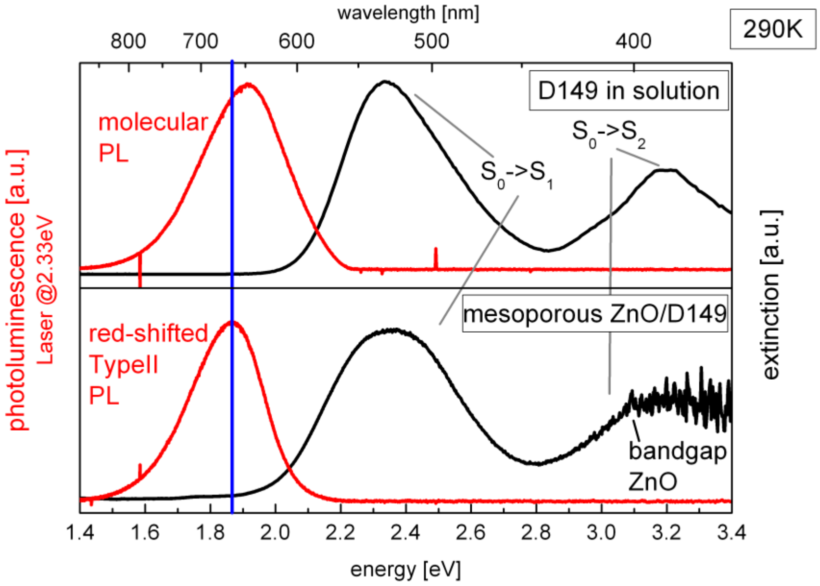

Photoluminescence and absorption spectroscopy of typeII organic-inorganic interface

Fig.1:
Indoline dye D149 on mesoporous ZnO (prepared by electrodepositon) shows a clear redshift in PL spectra which can be assigned to the typeII recombination from the conduction band of ZnO across the interface into indoline HOMO.

Spectroscopy of hybrid structures: Crystal formation leads to viewable exciton-PL

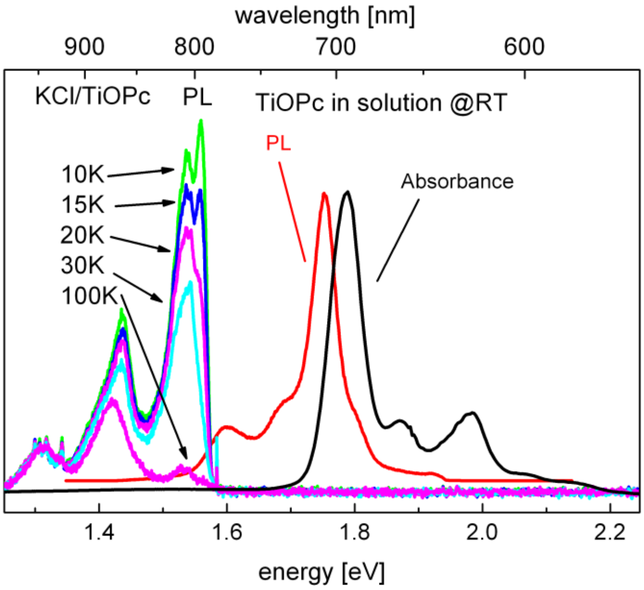

Fig.2:
As a promising typeII candidate of the wide variety of the group of phthalocyanines TiOPc is investigated. A strong red-shift from molecular to crystal absorption can be seen which is due to crystal formation. On KCl the temperature dependent PL measurements show a sharp peak at highest energy of the PL spectrum (about 790nm) which can be interpreted as exciton PL.

Conclusions

Mesoporous ZnO was revealed as a suitable wide gap semiconductor for organic-anorganic hybrid structures while mesoporous TiO2 Is difficult to investigate due to too many defect states.

Outlook

Further investigations with the hybrid structure ZnO_mesoporous/indoline will be performed in order to determine the precise level alignments at the interface.

References

[1] J.Helzel, Applied Physics Letters, 99 (2011) 211102
[2] M.Grätzel, Inorg.Chem., 44 (2005) 6841
[3] M. Nazeeruddin, J. Am. Chem. Soc., 127 (2005) 16835
[4] Shun Yu, J. Phys. Chem. C, 113 (2009) 13765
[5] E. Rohwer, ChemPhysChem, 14 (2013) 132

Development of a Double Resonant Probe Head For NMR Experiments

by Lars P. Kraft

My work started with the introductory training of the principles of NMR. Therefore I dealt with the theoretical background of the interaction between nuclear spins and magnetic fields. Also the interactions among nuclei was considered. However the whole understanding of the complex spin systems is an ongoing process by now.

As a precursor measurements of ^{13}Boron situated in the borosilicate glass of the probe head housing were carried out to become acquainted with the actual laboratory setup. Furthermore the results of these experiments act as reference for future experiments.

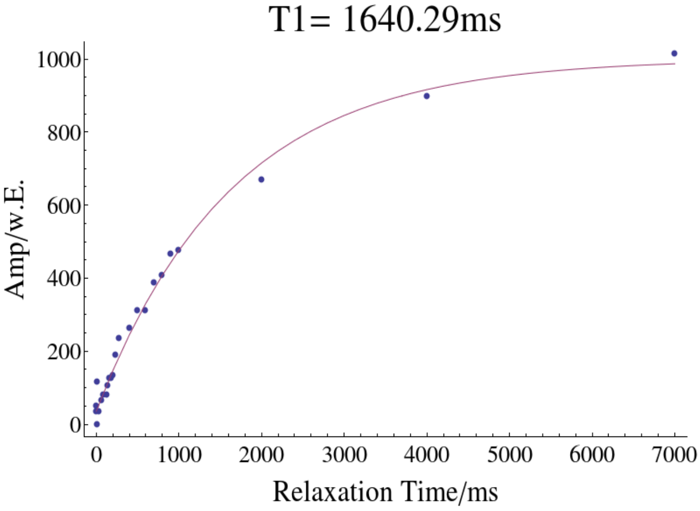

Figure 1: T1 relaxation time of ^{13}Boron in borosilicate glass in the stray field of the NMR measuring coil.

Once the principle of Dynamic Nuclear Polarization (DNP) was sufficiently understood a plan was conceived to build up a new installation for double resonance experiments. It is a sensitive and time-consuming job adapting NMR coils so precisely, that sufficiently homogeneous and definable fields can be applied at the probe volume. For that reason it was decided not to change the existing probe head but to design an extension that can be connected with the existing probe head by a cable.

For making a concept for the double resonance extension the paper of *Haase J. et al. (J. Magn. Reson. 1998 Dec; 135 (2): 273-9)* and the diploma thesis of *Schaffner A. (formally Schmitt) 2008, Marburg* were used. These works deal with the design of a double resonance circuit, to be more precise, with the coupling of two parallel oscillating circuits which are resonant at two near frequencies simultaneously. On the one hand these concepts appear handy but on the other hand they cannot be employed on the existing probe head because the latter is a series circuit. Therefore only the idea was taken as an example of coupling circuits.

There exist a lot of possibilities to accomplish coupled circuits, i.e. the matching to 50 Ω is possible. Thus there is a numerousness of solutions with different dimensions of the capacitors and coils. But only a few solutions provide the demanded q-factors and signal strengths for both frequencies concurrently by realistic dimensions of the components.

To find an appropriate solution a little *Mathematica* script was implemented to simulate a manifold of circuits. Hereby the existing probe head appears as a series oscillating circuit that is connected to a cable represented by a combination of capacitors and coils, which in turn is connected to the extension circuit providing the second resonance. The scheme of the extension circuit was variated as well as the number of subdivisions of the cable.

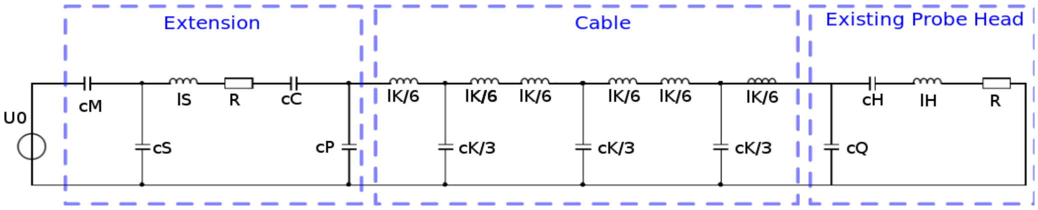

Figure 2: Model Circuit

The more parts are considered the more parameters have to be adjusted. Hence the task of impedance matching involves an optimization problem with in fact 19 variables. To lead numerical optimization algorithms to success suitable assumptions have to be applied. For example the range of capacities is limited, the power arising in the measuring coil should be maximized and estimations for the existing probe head's components and the cable's capacity/inductivity are made.

By reduction of the parameters to 5 and presetting suitable start values it became possible to solve the optimization problem. Still there can be considered many solutions but the encountered ones led to satisfying q-factors as high as 200...300.

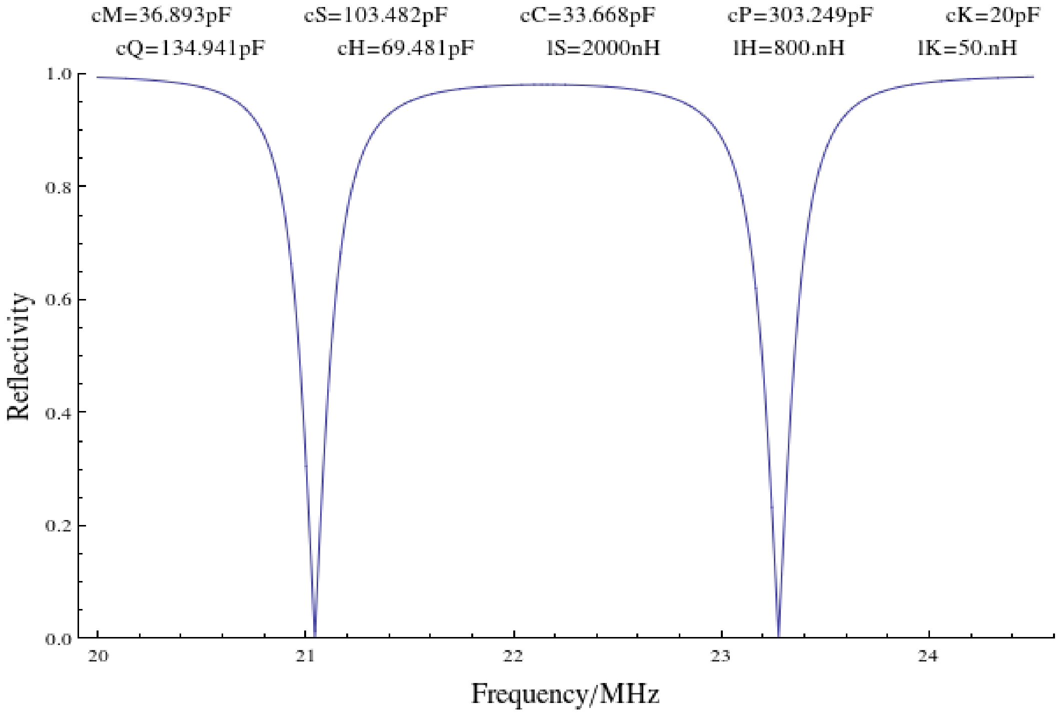

Figure 3: Simultaneously optimized reflectivity for 21.044 MHz and 23.275 MHz. R=1 Ω

The remaining subject of matter that is not treated in the simulation is the influence of the housing's walls and the power losses by additional resistances (cable, eddy currents, etc.). This influence is handled by establishing a preliminary setup.

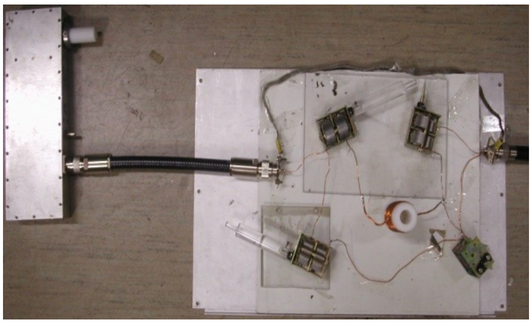

Figure 4: Preliminary test setup

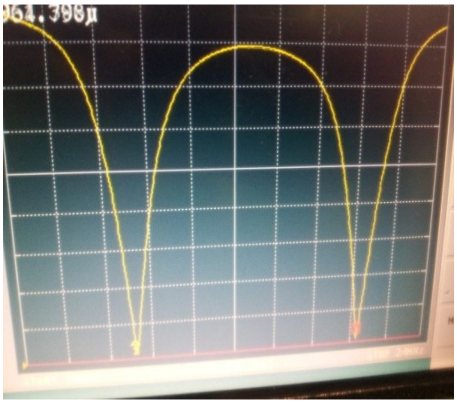

Figure 5: Measurement of signal reflectivity. Spectral range is the same as in the simulation

Therefore a similar probe head as the one in the actual experimental setup is connected to the preliminary setup by a coaxial cable with low damping (This cable will be used in the final setup). It was possible to accomplish the 50 Ω impedance matching for both frequencies simultaneously in fact.

From the measurement of reflectivity a q-factor arises of approximately 100. The gap between the simulation and the preliminary setup arises from resistances. This was qualitatively tested in the simulation by taking additionally resistances into consideration.

Stray capacities or stray inductivities as well as the mentioned resistances are not discussed in detail furthermore because this will first be necessary in the final setup. In a preliminary experiment the field in the measuring coil was gauged and it suited the expectations.

Hence it was shown that this concept fulfills the requirements. The main extension circuit is under construction.